R. & M. No. 2535
(8739, 7596, 7045, 9559, 8707)
A.R.C. Technical Report

MINISTRY OF SUPPLY

AERONAUTICAL RESEARCH COUNCIL
REPORTS AND MEMORANDA

High-speed Wind-tunnel Tests on Models of Four Single-engined Fighters (Spitfire, Spiteful, Attacker and Mustang) Parts 1 — 5

By

The Staff of the R.A.E. High Speed Wind Tunnel

Edited by W.A. Mair, M.A.

LONDON : HIS MAJESTY'S STATIONERY OFFICE

1951

PRICE £1 0s 0d NET

High-speed Wind-tunnel Tests on Models of Four Single-engined Fighters (Spitfire, Spiteful, Attacker and Mustang)

Part I

Tests on the Spitfire I

By

W. A. MAIR, M.A., S. P. HUTTON, M.Eng. and H. E. GAMBLE, B.Sc.

Part II

Tests on the Spiteful (F. 1/43)

By

W. A. MAIR, M.A., S. P. HUTTON, M.Eng. and H. E. GAMBLE, B.Sc.

Part III

Tests on Cabins for the Spiteful

By

W. A. MAIR, M.A. and S. P. HUTTON, M.Eng.

Part IV

Tests on the Attacker (E. 10/44)

By

S. P. HUTTON, M.Eng., D. A. CLARK, B.Sc. (Eng.), A.C.G.I. and D. J. TREMLETT, B.Sc, (Eng.), A.C.G.I.

Part V

Tests on the Mustang I

By

J. Y. G. EVANS, B.Sc., J. CALDWELL, B.Sc., Wh.Sch., A.M.I.Mech.E. and C. M. BRITLAND

High-speed Wind-tunnel Tests on Models of Four Single-engined Fighters (Spitfire, Spiteful, Attacker and Mustang)

By

The Staff of the R.A.E. High Speed Wind Tunnel

COMMUNICATED BY THE PRINCIPAL DIRECTOR OF SCIENTIFIC RESEARCH (AIR), MINISTRY OF SUPPLY

Reports and Memoranda No. 2535*

April, 1945

Summary.—This report describes measurements of lift, drag, and pitching moment made in the R.A.E. High Speed Wind Tunnel on models of the Spitfire, Spiteful (F.1/43), Attacker (E.10/44), and Mustang. On the Spiteful model, pressure distributions on the front radiator flap were also measured. An introduction (written in 1949) gives a general account of the tests described in the separate parts of the report.

INTRODUCTION

1. *Range of Tests.*—Each model was tested for a range of incidences at a series of Mach numbers up to about 0·8, and the wind-tunnel pressure was adjusted to keep the Reynolds number constant at a value of about 1×10^6. Measurements were made on the model with and without tail, and for various elevator and tailplane settings.

In addition to these high-speed tests, measurements were made at low Mach numbers (less than 0·2) for a range of Reynolds numbers up to about 4×10^6. On the Spiteful model these also included tests of landing flaps.

2. *Model Rig.*—The models were made of teak, and were supported on two main struts under the wings and a third strut under the after end of the body which was used to alter incidence. These struts were mounted on a balance under the floor of the tunnel. The main struts were shielded by hollow streamlined guards for about two-thirds of their height from the floor. Two cross-bracing wires of oval section were connected from the tops of the struts to the balance to provide lateral rigidity.

The engine air flow on the jet-propelled Attacker was represented by open ducts. These gave a flow at the entry roughly appropriate to top-speed flight conditions. On the other models, the radiators for the piston engines were represented by slotted metal baffle plates in the ducts, arranged to give roughly the correct pressure drop for top-speed flight conditions.

* R.A.E. Report No. Aero. 1810 (A.R.C. 6739)—received 24th May, 1943.
R.A.E. Report No. Aero. 1908 (A.R.C. 7596)—received 4th April, 1944.
R.A.E. Test Note No. Aero. 1247 (A.R.C. 7045)—received 15th September, 1943.
R.A.E. Report No. Aero 2112 (A.R.C. 9559)—received 29th April, 1946.
R.A.E. Report No. Aero. 2038 (A.R.C. 8707)—received 28th May, 1945.

3. *Presentation of Results.*—The results of the tests are given in the form of diagrams of force, moment and pressure coefficients, the pitching moments being referred to the C.G. position as given for each aircraft. The conclusions for each series of tests are given at the ends of the separate parts of the report.

4. *Corrections Applied.*—The tunnel interference effect produced by the model lift has been allowed for by applying the usual corrections, modified for compressibility by the linear perturbation theory given by Goldstein and Young in 1943 (R. & M. 1909). For high-speed tests the so-called " blockage " correction is of greater importance, because it involves a correction to the measured Mach number. For all the results given in this report except those in Part I, this correction was calculated by the method given by Thom in 1943 (R. & M. 2033), the order of the correction to Mach number being about $+0{\cdot}03$ at $M=0{\cdot}8$, and negligible below $M=0{\cdot}7$. Later work has indicated that this method underestimates the magnitude of the correction at Mach numbers above about $0{\cdot}8$.

In the case of the Spitfire tests described in Part I, this blockage correction was not applied when the original report was issued. The appropriate values of the correction, which should be applied to all the results given in Part I, are as follows :—

Uncorrected Mach number	0·60	0·70	0·75	0·78	0·80
Corrected Mach number	0·607	0·712	0·768	0·807	0·838

The strut support system described above introduces serious disturbances in the air flow over the model at high speeds. Various attempts have been made to allow for these by measuring the effects of the struts, guards, and bracing wires, and then correcting the measured forces and moments. These methods are not now regarded as reliable (1949), and there is some uncertainty about the results of the tests for Mach numbers (corrected for blockage) above about $0{\cdot}8$. In the case of drag the difficulties are particularly serious, and results above $M=0{\cdot}75$ are unreliable.

The authors consider that although some caution is needed in interpreting the results at high Mach numbers, useful comparisons can be made, provided that due regard is paid to the above limitations and their causes.

LIST OF SYMBOLS

a_1	Tail plane lift-curve slope $(dC_{LT}/d\alpha_T)$
a_2	Elevator effectiveness $(dC_{LT}/d\eta)$
C_D	Drag coefficient
C_F	Normal-force coefficient for radiator flap
C_H	Hinge-moment coefficient for radiator flap
C_L	Lift coefficient, for wing or complete aircraft
$C_{L\,\mathrm{MAX}}$	Maximum lift coefficient
C_{LT}	Tailplane lift coefficient
C_m	Pitching-moment coefficient
C_{m0}	Pitching-moment coefficient at zero lift, for aircraft without tail

LIST OF SYMBOLS—*continued*

C_p	Pressure coefficient $(p-p_1)/(\frac{1}{2}\rho V^2)$
c	Wing chord
$\bar{c}$	Mean wing chord
h_n	$1/\bar{c}$ (distance from neutral point to leading edge of mean chord)
M	Mach number
p	Static pressure at any given point
p_1	Static pressure in undisturbed stream
R	Reynolds number
T.A.S.	True air speed (in flight)
V	Velocity of air in tunnel
α	Wing incidence
α_T	Tailplane incidence
ε	Downwash angle at tail
η	Elevator angle
η_T	Tailplane setting (to wing root chord)
ρ	Air density

CONVERSION FACTORS

To convert British units to metric units multiply by the figure given.

1 inch in = 25·400 millimetres mm

1 foot ft = 30·480 centimetres cm

1 square foot ft² = 929·03 square centimetres cm²

1 pound per square foot Lb/ft² = 4·882 4 kilogrammes per square metre Kg/m²

ABBREVIATIONS

N.P.L.	..	National Physical Laboratory
R.A.E.	..	Royal Aircraft Establishment
F.S.	..	Full scale
L.E.	..	Leading edge
T.A.S.	..	True air speed

PART I

Tests on the Spitfire I

By

W. A. MAIR, M.A., S. P. HUTTON, B.Eng., and H. E. GAMBLE, B.Sc.

1. *Introduction.*—Flight tests[1] on a Spitfire at high speeds have shown no important changes of trim or stability at Mach numbers up to 0·775, but a large increase of drag* was found at Mach numbers above about 0·7.

High-speed tunnel tests were required to provide further information on the characteristics of the Spitfire at high speeds and for comparison with measurements made in flight.

2. *Details of Model.*—The tests were made on a $\frac{1}{6}$ scale model Spitfire I. Model and full-scale dimensions are given in Table 1, and the general arrangement of the model is shown in Fig. 1.

3. *Results.*—In presenting the results of the tests all incidences refer to the wing root chord.

3.1. *Lift.*—The variation of trimmed lift coefficient with incidence and Mach number is shown in the form of a lift carpet in Fig. 2. Fig. 3 shows the variation of lift-curve slope with Mach number for a lift coefficient of 0·1. The lift-curve slope increases with Mach number up to about 0·75, then falls off rapidly with further increase of Mach number.

Fig. 4 shows values of C_L and C_D for the complete model at a low Mach number, plotted against incidence for two different Reynolds numbers. There is no appreciable scale effect on lift-curve slope, but the no-lift angle appears to be about 0·1 deg greater at $R=4\cdot8\times10^6$ than at $R=2\times10^6$.

3.2. *Drag.*—Fig. 5 shows the variation of drag coefficient with Mach number for four different values of C_L. These curves show that the drag critical Mach number is greatest at a lift coefficient of about 0·1. At this value of C_L the drag coefficient at $M=0\cdot7$ is about 18 per cent greater than at low speed.

3.3. *Longitudinal Stability and Trim.*—Figs. 7 and 8 show pitching-moment coefficients plotted against lift coefficients (untrimmed) for different Mach numbers, tail settings and elevator angles.

In Figs. 15 and 16 pitching-moment coefficients are plotted against Mach number for several different values of C_L, with and without the tail. Figs. 10 and 14 show elevator angle to trim and downwash angle at the tail respectively, plotted against Mach number. It can be seen from Figs. 10 and 15 that the change of trim with Mach number is smallest at zero lift, and is then only about $\frac{1}{2}$ deg of elevator angle at a Mach number of 0·79. Even at higher lift coefficients the change of trim is not dangerously large, at least for Mach numbers up to about 0·8. Comparison of Figs. 15 and 16 shows that at high Mach numbers and moderate lift coefficients there is a large negative pitching moment due to the tail. This effect is due partly to the reduction of main-plane lift-curve slope, causing an increase of incidence for a given value of C_L, and partly to the reduction of downwash at the tail at high Mach numbers, as shown by Fig. 14.

The large reduction of downwash at high Mach numbers is probably due to the gradual spreading of the shock stall along the wing from root to tip. Because of the wash-out and change of thickness along the wing the critical speed at the root is less than at the tip, so that there is a

* Later flight tests, using improved methods, have shown that the drag of the Spitfire does not increase appreciably until much higher Mach numbers are reached.

pronounced change of lift distribution and the resulting change in the trailing vortex system affects the downwash at the tail. In addition to this change of downwash due to the effect of the trailing vortices, there must also be a reduction of downwash as a direct result of the loss of lift on the part of the wing in front of the tail. If the shock-stalling speed were the same for all parts of the wing, it might be expected that the downwash for a given lift coefficient would be nearly independent of Mach number.

Fig. 9 shows the effect of Mach number on C_{m0} for the model without the tail. This coefficient gives the tailplane load required for trim at zero lift. The increase in the numerical value of the coefficient with Mach number is given approximately by the Glauert law, except at very high Mach numbers. Values of C_{m0} for wing and body, derived from tail deflection measurements in flight[1], have been corrected to zero aileron float by Glauert's theoretical method[2] and plotted in Fig. 9 for comparison with the tunnel results. There is a considerable difference between the flight and tunnel results, but part of this may be attributed to scale effect. This is shown by the values of C_m measured in the tunnel at two different Reynolds numbers at low speed, which are given in Fig. 6. The value of C_{m0} at low Mach numbers for the higher Reynolds number is also shown in Fig. 9.

From the slopes of the curves in Figs. 7 and 8 the value of $(\partial C_m/\partial C_L)$ at constant Mach number has been found, for different lift coefficients and Mach numbers, and the results are given in Fig. 11. At Mach numbers below 0·6 this quantity is very nearly independent of C_L and Mach number. As the Mach number increases from 0·6 to about 0·7 $(\partial C_m/\partial C_L)_M$ increases, and with further increase of Mach number there is a considerable decrease. This decrease of $(\partial C_m/\partial C_L)_M$ at very high Mach numbers is considerably greater for moderately high values of C_L than for zero lift, and is apparently due to the shock-stalling of the wing causing a reduction of lift-curve slope, while the tailplane does not shock-stall and so has a relatively large lift-curve slope.

From the curves of Fig. 8 the tailplane lift-curve slope a_1 has been calculated for different incidences and Mach numbers. The results are given in Fig. 12 for wing root incidences from 0 to 6 deg over a range of Mach numbers. It is evident from these curves that the tailplane retains its full stabilising effect at all Mach numbers up to 0·8. Similar calculations of a_2, the tailplane lift due to change of elevator angle, have been made and are given in Fig. 13. The elevator is fully effective at all Mach numbers up to 0·8.

In Fig. 6, pitching-moment coefficients for the complete model and for the model without the tail are plotted against C_L for two different Reynolds numbers at low speed. Although the scale effect on the model without the tail is very small, the pitching moment of the complete model increases with Reynolds number. This change of trim must be caused by a change of downwash at the tail due to some change in the flow over the body, since the effect is present even when the pitching moment due to the tail is zero. The increase of pitching moment between $R=2\times10^6$ and $R=4\cdot8\times10^6$ is equivalent to an increase of about $\frac{1}{3}$ deg in the elevator angle to trim. The pitching-moment coefficients shown in Fig. 6 for the model with tail do not agree exactly with the values for the same tail setting, elevator angle, and Reynolds number given in Fig. 7A. The results given in Fig. 6 were derived from a later test than those given in Fig. 7A, and it must be supposed that some change in the model had occurred between the two tests.

Measurements made in flight have shown that the elevator angle to trim at low Mach number and low C_L is about 4 deg, whereas Fig. 20 gives about 3·2 deg. Part of this discrepancy may be due to the difference of Reynolds number between the model and full-scale tests.

4. *Conclusions.*—These tests have shown that the only important change that occurs at Mach numbers up to 0·8 is an increase of drag coefficient. This conclusion is in agreement with the results of flight tests.

REFERENCES

No.	*Author*	*Title, etc.*
1	Mair	Measurements of Tailplane Deflection in High Speed Dives. A.R.C. 5989. (June, 1942.)
2	Glauert	Theoretical Relationships for an Aerofoil with a Hinged Flap. R. & M. 1095. (April, 1927.)

TABLE 1

Spitfire Dimensions (Full Scale)

Wing span	36·92 ft
Standard mean chord	6·54 ft
Wing root chord	8·26 ft
Gross wing area	242·0 sq ft
Aspect ratio	5·65
Tailplane span	10·50 ft
Tailplane mean chord	3·215 ft
Gross tailplane area	33·75 sq ft
Distance from tailplane quarter-chord point to aft centre of gravity position	17·92 ft
Tailplane volume coefficient	0·382
Aft centre of gravity position	
Aft of leading edge mean chord	$0 \cdot 340\bar{c}$
Above root chord	$0 \cdot 246\bar{c}$
Aft of root leading edge	2·638 ft
Above root chord	1·705 ft
Fuselage datum incidence	—2 deg to wing root chord.
Wing tip incidence	$-2\frac{1}{2}$,, ,, ,, ,, ,,
Normal tailplane setting	—2 ,, ,, ,, ,, ,,
Wing section at root	NACA 2213
Wing section near tip	NACA 2208

Tailplane and elevator $\frac{t_{max.}}{c} = 0 \cdot 10$.

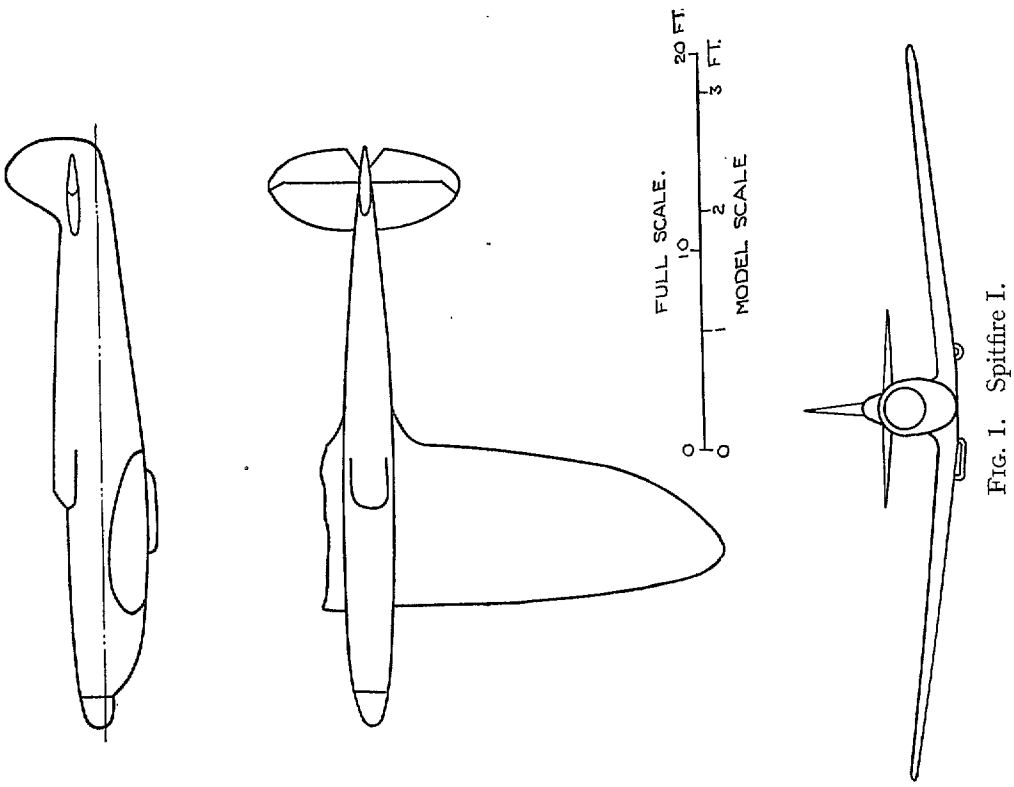

FIG. 1. Spitfire I.

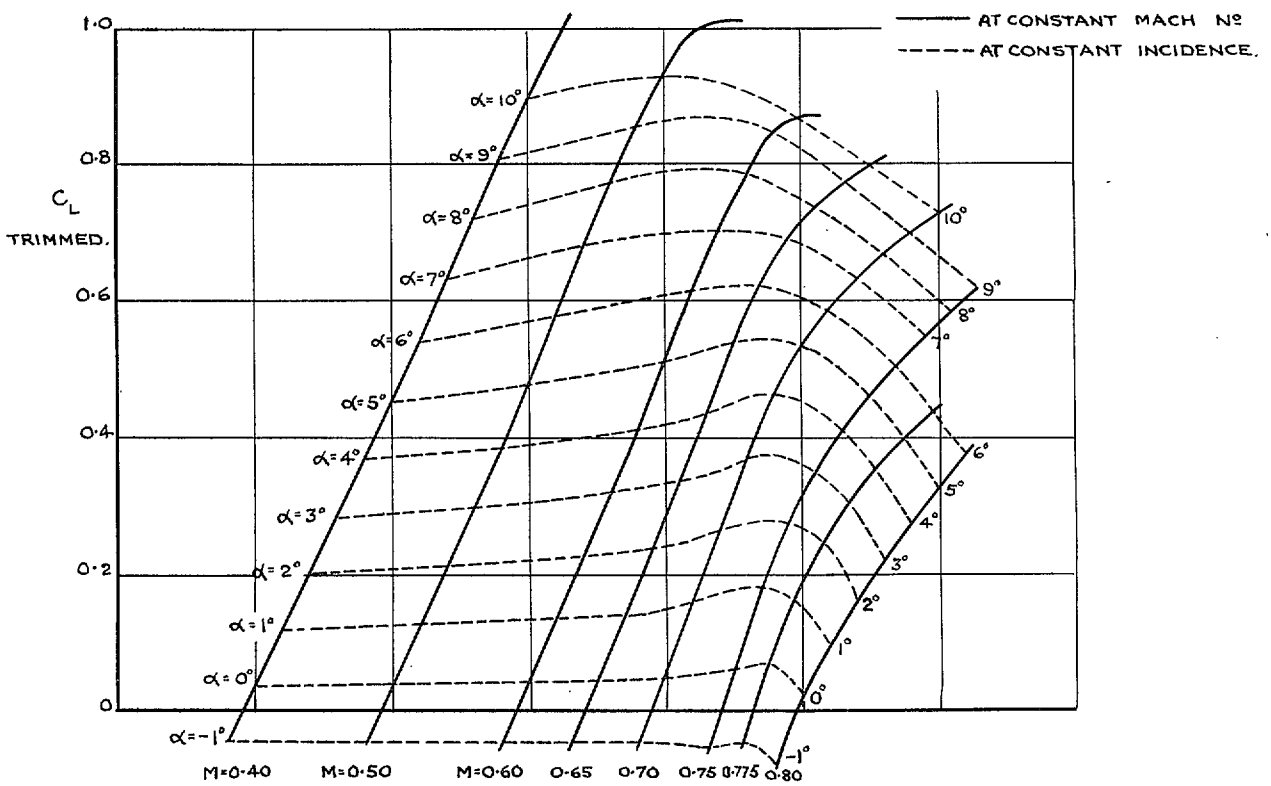

FIG. 2. Lift carpet. (Not corrected for blockage.)

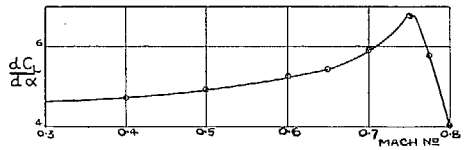

FIG. 3. Lift-curve slope at $C_L = 0 \cdot 1$.
(Not corrected for blockage.)

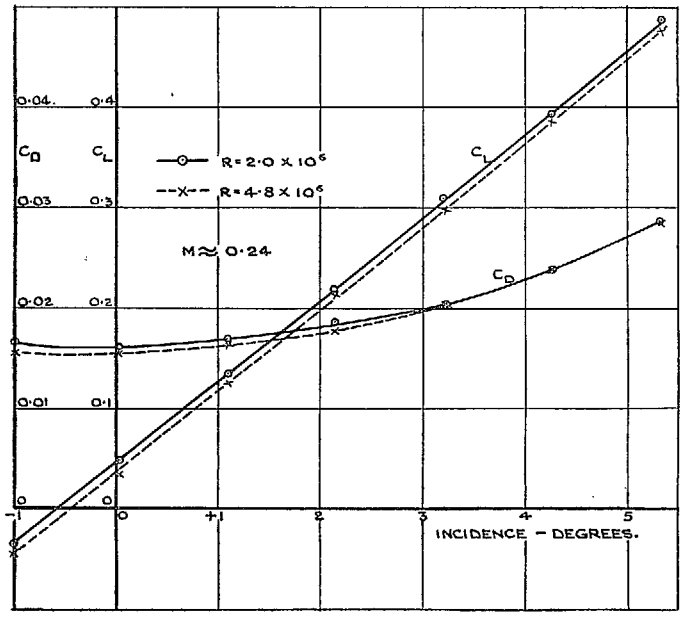

FIG. 4. Lift and drag coefficients at low speed.

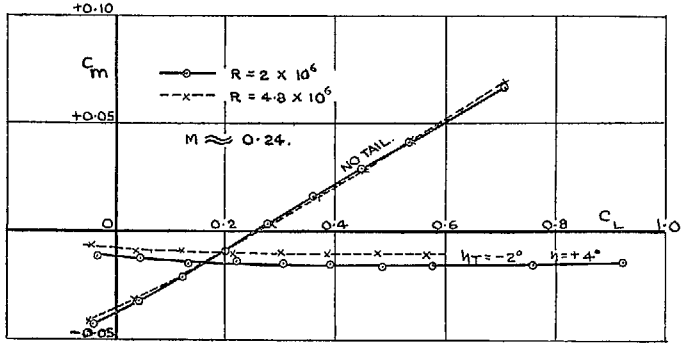

FIG. 6. Pitching moment at low speed.

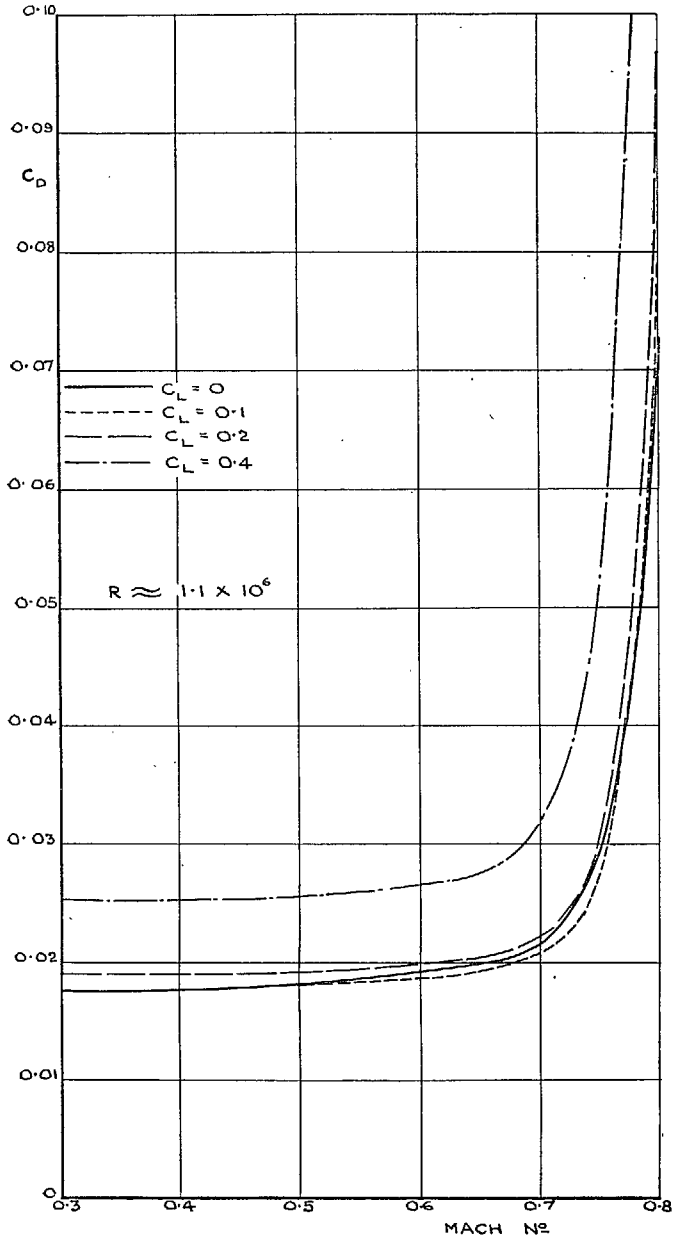

FIG. 5. Effect of Mach number on drag at constant C_L.
(Not corrected for blockage.)

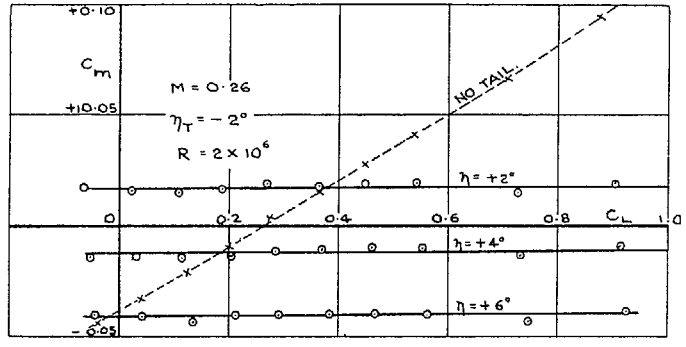

A

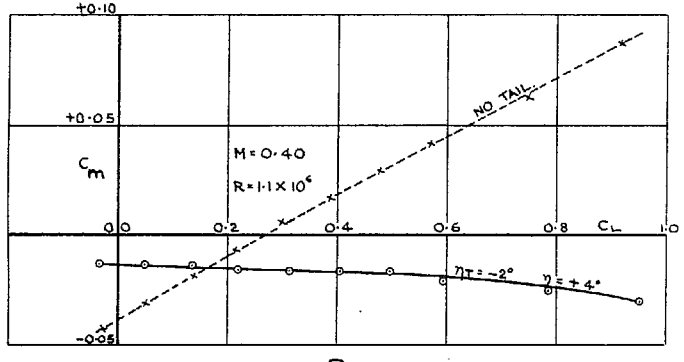

B

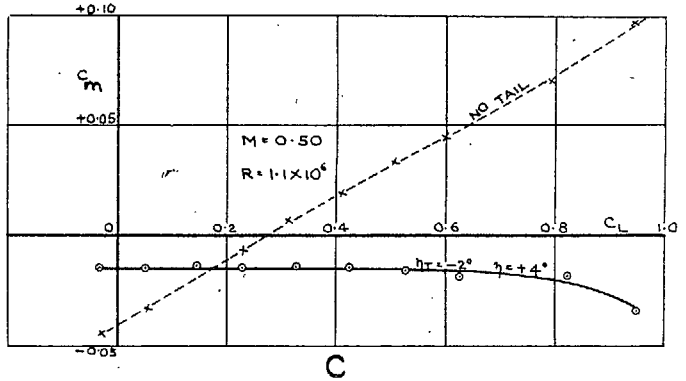

C

FIG. 7. Pitching-moment curves.

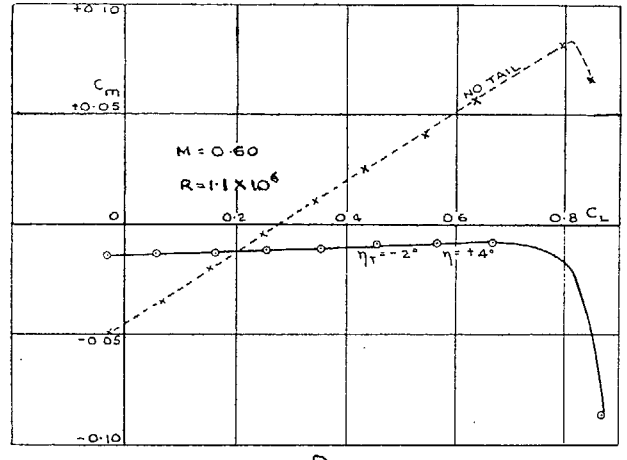

D

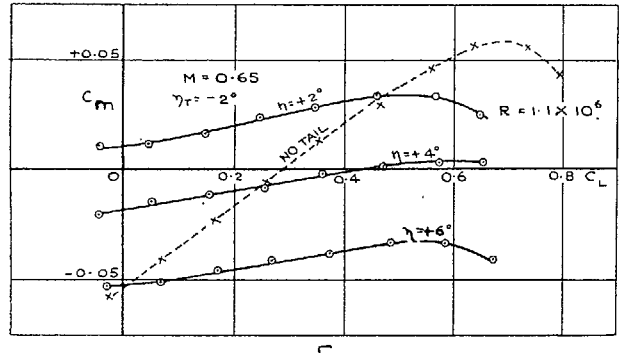

E

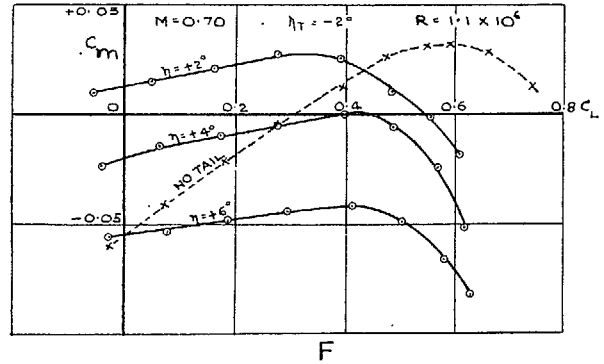

F

FIG. 7. Pitching-moment curves. (Not corrected for blockage.)

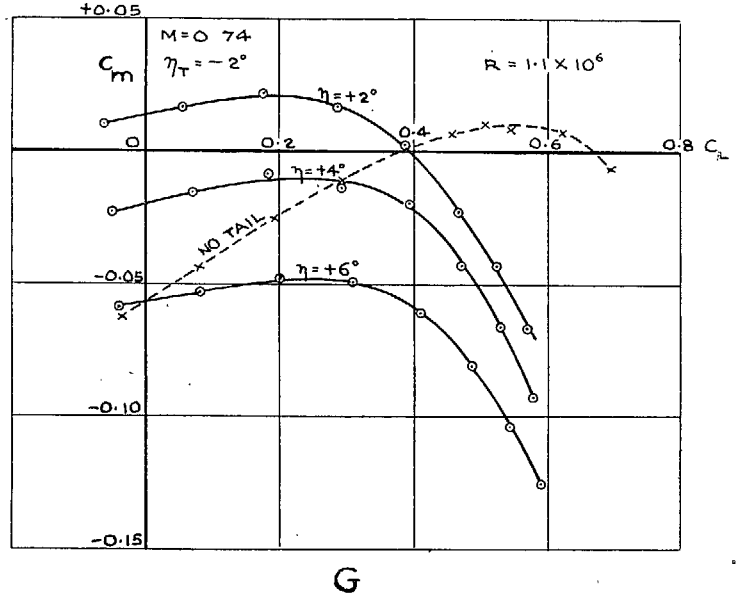

G

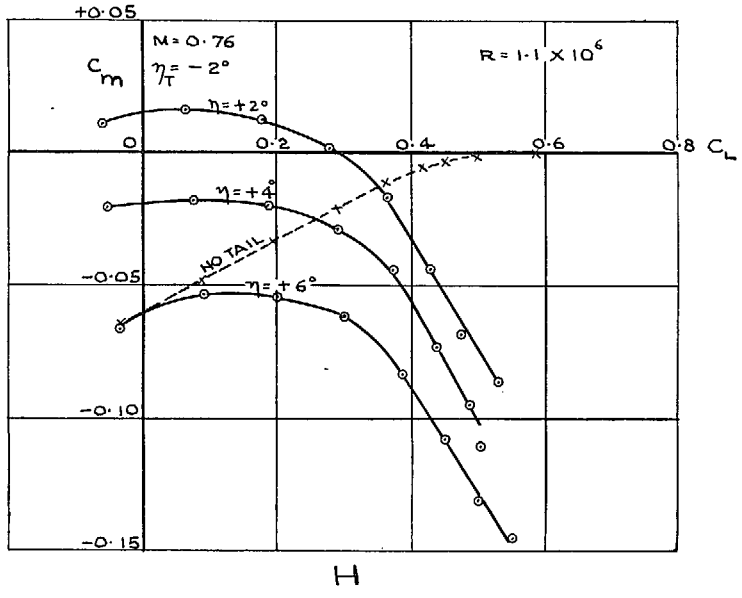

H

FIG. 7. Pitching-moment curves. (Not corrected fo blockage.)

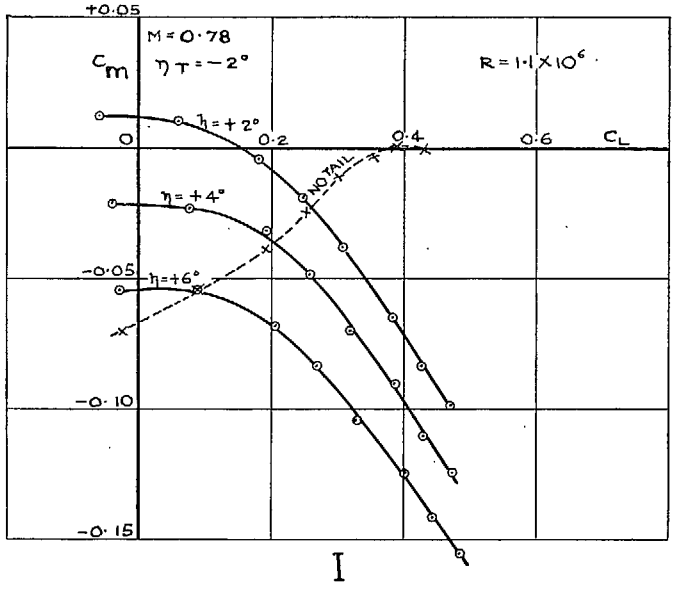

I

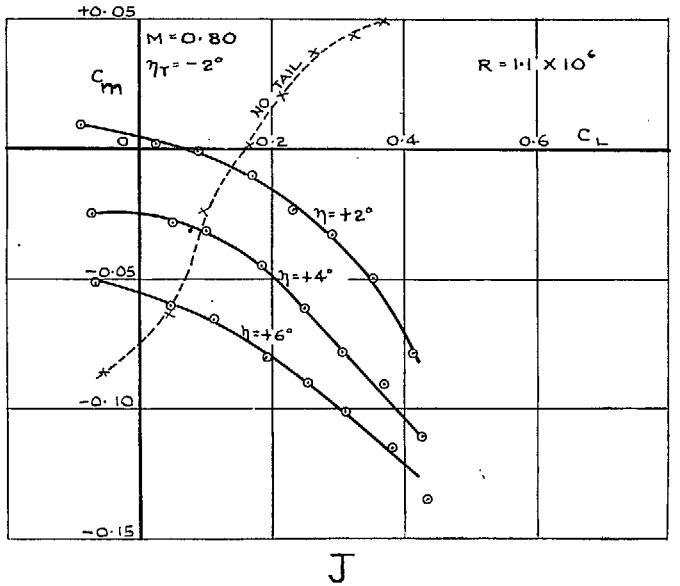

J

FIG. 7. Pitching-moment curves. (Not corrected for blockage.)

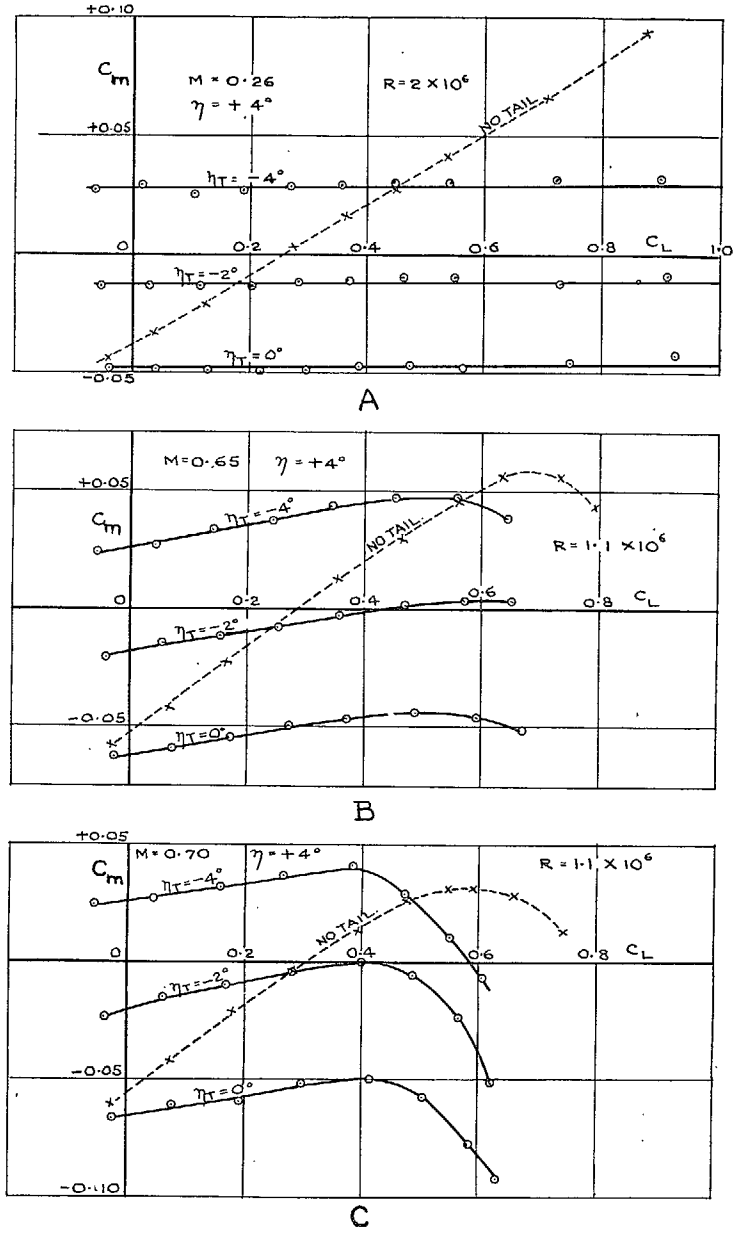

FIG. 8. Pitching-moment curves. (Not corrected for blockage.)

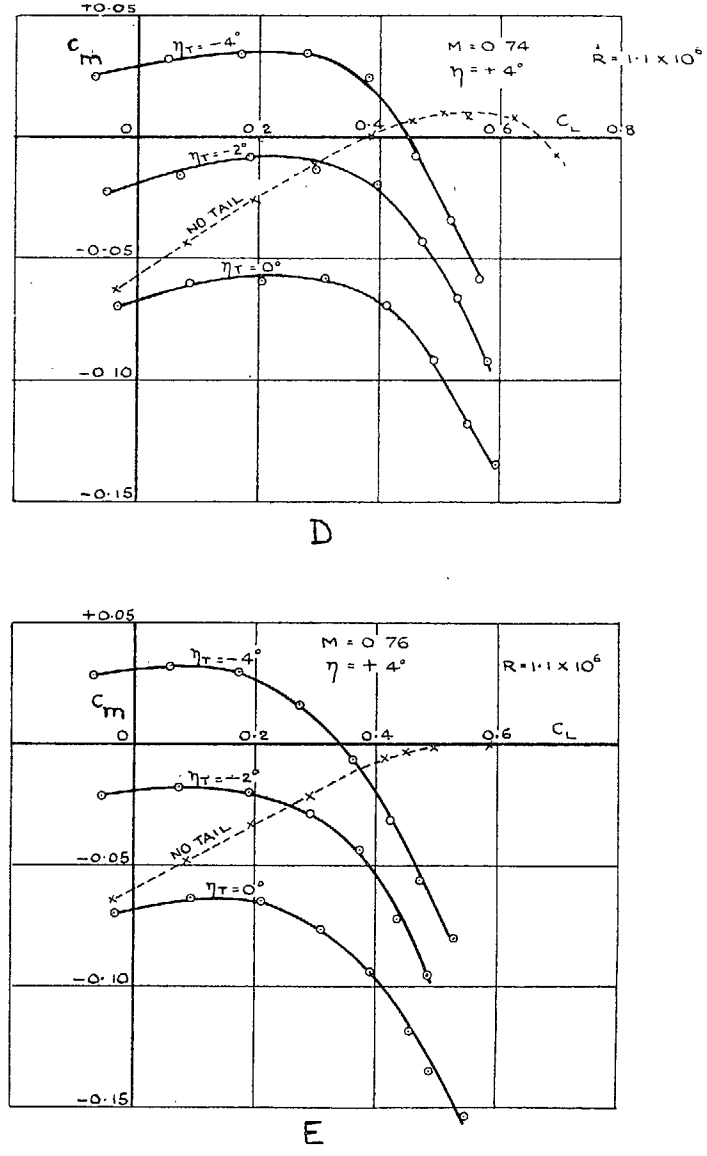

FIG. 8. Pitching-moment curves. (Not corrected for blockage.)

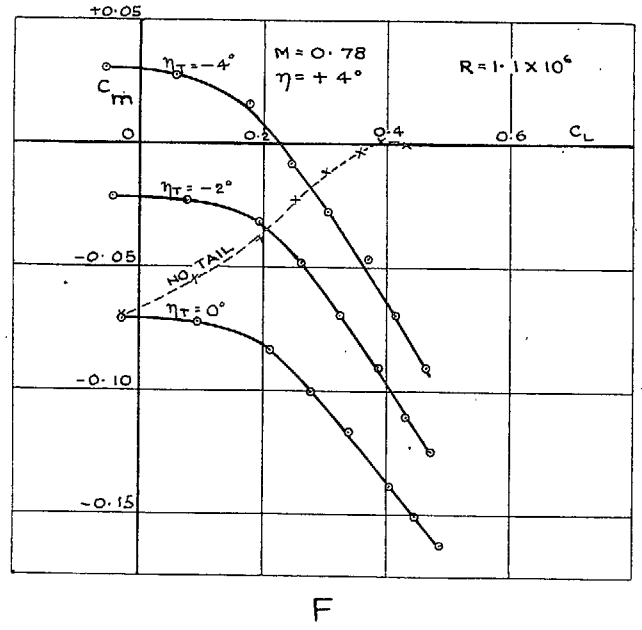

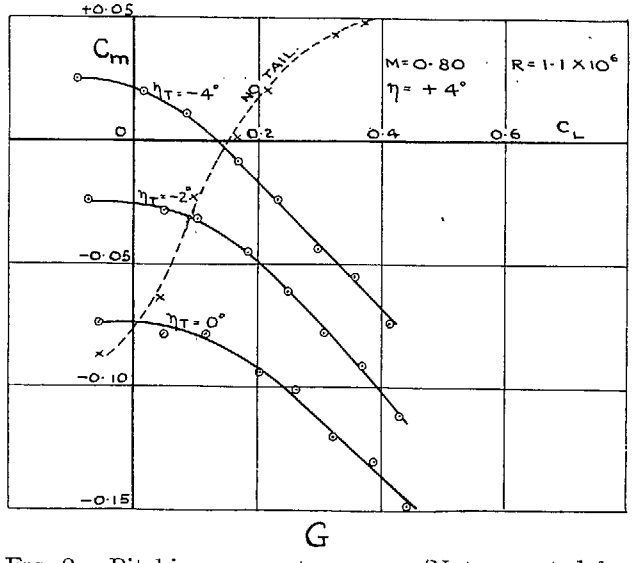

FIG. 8. Pitching-moment curves. (Not corrected for blockage.)

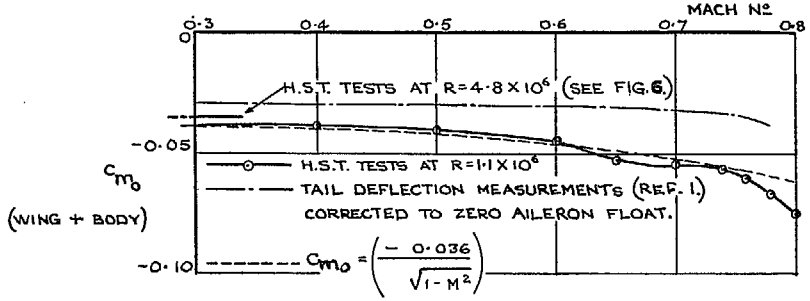

FIG. 9. Pitching moment (no tail) at $C_L = 0$. (Not corrected for blockage.)

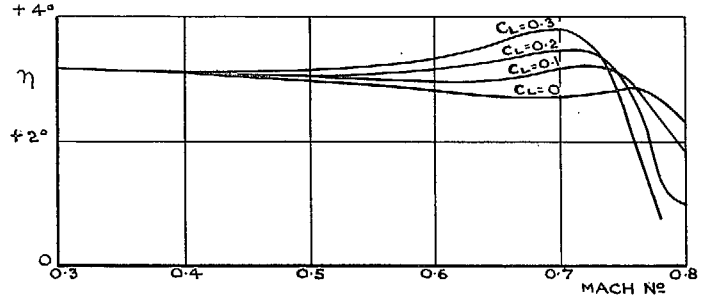

FIG. 10. Elevator angle to trim. (Not corrected for blockage.)

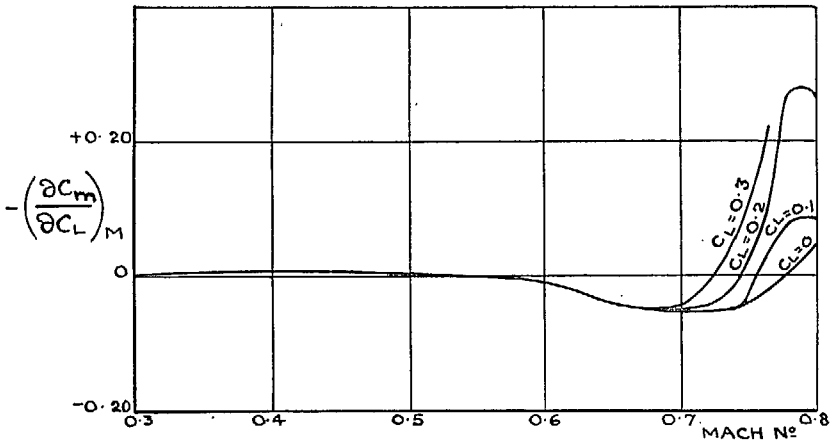

FIG 11. Effect of Mach number on $-\left(\frac{\partial C_m}{\partial C_L}\right)_M$ (Not corrected for blockage.)

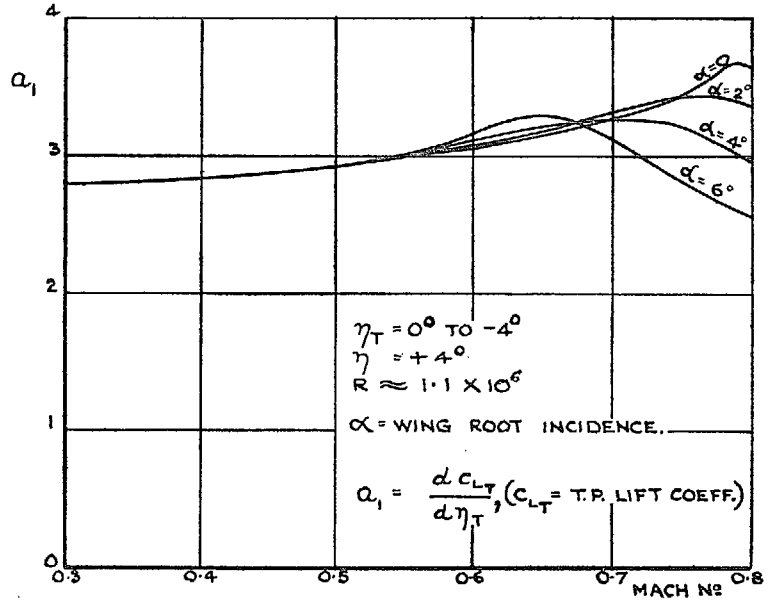

FIG. 12. Tailplane lift-curve slope. (Not corrected for blockage.)

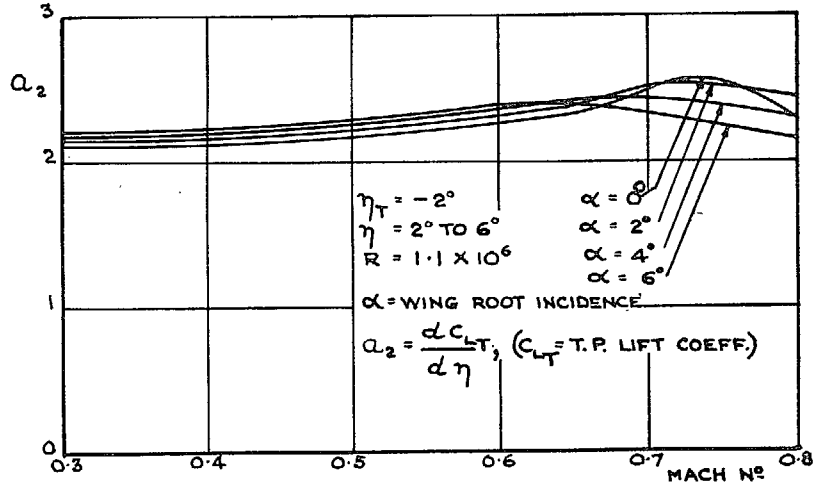

FIG. 13. Tailplane lift due to elevator. (Not corrected for blockage.)

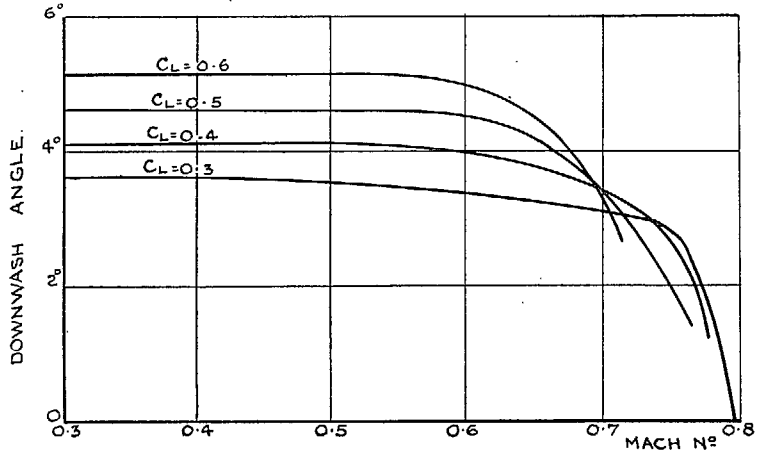

FIG. 14. Downwash angle at tail. (Not corrected for blockage.)

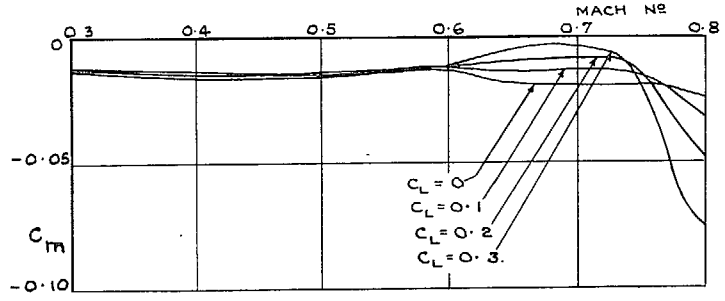

FIG. 15. Pitching moment with tail ($\eta_T = -2$ deg, $\eta = +4$ deg). (Not corrected for blockage.)

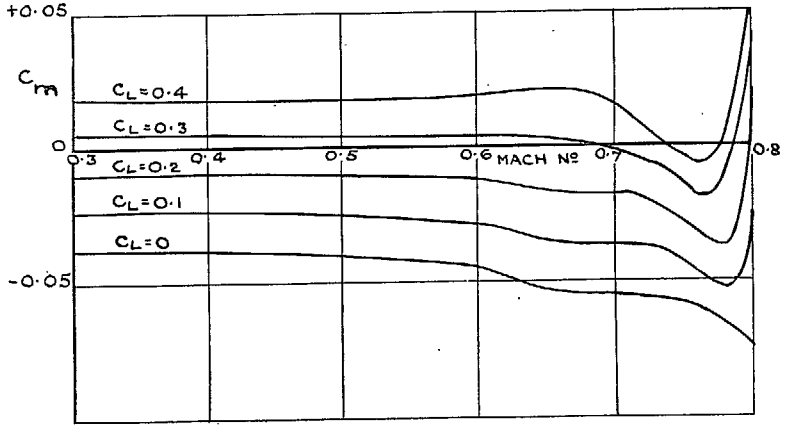

FIG. 16. Pitching moments without tail. (Not corrected for blockage.)

PART II

Tests on the Spiteful (F.1/43)

By

W. A. MAIR, M.A., S. P. HUTTON, B.Eng. and H. E. GAMBLE, B.Sc.

1. *Introduction.*—The Spiteful (F.1/43) is a single-engine fighter with fuselage and tail unit similar to the Spitfire. The wing has been designed for low drag and has a cusped trailing edge. The inboard sections of the wing were designed to have a high critical Mach number, and the outboard sections to maintain extensive laminar boundary layers. The mean wing thickness is slightly greater than that of the Spitfire.

High-speed wind-tunnel tests were required to supplement the earlier low-speed tests[1, 2] and for comparison with the high-speed tests on the Spitfire I (Part I). High Reynolds-number tests were also required, to determine the scale effect on maximum lift and longitudinal stability at low speeds.

Pressure measurements on the front radiator flaps at high speeds were required, for the estimation of loads in the flap operating mechanism, and for the determination of critical Mach number.

2. *Description of Model.*—Particulars of the 1/5·75 scale model are given in Table 1 and in Fig. 1. The wing and fuselage were made of hardwood and the radiators were made from brass castings with steel flaps and baffle plates. The wing sections at root and tip are shown in Fig. 2. Fig. 3 shows a typical section of the tailplane and elevator, this being the same as on the Spitfire. Fig. 4 shows a typical section of the radiator duct, and in Fig. 5 a section of the front radiator flap is given, indicating the positions of the static holes used for the pressure measurements. The baffle constant* was 0·50 for both radiators. The cabin was one with a curved front fairing, described as cabin A in Part III. In all tests with the fuselage the cabin and fin were fitted, and the engine air intake was represented by a faired shape. Ailerons, rudder and engine exhaust pipes were not represented.

For the tests with landing flaps down the rear radiator flaps were opened 87·5 deg to form part of the landing flap system (*see* Table 1). For all other tests with the radiators fitted the rear flaps were in the shut position, and except where otherwise stated the front radiator flaps were also in the shut position (Fig. 4). For the tests without radiators the ducts in the wing were filled with wood blocks.

3. *Correction of Pressure Measurements.*—The diameter of the pressure holes in the front radiator flap was about 0·05 in, and a correction has been applied for this rather large hole diameter. Measurements by Thom[3], confirmed by Linke[4], have shown that on a circular cylinder the measured pressure can be assumed to act at a point that is displaced from the centre of the hole by one-quarter of the hole diameter towards the front of the cylinder. This rule was established by Thom only for a circular cylinder upstream of the minimum pressure, and thus the displacement towards the front of the cylinder was upstream and towards the high-pressure side of the hole. In forming a rule for general application, it is not known whether the displacement should be upstream or towards the high-pressure side. The measured pressure distributions on the front radiator flap have been corrected for size of hole by displacing the measured pressure towards the high-pressure side by one quarter of the hole diameter. However, the correction is unimportant except on the part of the flap where the high-pressure side is also the upstream side, this being the region of steep pressure gradients. Thus the uncertainty of the direction of the displacement in a region of rising pressure has no appreciable effect on the pressure distribution.

* The baffle constant is defined as (drop of total head across baffle)/$\frac{1}{2}\rho V^2$, where V is the velocity in the duct immediately in front of the baffle.

4. *Results.*—Where results of tests on the Spitfire are given in this part of the report for comparison, the blockage corrections given in the Introduction have been applied. Thus these results are not exactly the same as those given in Part I, but they are directly comparable with the results of the tests on the Spiteful.

4.1. *Lift.*—The increase of lift gradient of the wing with Mach number (Fig. 12) is greater than that given by linear theory for finite aspect ratio[5]. The increase of lift gradient of the wing and body is rather less than that of the wing, and follows the theoretical curve fairly closely up to about $M = 0{\cdot}7$. At higher Mach numbers the lift gradient falls fairly rapidly.

The effect of Mach number on maximum lift coefficient is fairly small up to $M = 0{\cdot}7$ (Fig. 6). However, in considering the maximum lift at high Mach numbers it should be noted that the Reynolds number of the tests was only $1{\cdot}15 \times 10^6$. The scale effect on maximum lift at low speed has been measured and is discussed below, but the effect at higher Mach numbers is not known.

Figs. 9, 10 and 11 show that there is considerable scale effect on maximum lift coefficient at low Mach numbers, especially between Reynolds numbers of about $1{\cdot}5 \times 10^6$ and $3{\cdot}0 \times 10^6$. The maximum lift coefficient of the wing is about the same as that of the complete model (trimmed) with flaps up. The increment of $C_{L\,\max.}$ due to lowering the landing flaps is about $0{\cdot}40$ at all values of R. The scale effect on lift gradient is small at low incidences but larger at the higher incidences. The values of $C_{L\,\max.}$ found for high Reynolds numbers correspond to stalling speeds of 117 m.p.h. with flaps up and 101 m.p.h. with flaps down, with a wing loading of $41{\cdot}5$ lb/sq ft.

4·2. *Drag.*—For low values of C_L the drag coefficient of the wing does not start to increase appreciably until the Mach number exceeds about $0{\cdot}72$ (Fig. 14). This Mach number agrees with the critical value found theoretically.

The effect of Mach number on the drag of the complete model is more serious than for the wing (Fig. 13). At zero lift there is a considerable increase of drag as the Mach number rises above about $0{\cdot}62$, but this early rise is caused by the radiators (*see* Fig. 19). At higher values of C_L (*e.g.* $C_L = 0{\cdot}2$) the critical speed of the radiators is higher, and the drag of the complete model does not rise appreciably until the Mach number exceeds about $0{\cdot}66$. At this Mach number shock waves at the wing-fuselage fillet would be expected, as shown by low-speed measurements of pressure distribution made at the N.P.L.[6]

Comparisons of the drag of the Spiteful with that of the Spitfire are shown in Figs. 15, 16 and 17. At $C_L = 0{\cdot}1$ the Mach number at which the drag of the wing rises steeply is about the same as for the Spitfire wing, although the critical speed (where the drag first starts to rise) is lower for the Spitfire wing than for the Spiteful. At $C_L = 0{\cdot}3$ the Spiteful wing has a lower drag than that of the Spitfire at all Mach numbers covered by the tests. Comparing the drag of the wing and body, without radiator or tailplane, Fig. 17 shows that the drag increase starts at a higher Mach number on the Spiteful than on the Spitfire, although at very high Mach numbers the Spiteful has the greater drag. However, since the wing area of the Spiteful is less than that of the Spitfire, the increment of drag coefficient due to the same actual fuselage drag would be greater on the Spiteful. The drags of the complete models are compared in Fig. 15. At $C_L = 0{\cdot}1$ the increase of drag between $M = 0{\cdot}60$ and $0{\cdot}65$ is less on the Spiteful than on the Spitfire, but at higher Mach numbers the drag of the Spiteful appears to be consistently greater than that of the Spitfire. At $C_L = 0{\cdot}3$, the Spiteful is considerably better than the Spitfire, except at very high Mach numbers. The two complete models are not really comparable, however, because the Spiteful has a much larger radiator system than the Spitfire I. Thus the improvement in changing from the Spitfire to the Spiteful is probably rather greater than would appear from Fig. 15.

4.3. *Longitudinal Stability and Trim.*—Low-speed wind-tunnel tests[1, 2] have shown that the effect of the propeller on the longitudinal stability of the Spiteful is very large. For example a six-blade contra-rotating propeller at zero thrust moves the neutral point forward by about

$0 \cdot 14\bar{c}$. The high-speed tunnel tests were all made on a model without a propeller, and thus the stability as shown by the results of these tests is considerably greater than it would be with a propeller. The influence of Mach number on the destabilising effect of a propeller is not yet known, but if it is assumed that this effect is independent of Mach number then the changes of stability with Mach number are given correctly by the results of the high-speed tunnel tests.

Fig. 30 shows the variation of $-(\partial C_m/\partial C_L)_M$ with Mach number, for the complete model with tail. These curves show that there is a considerable decrease of manoeuvre margin at the higher lift coefficients between $M = 0 \cdot 6$ and $0 \cdot 7$. This may mean that large normal accelerations can occur very easily in high-speed manoeuvres at high altitudes. The rapid increase of $-(\partial C_m/C_L)_M$ at high Mach numbers is usually found in high-speed tunnel tests on complete models, and shows the large stick movement required for pulling out of a high-speed dive. It is satisfactory, however, that for zero lift this increase does not occur at any Mach number up to $0 \cdot 82$.

Table 2 shows that the scale effect on longitudinal stability at low Mach numbers is fairly small. For the complete model with radiators and tail an increase of Reynolds number from $1 \cdot 5 \times 10^6$ to $4 \cdot 5 \times 10^6$ causes a forward movement of the neutral point of less than $0 \cdot 01\bar{c}$.

For the complete model with tailplane, the change of trim with Mach number is least for $C_L = 0 \cdot 2$ (Fig. 25). At lower values of C_L there is an increasing (positive) pitching moment with rising Mach number, and at higher values of C_L there is a decreasing pitching moment with rising Mach number. For values of C_L between 0 and $0 \cdot 35$, the change of trim between $M = 0$ and $M = 0 \cdot 82$ is equivalent to less than 1 deg of elevator movement (Fig. 26).

Fig. 34 shows that there is a very large increase in the numerical value of C_{m0}, as M is increased from $0 \cdot 3$ to $0 \cdot 8$. The variations with Mach number of C_{m0} for the wing and for the wing and body without radiators are similar to the effects found on other models, but the effect of the radiators is unusual.

The effect of Mach number on the downwash angle at the tail (Fig. 35) is very different from the effect on the Spitfire (Fig. 14 of Part I). On the Spitfire the downwash at a given value of C_L falls severely as the Mach number increases above about $0 \cdot 7$ or $0 \cdot 75$. On the Spiteful the downwash angle at a given value of C_L is nearly independent of Mach number up to $M = 0 \cdot 8$ This difference may be explained by the wash-out and greater thickness taper of the Spitfire wing, which tend to make the root sections shock-stall before the outer sections. The Spiteful wing has no wash-out and a more uniform thickness distribution.

Figs. 31 and 32 show that the tailplane and elevator both remain fully effective at all Mach numbers up to about $0 \cdot 82$. These curves are similar to those given in Part I for the Spitfire I, the tailplane and elevator being identical on the two aircraft.

4.4. *Radiators.*—The pressure distributions on the front radiator flap are shown in Figs. 39 to 47. The peak suction coefficients are rather high, and further tests are being made in a low-speed wind tunnel to investigate the pressure distributions for different combinations of front and rear flap settings These tests have shown that the suction coefficients near the middle of the flap are slightly higher than those at the pressure holes used in the high-speed tunnel tests, so that the values given in this report for the critical speeds may be a little too high.

As the Mach number increases above about $0 \cdot 7$ the pressure distribution curves change their form, possibly because of a separation of flow near the leading edge of the front radiator flap. At about the same Mach number the increment of C_L due to the radiators starts to increase suddenly (Fig. 18). The change of sign of the radiator lift increment explains the large change in the increment of C_{m0} due to the radiators, shown in Fig. 34. At low speeds the negative radiator lift increases the no-lift angle of the wing and so reduces C_{m0} numerically. At high speeds this effect becomes reversed, giving a high numerical value of C_{m0}.

The observed peak suction coefficients for the radiator front flap are shown in Fig. 48 plotted against Mach number. The curve marked ' critical ' on the same diagram is derived from the theoretical relationship for isentropic flow, and shows the value of C_p giving a local velocity equal

to the local speed of sound. From the critical Mach number with front and rear flaps shut the critical speeds in level flight have been calculated, assuming a wing loading of 41·5 lb/sq ft (Fig. 49). At 35,000 ft the critical speed is only about 430 m.p.h., which is below the probable top speed at that height. However, with both radiator flaps shut the increase of radiator drag with Mach number is fairly small for level flight conditions (Fig. 19). With the front flap open the radiator critical speed is lower and the increase of drag with Mach number is more serious (Figs. 20 and 21).

Comparison of Figs. 25 and 29 shows that the radiators do not have any large effect on the general form of the pitching-moment curves, but the curves of Fig. 25 are spaced more widely, indicating an increase of stability due to the radiators. Table 2 shows that, at low Mach number and low C_L, this effect on stability disappears at high Reynolds number. At high C_L the radiators increase stability at all Reynolds numbers.

Coefficients of normal force and hinge moment have been calculated for the radiator front flap, assuming free-stream stagnation pressure inside the radiator duct (Fig. 50). This assumption is not accurate, but is sufficient to show the general form of the variation of the coefficients with Mach number.

Fig. 50 shows that the variation of hinge-moment coefficient with Mach number is fairly small, the maximum increase due to compressibility effects being only about 10 per cent of the low-speed value.

5. *Conclusions.*—The Mach number at which the drag coefficient starts to rise is higher for the Spiteful than for the Spitfire. However, in changing from the Spitfire to the Spiteful only a small improvement of performance would be expected from the suppression of compressibility effects, because the increase of drag of the Spitfire with Mach number is at first very gradual. At very high Mach numbers and low values of C_L the drag coefficient of the Spiteful is greater than that of the Spitfire, this being probably due to the greater mean wing thickness of the former aircraft.

At Mach numbers up to 0·82 there are no large changes of trim at low values of C_L, and elevator control is satisfactory. There is the usual increase of stability in dives at very high Mach numbers, except near zero lift, where there is very little change of stability in the dive.

For all Mach numbers up to 0·70 the static margin of the model without propeller is about $0 \cdot 10\bar{c}$. As shown in Refs. 1 and 2 this margin would be greatly reduced by the addition of a propeller.

At $R = 4 \times 10^6$ and low Mach number, $C_{L\,\max.}$ (trimmed) is 1·16 with flaps up and 1·58 with flaps down. The corresponding stalling speeds are 117 and 101 m.p.h., assuming a wing loading of 41·5 lb/sq ft.

REFERENCES

No.	*Author*	*Title, etc.*
1	Warren and Kirk	Wind Tunnel Tests with Propeller on the Supermarine F.1/43. R.A.E. Report No. Aero 1860. (October, 1943.)
2	Warren and Becker	Wind Tunnel Tests on the Supermarine F.1/43 with a Five-Bladed Propeller, and at Two Wing Settings. A.R.C. 7395. (November, 1943. (To be published.)
3	Thom	Flow Past Circular Cylinders at Low Speeds. R. & M. 1539. (June, 1932.)
4	Linke	Neue Messungen zur Aerodynamik des Zylinders, insbesondere seines reinen Reibungswiderstandes. *Physik. Zeit.* 32. (1931.)
5	Young	Note on the Effect of Compressibility on the Lift Curve Slope of a Wing of Finite Aspect Ratio. A.R.C. 7046. (August, 1943.)
6	Warden	Pressure Distribution Measurements on the Supermarine F.1/43. (Unpublished.)

TABLE 1

Leading Dimensions, Full Scale

(Model scale = 1/5·75)

Wing:	
Gross area	209 sq ft
Span	35·0 ft
Standard mean chord	5·98 ft
Aspect ratio	5·85
Chord at theoretical centre-line	8·33 ft
Chord at change in taper	7·08 ft
Chord at 6 in from tip	3·33 ft
Maximum thickness at theoretical centre line	13·0% at 40% chord from leading edge
Maximum thickness at change in taper	13·0% at 40% chord from leading edge
Maximum thickness at 6 in from tip	8·4% at 50% chord from leading edge
Camber (constant along span)	0·93% at 50% chord from leading edge
Dihedral angle	3 deg
Geometric twist	0
Angle to fuselage datum*	1·5 deg
Line of no sweepback	39% chord
Sweepback of quarter-chord line (inboard)	1·67 deg
Sweepback of quarter-chord line (outboard)	2·74 deg
Distance of mean quarter-chord point behind leading edge at theoretical centre-line	2·36 ft
Distance of mean quarter-chord point above chord at theoretical centre-line	0·40 ft
Tailplane:	
Gross area	33·75 sq ft
Span	10·5 ft
Mean chord	3·21 ft
Arm	18·9 ft
Volume coefficient	0·510
Normal setting (to wing chord)	−1·5 deg
Height of mean quarter-chord point above wing chord at theoretical centre-line	3·65 ft
Maximum thickness	10% at 30% chord from leading edge
Elevator area behind hinge	12·21 sq ft
C.G. position:	
Behind leading edge at theoretical centre-line	2·68 ft
Behind leading edge at change in taper	2·19 ft
Behind leading edge mean chord	0·304$\bar{c}$
Above chord at theoretical centre-line	1·18 ft
Above chord at change in taper	0·86 ft
Below fuselage datum	0·79 ft
Above mean chord	0·131$\bar{c}$

* 1·5 deg is the correct full-scale wing setting. The model wing setting was 0·2 deg too high.

TABLE 1 (*contd.*)

Landing flaps:

Rear radiator flaps:

Chord	1·38 ft
Total span	8·10 ft
Maximum deflection (from shut position)	87·5 deg

Outer landing flaps:

Mean chord	1·48 ft
Total span	5·66 ft
Maximum deflection	70 deg

Total flap area .. .. 19·55 sq ft

TABLE 2

Scale Effect on Longitudinal Stability at Low Speeds ($M < 0{\cdot}2$)

$R \times 10^{-6}$		1·5	2·8	4·5
Condition of model	C_L	Values of h_n		
Wing only	0·2	0·231	0·231	0·233
Wing only	0·7	0·198	0·211	0·211
Wing + body. No radiators or tail	0·2	0·209	0·206	0·210
Wing + body. No radiators or tail	0·7	0·172	0·182	0·188
Wing + body + tail. No radiators	0·2	0·377	0·390	0·390
Wing + body + tail. No radiators	0·7	0·377	0·366	0·360
Wing + body + radiators. No tail	0·2	0·202	0·208	0·208
Wing + body + radiators. No tail	0·7	0·172	0·181	0·184
Complete with tail. Landing flaps up	0·2	0·395	0·390	0·387
Complete with tail. Landing flaps up	0·7	0·391	0·390	0·390
Complete with tail. Landing flaps down	1·0	0·380	0·383	0·387*

In the above Table, h_n is defined as :— $h_n = \dfrac{\textit{distance of neutral point behind leading edge mean chord}}{\textit{mean chord}}$

* at $R = 4{\cdot}0 \times 10^6$.

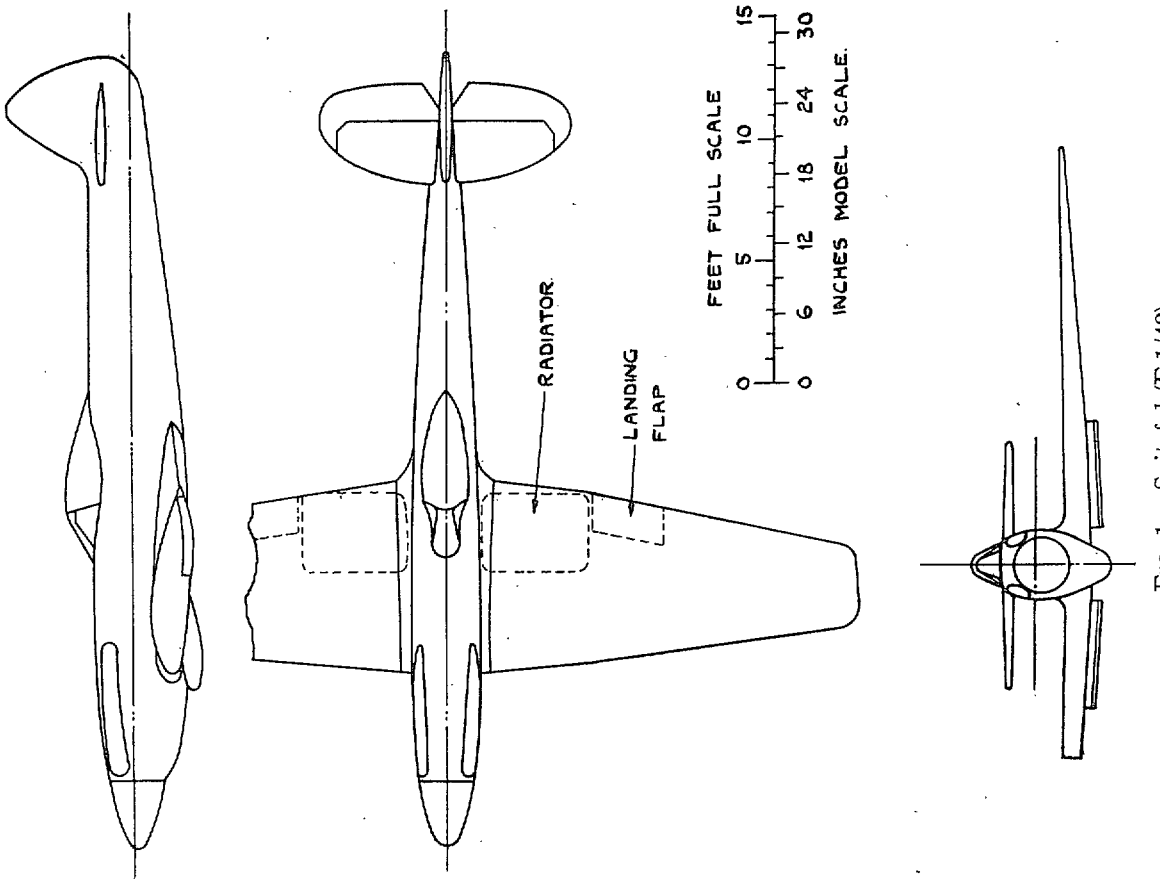

FIG. 1. Spiteful (F.1/43).

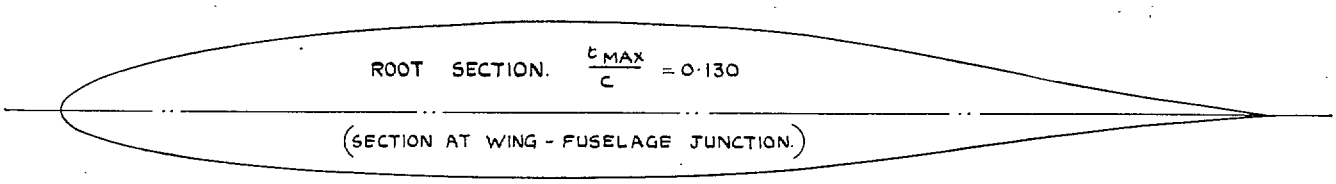

x/c	·005	·010	·025	·050	·075	·100	·15	·20	·25	·30	·35	·40	·45	·50	·55	·60	·65	·70	·75	·80	·85	·90	·95
y_u/c	·0105	·0149	·0238	·0337	·0410	·0468	·0559	·0625	·0674	·0709	·0730	·0741	·0740	·0728	·0703	·0657	·0589	·0507	·0417	·0323	·0230	·0142	·0069
y_l/c	·0097	·0135	·0207	·0284	·0349	·0380	·0444	·0490	·0522	·0543	·0556	·0559	·0555	·0542	·0519	·0484	·0431	·0368	·0299	·0229	·0161	·0098	·0044

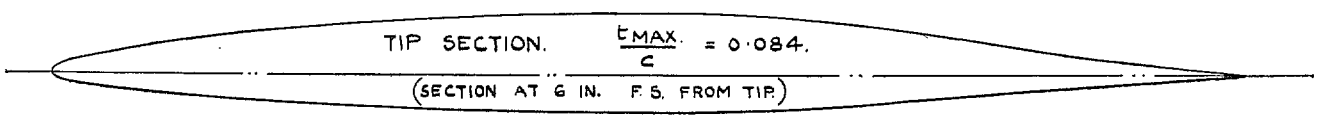

x/c	·005	·010	·025	·050	·075	·100	·15	·20	·25	·30	·35	·40	·45	·50	·55	·60	·65	·70	·75	·80	·85	·90	·95
y_u/c	·0055	·0079	·0127	·0185	·0230	·0269	·0331	·0382	·0424	·0456	·0482	·0500	·0510	·0511	·0501	·0476	·0430	·0372	·0305	·0236	·0168	·0101	·0044
y_l/c	·0046	·0064	·0098	·0134	·0160	·0183	·0218	·0248	·0271	·0291	·0306	·0318	·0324	·0325	·0319	·0304	·0273	·0232	·0196	·0142	·0099	·0058	·0024

FIG. 2. Wing sections.

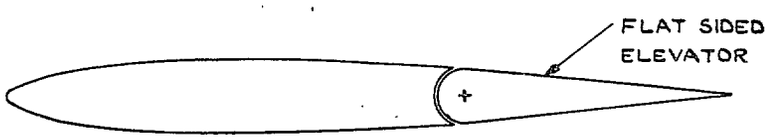

x/c	·0125	·025	·05	·075	·10	·15	·20	·30	·40	·50	·60	·70
y/c	·014	·019	·028	·033	·037	·042	·047	·049	·047	·045	·038	·030

FIG. 3. Typical section of tailplane and elevator (21 in from centre line, full scale).

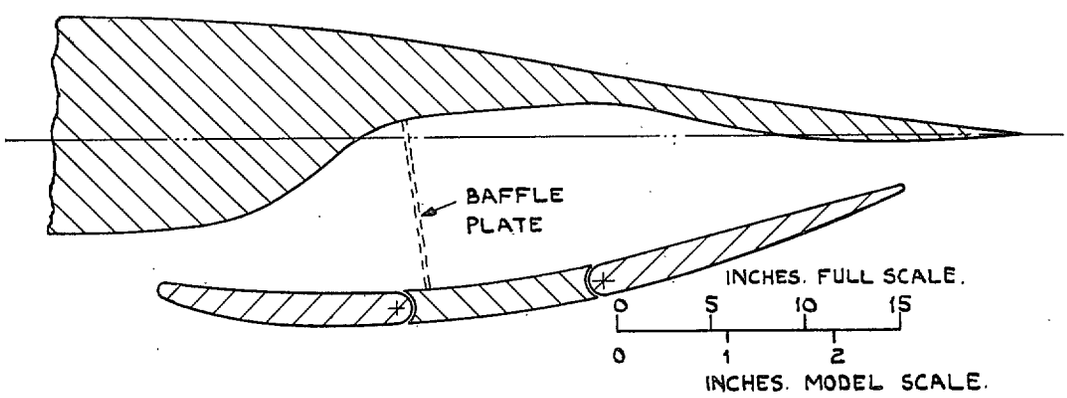

FIG. 4. Section of radiator duct half-way along radiator (flaps shown in shut position).

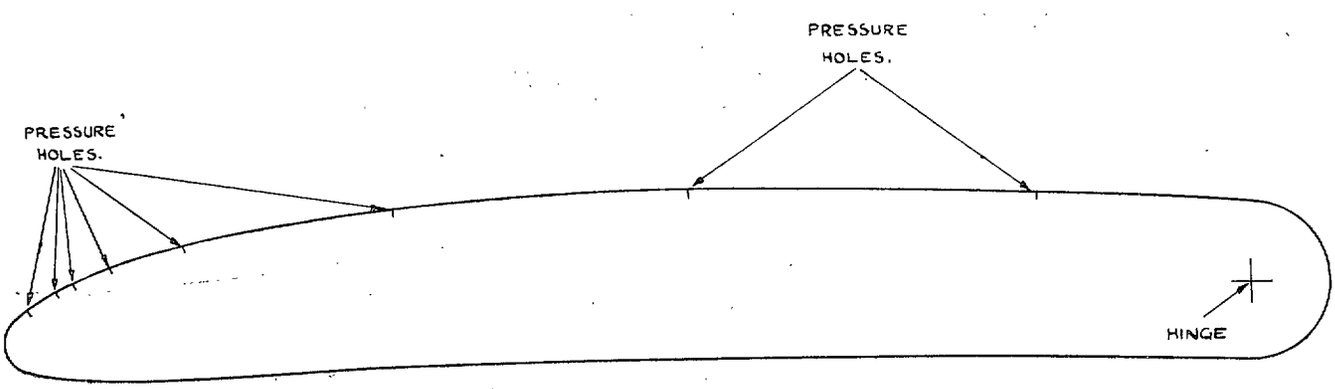

FIG. 5. Section of front radiator flap, showing positions of pressure holes.

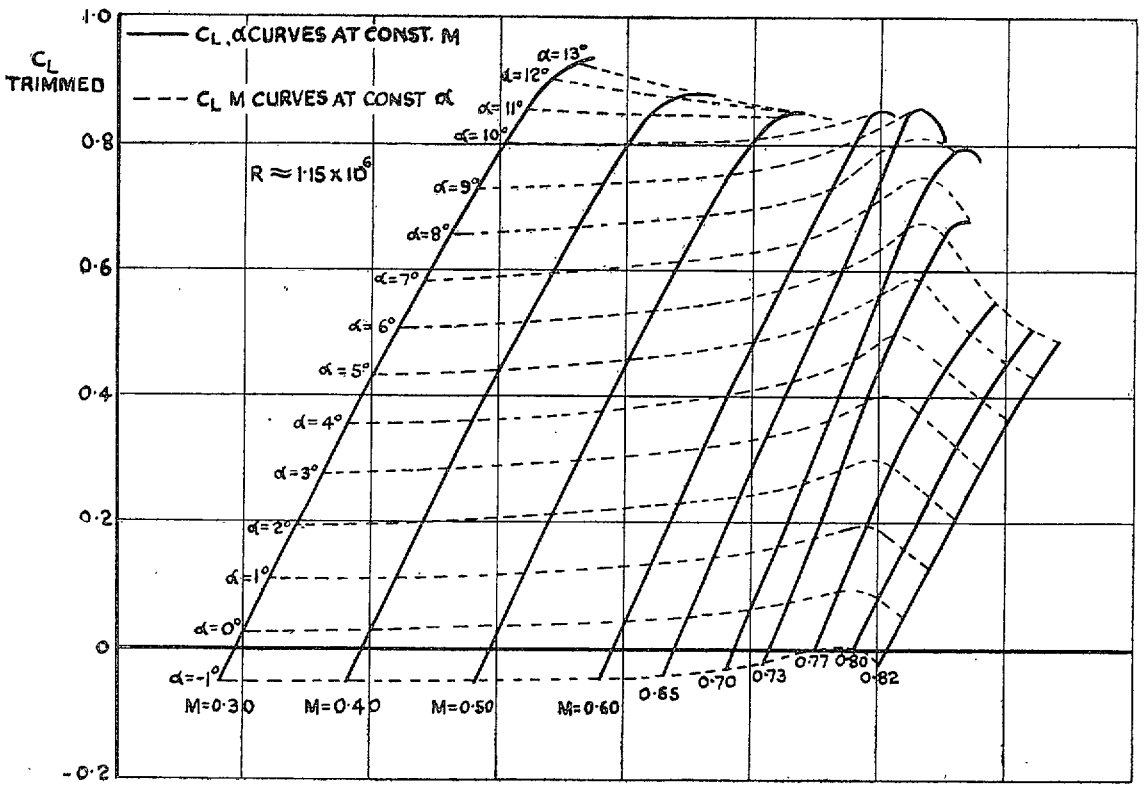

FIG. 6. Lift carpet—complete model.

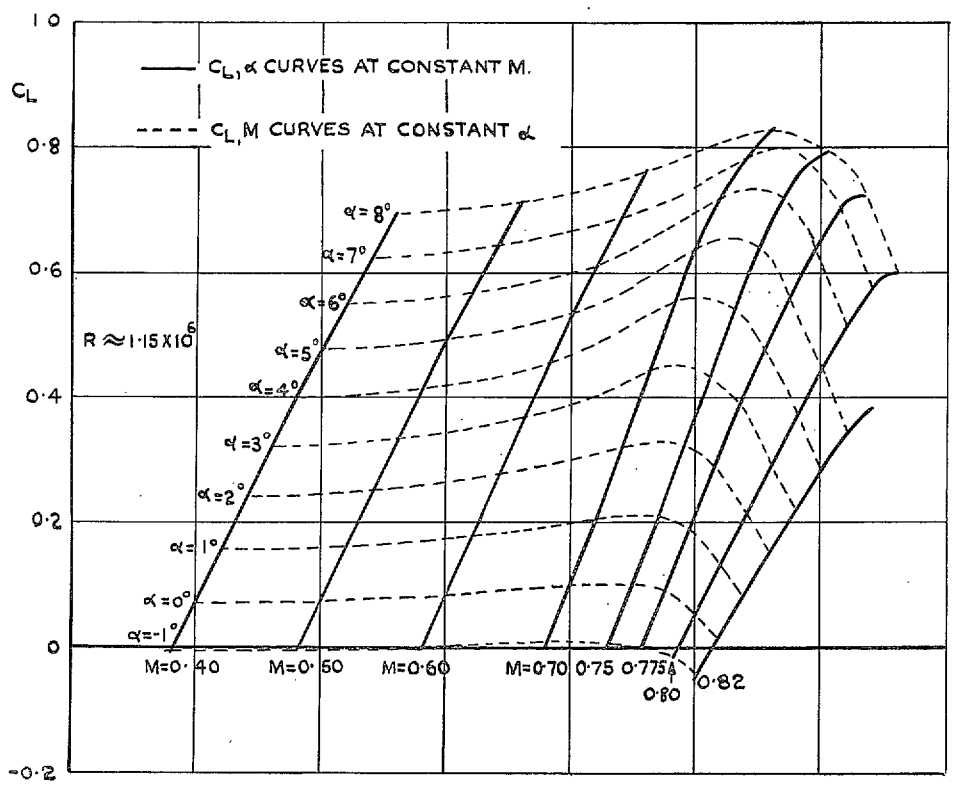

FIG. 7. Lift carpet—wing only.

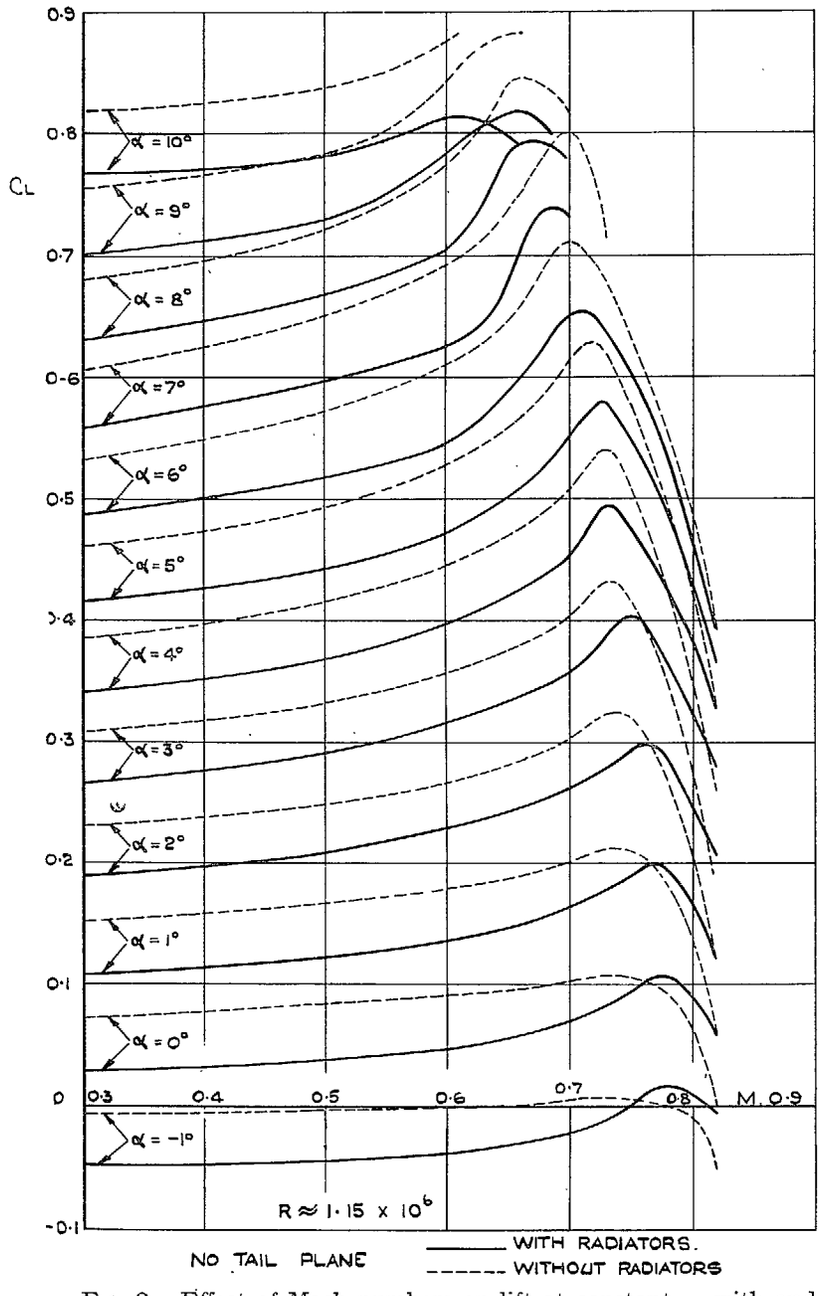

FIG. 8. Effect of Mach numbers on lift at constant α, with and without radiators.

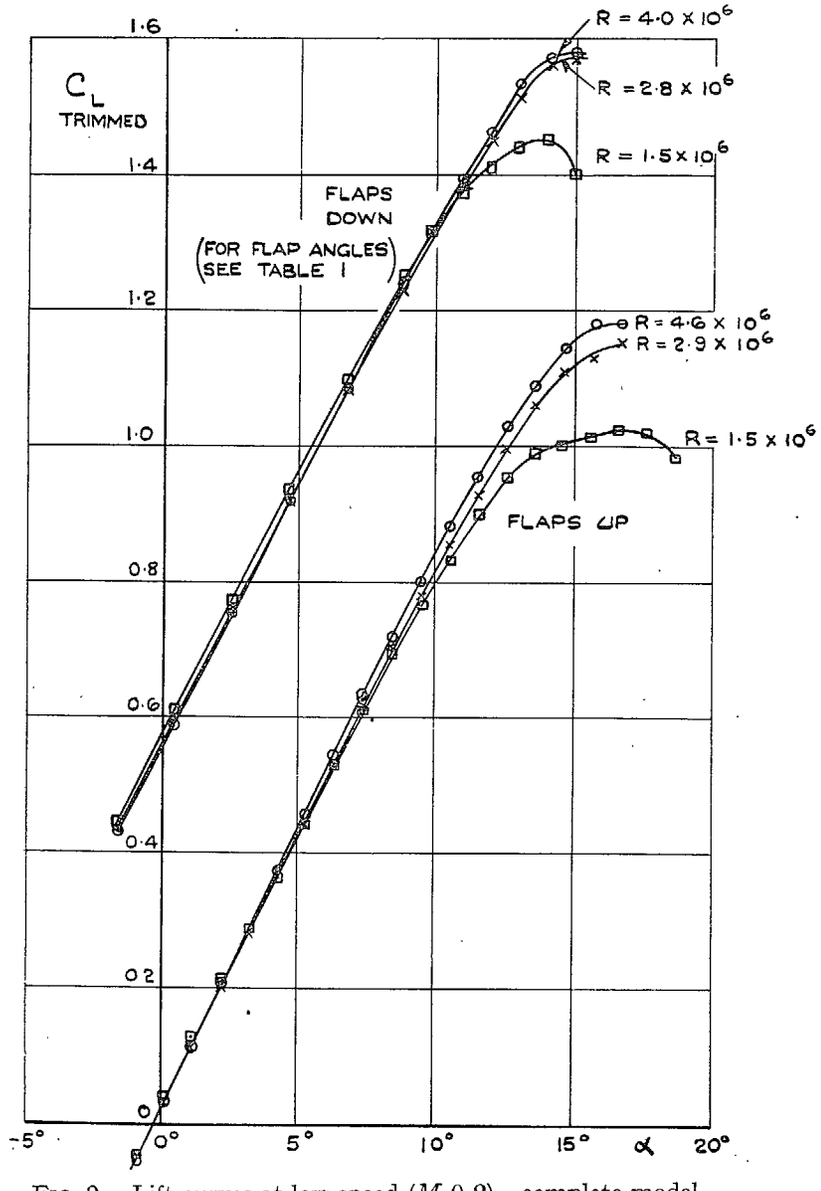

FIG. 9. Lift curves at low speed (M_o0·2)—complete model.

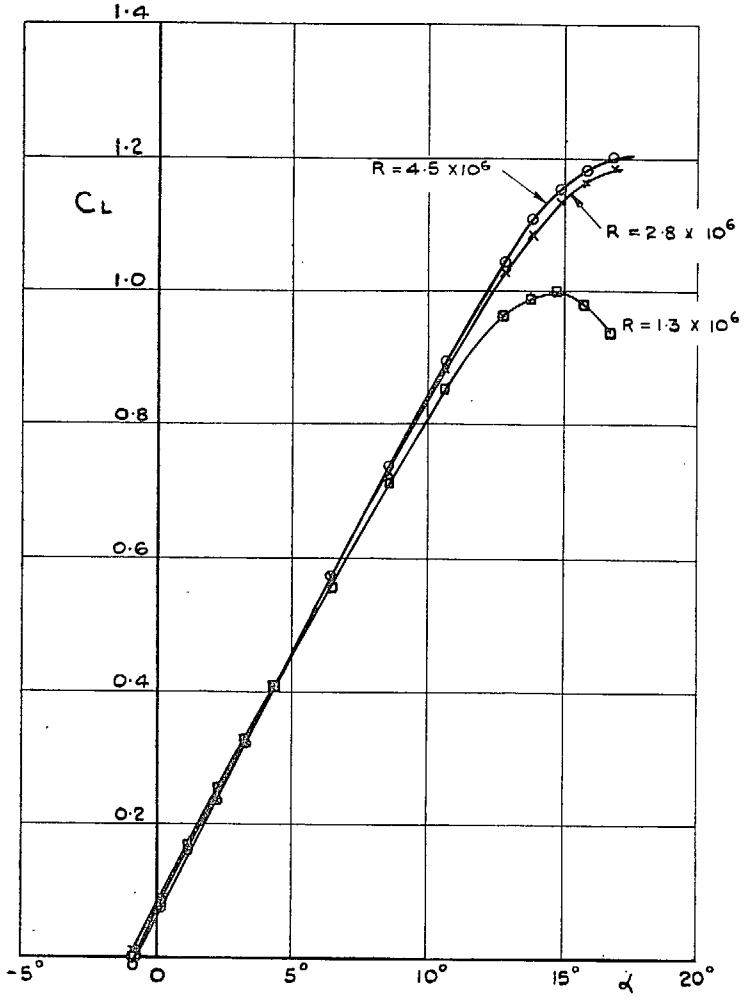

FIG. 10. Lift curves at low speed ($M < 0{\cdot}2$)—wing only.

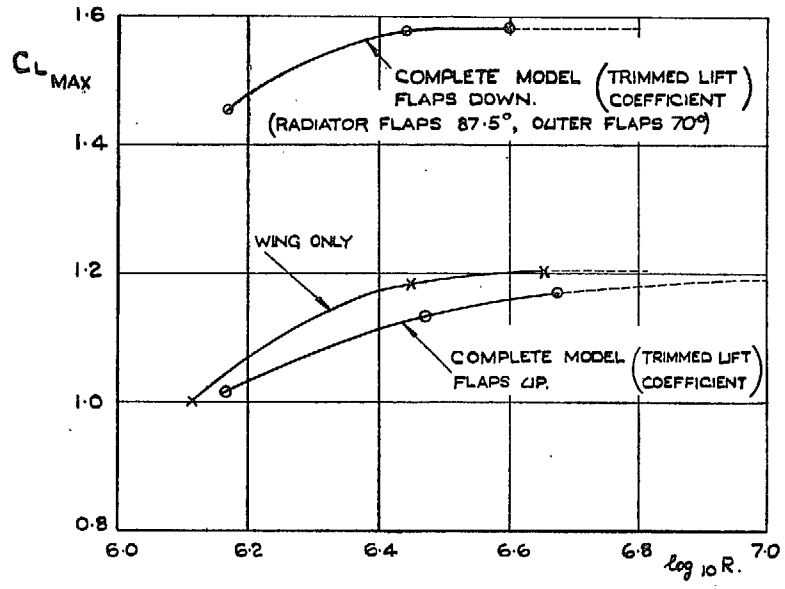

FIG. 11. Effect of Reynolds number on maximum lift. ($M < 0{\cdot}2$)

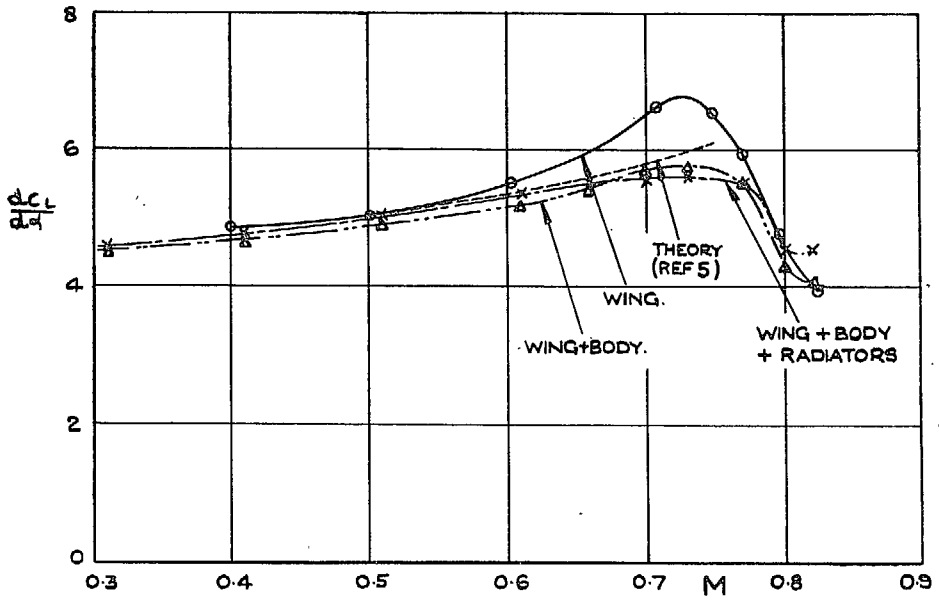

FIG. 12. Effect of Mach number on lift gradient. $R = 1{\cdot}15 \times 10^6$. $C_L = 0{\cdot}2$

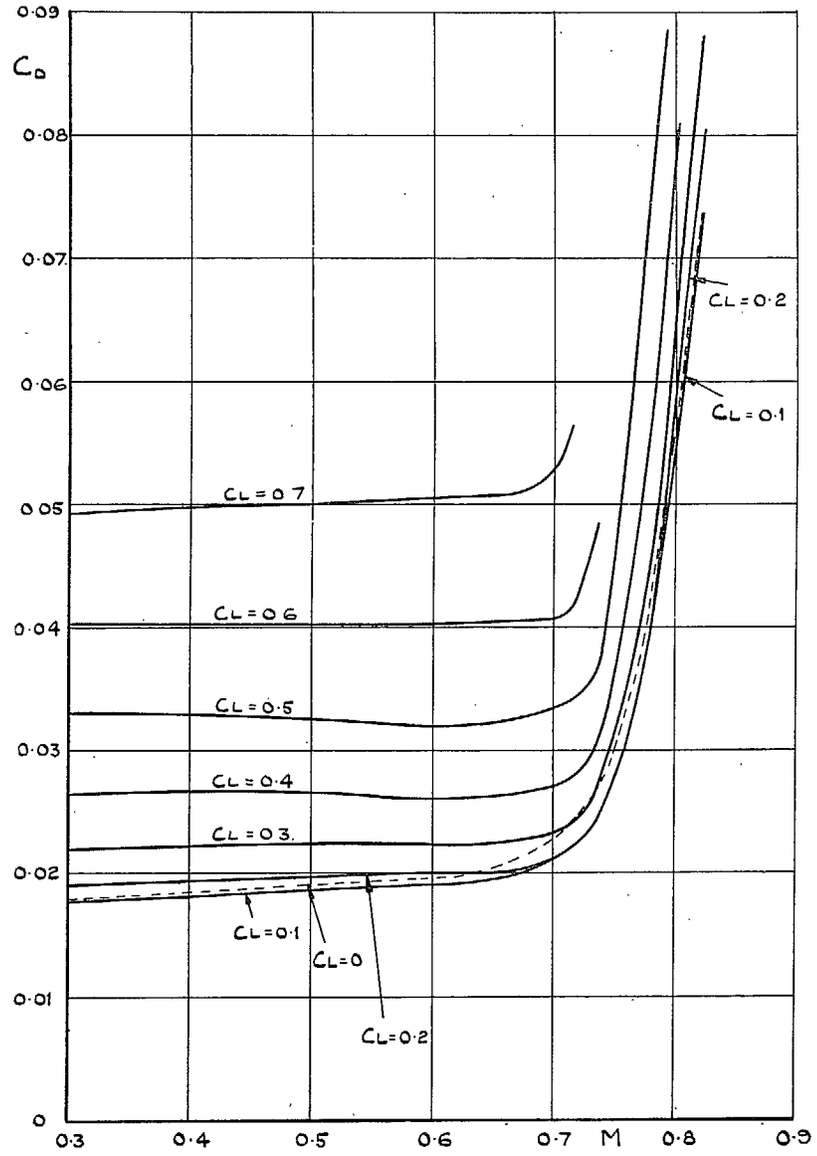

FIG. 13. Effect of Mach number on drag at constant C_L — complete model. $R = 1{\cdot}15 \times 10^6$.

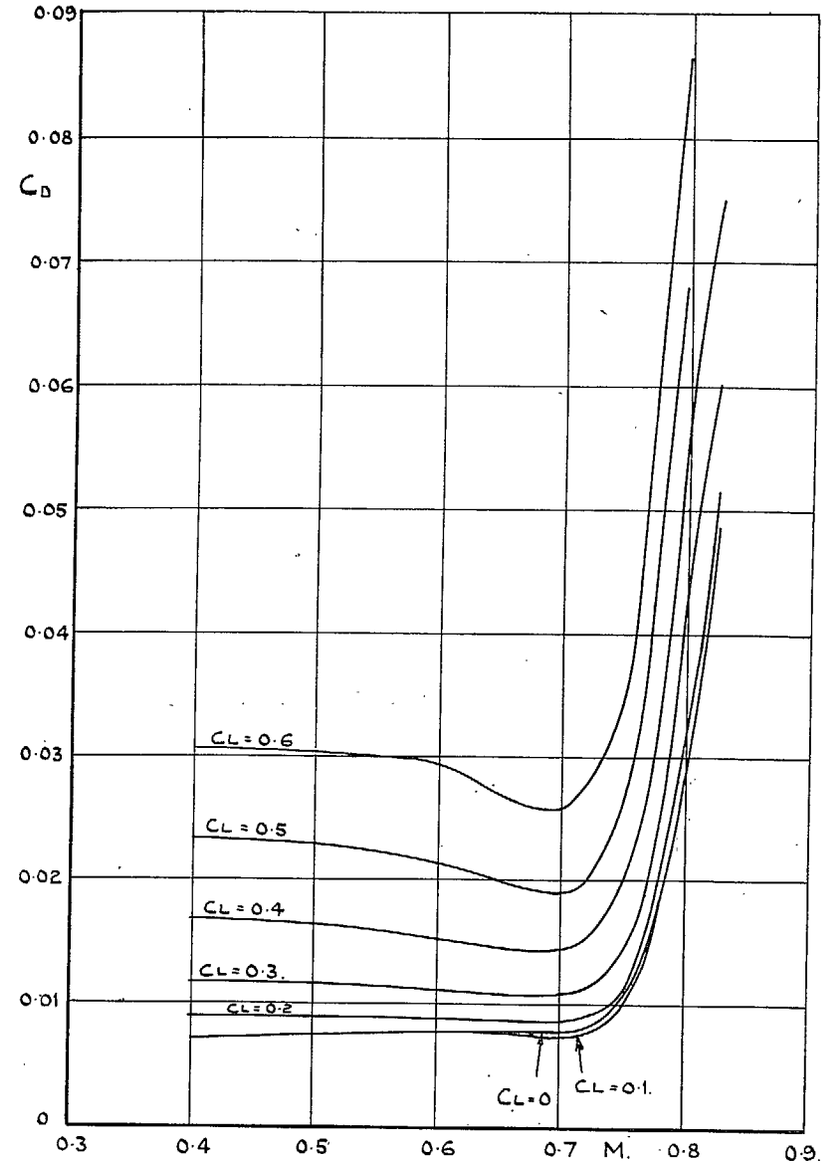

FIG. 14. Effect of Mach number on drag of wing at constant lift coefficient. $R = 1{\cdot}15 \times 10^6$.

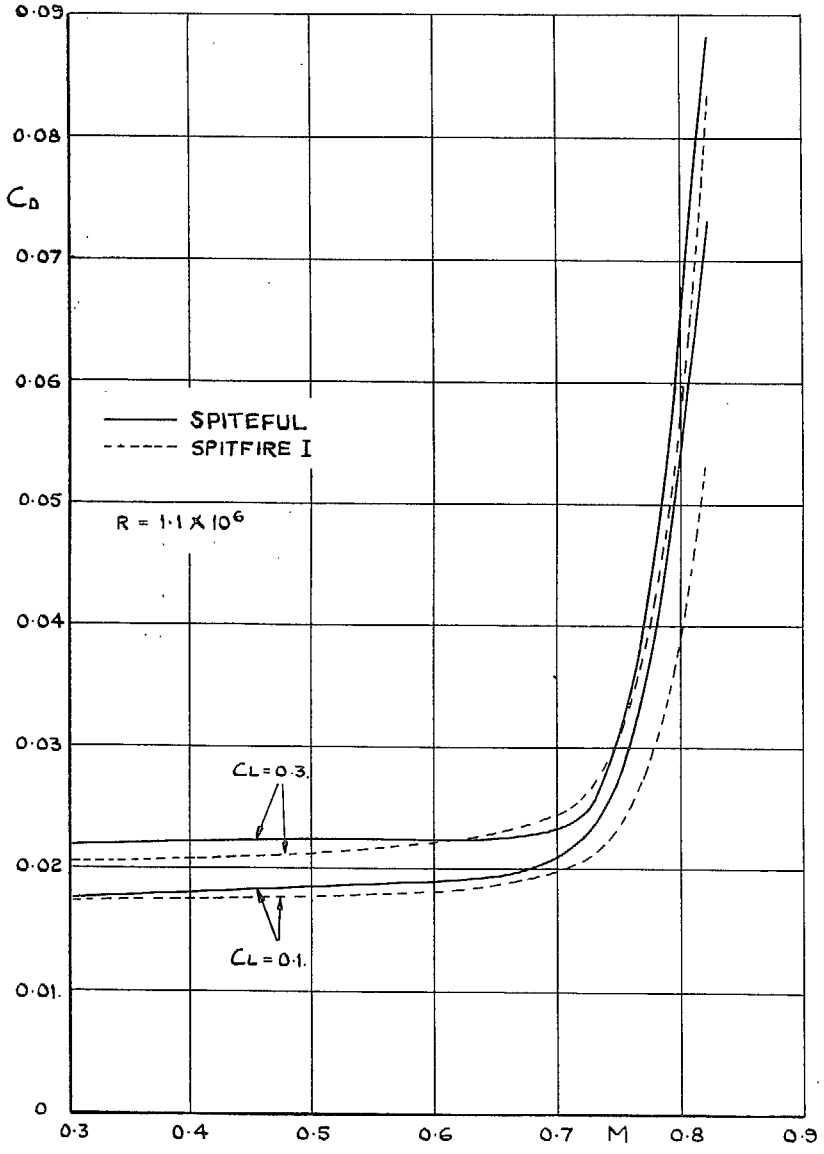

FIG. 15. Effect of Mach number on drag of complete model, comparison with Spitfire I.

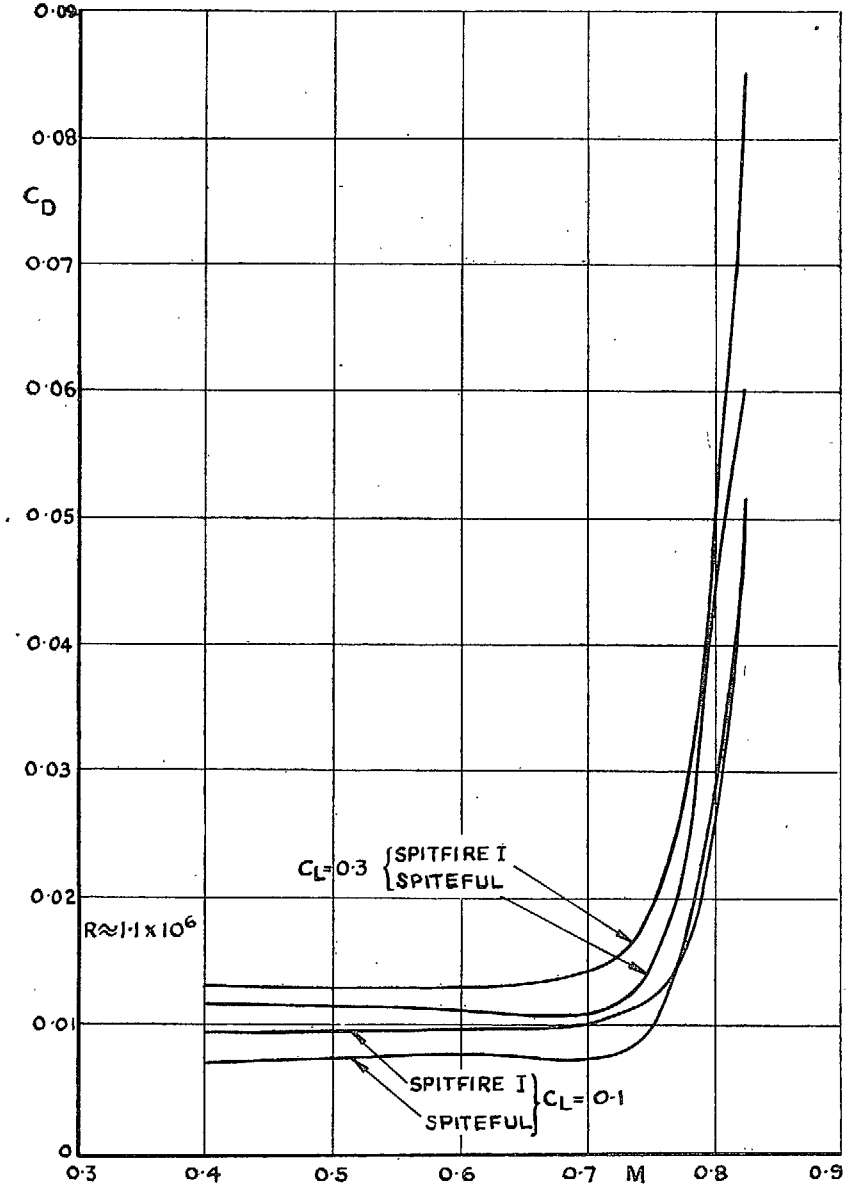

FIG. 16. Effect of Mach number on drag of wing, comparison with Spitfire I.

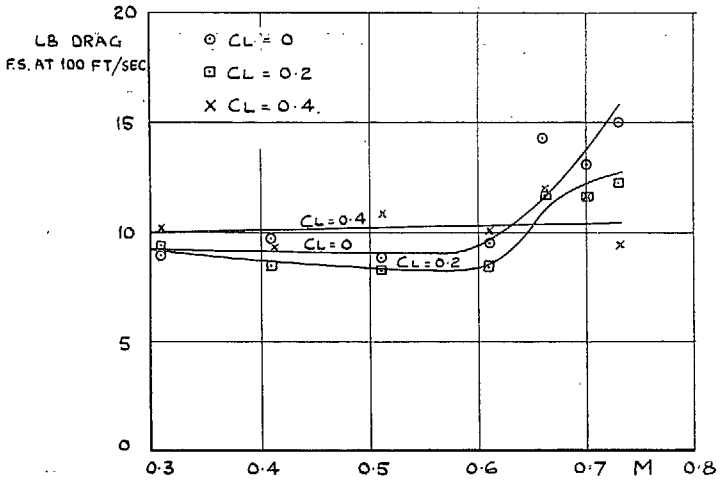

FIG. 20. Drag of radiators, rear flaps shut, front flaps 2 deg open.

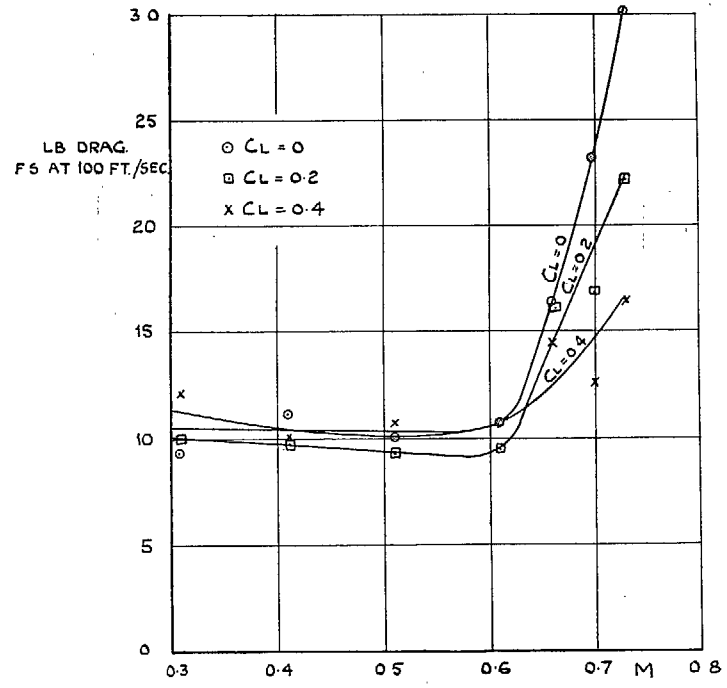

FIG. 21. Drag of radiators, rear flaps shut, front flaps 5 deg open.

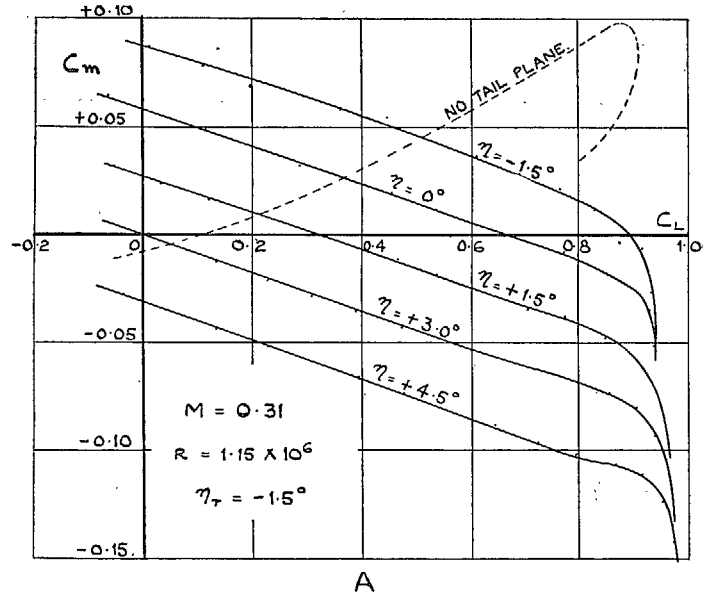

A

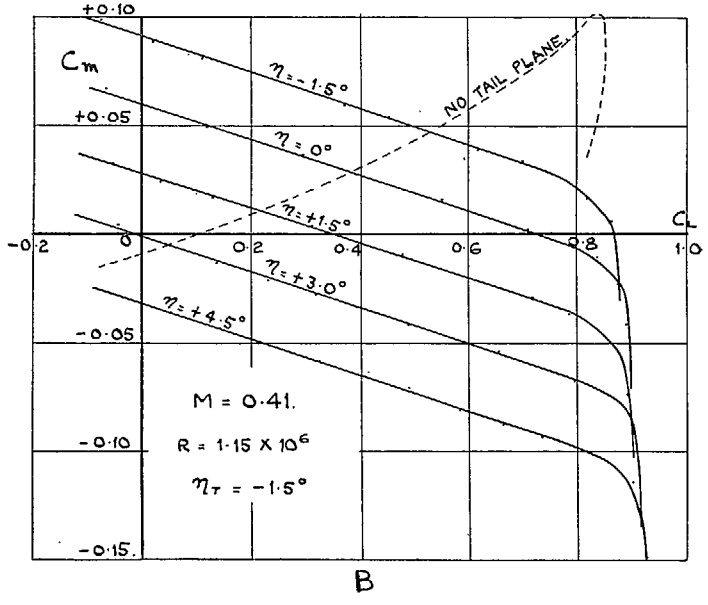

B

FIG. 22. Pitching moment curves (constant tailplane setting).

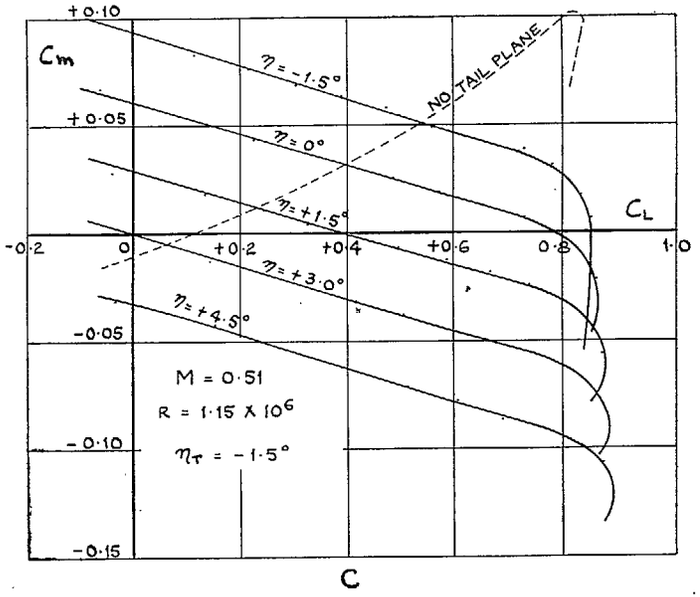

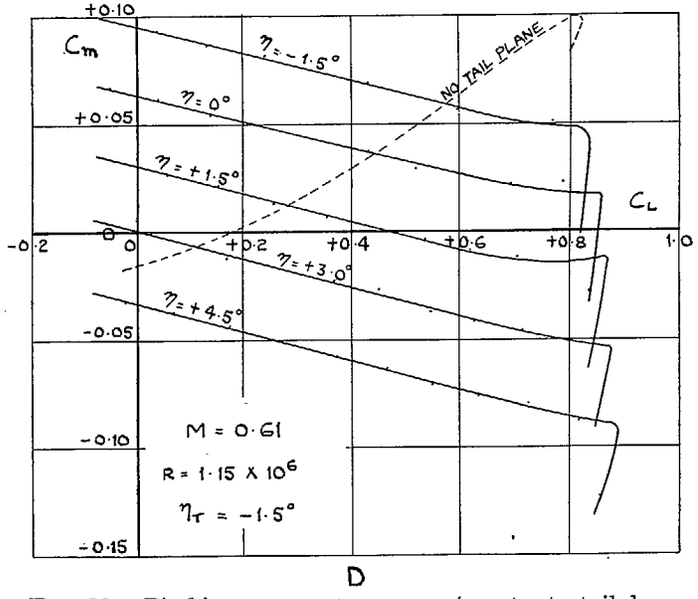

FIG. 22. Pitching moment curves (constant tailplane setting).

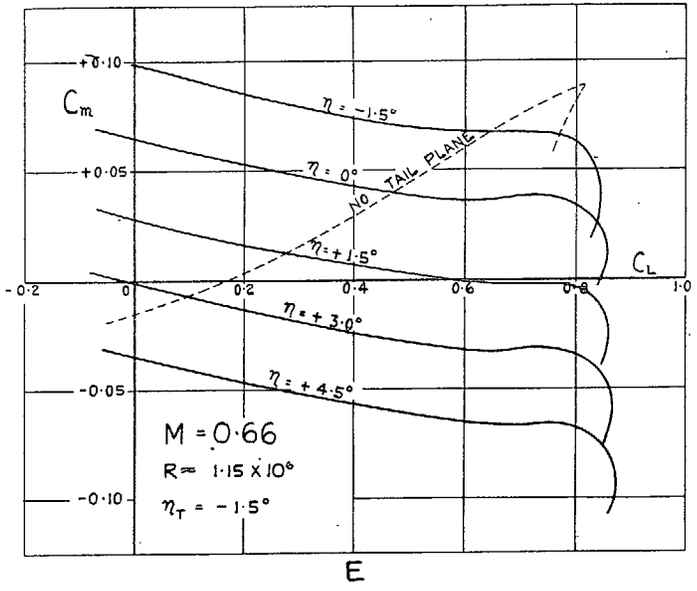

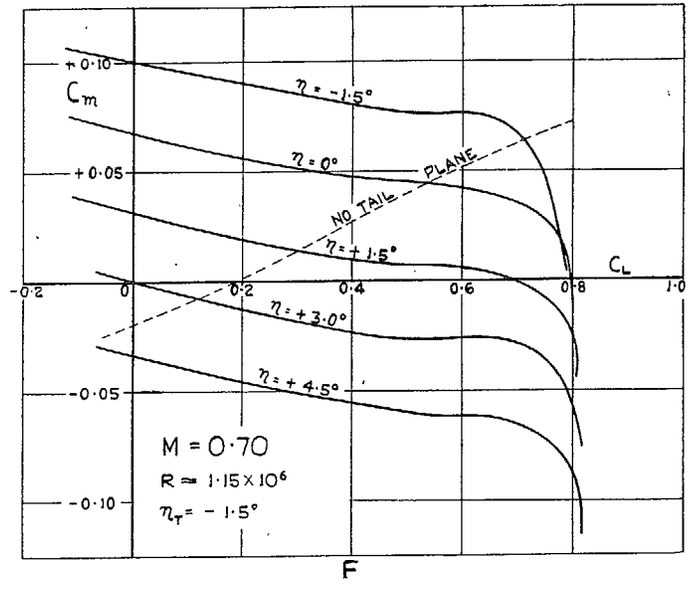

FIG. 22. Pitching moment curves (constant tailplane setting).

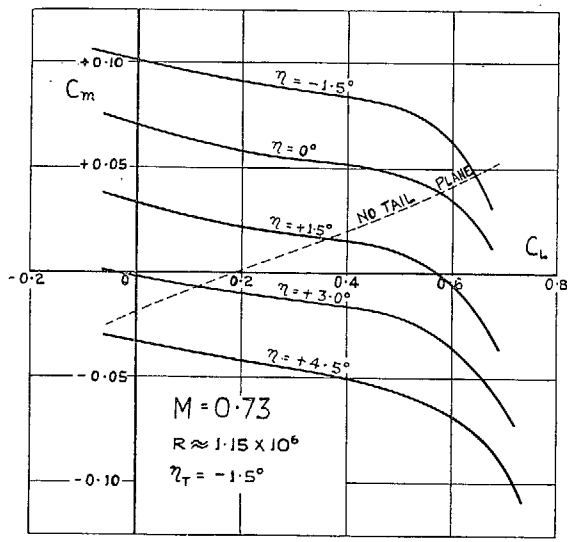

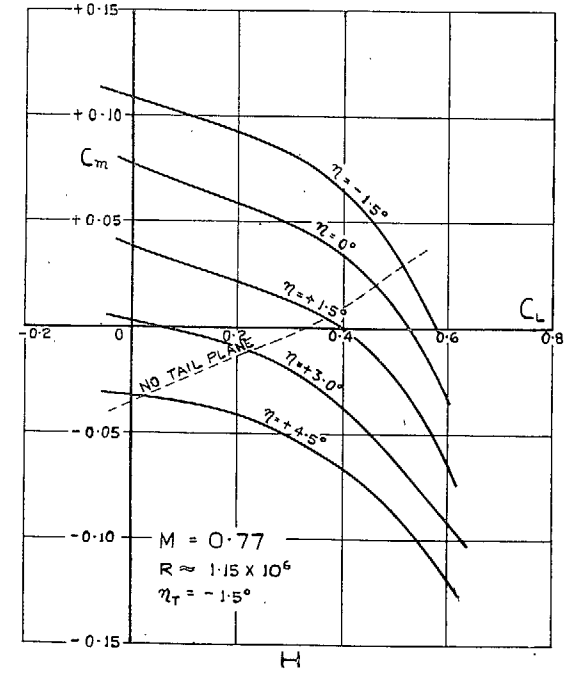

FIG. 22. Pitching moment curves (constant tailplane setting).

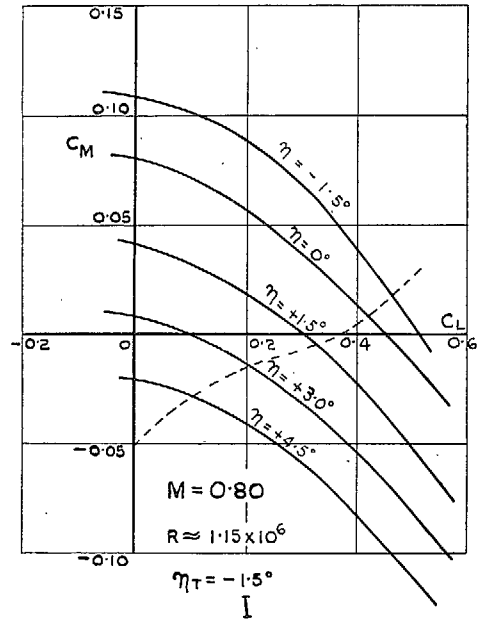

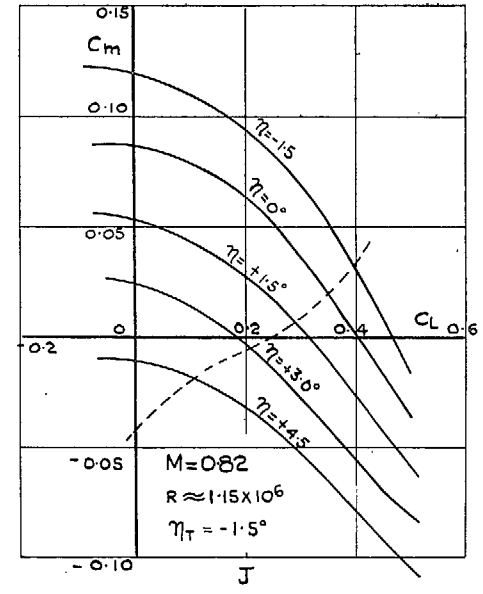

FIG. 22. Pitching moment curves (constant tailplane setting).

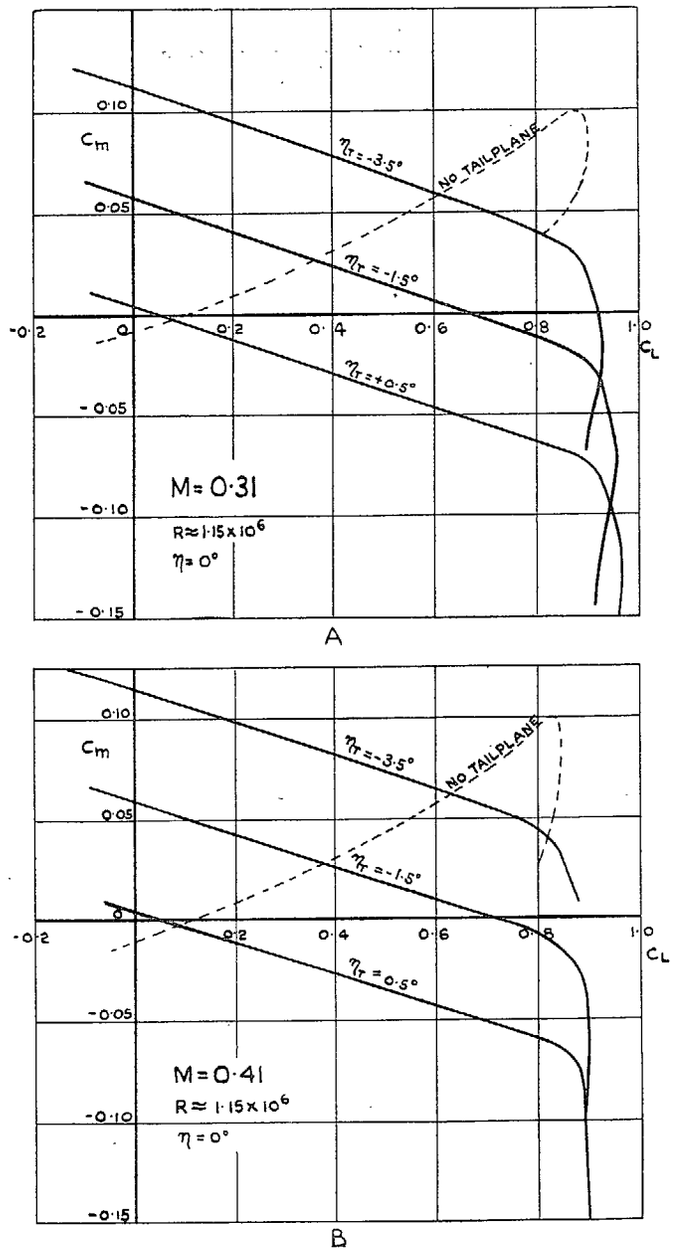

FIG. 23. Pitching moment curves (constant elevator angle).

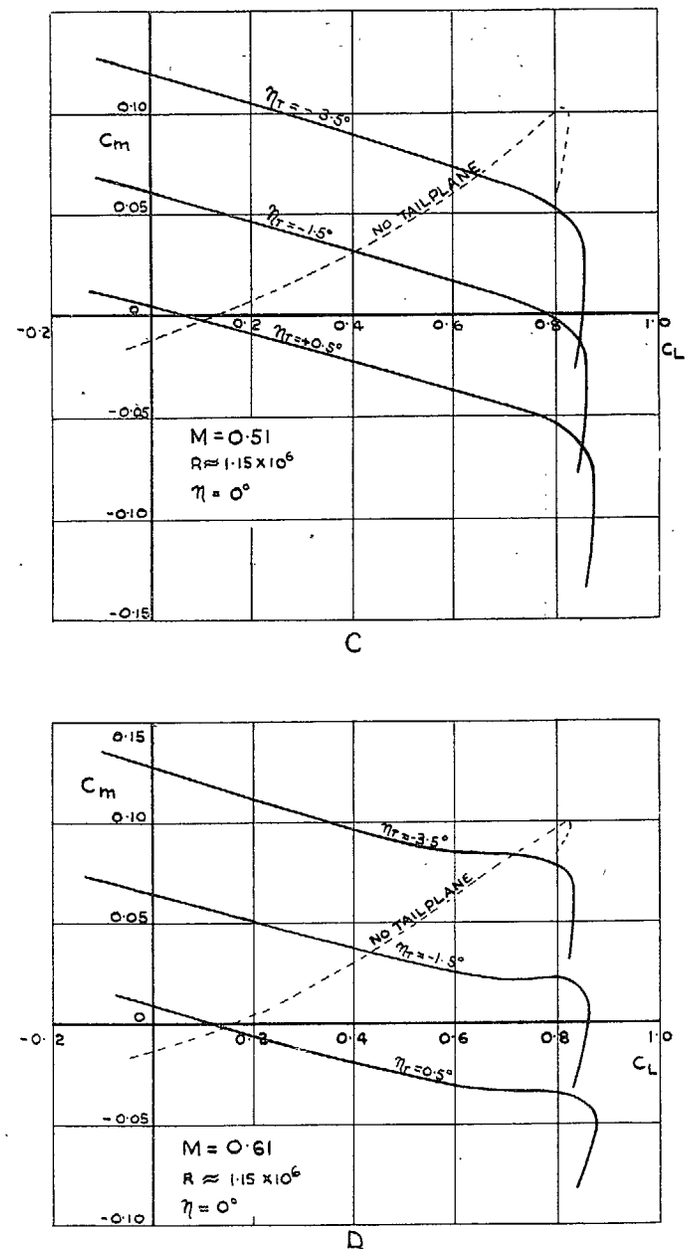

FIG. 23. Pitching moment curves (constant elevator angle)

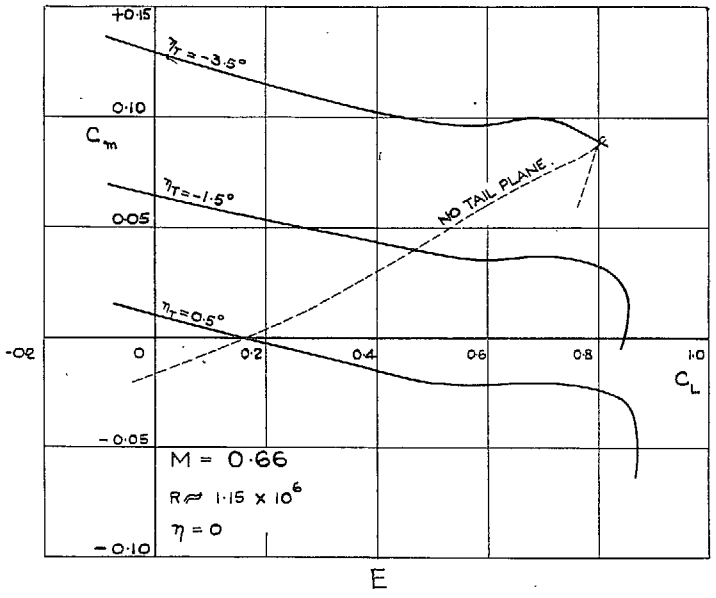

E

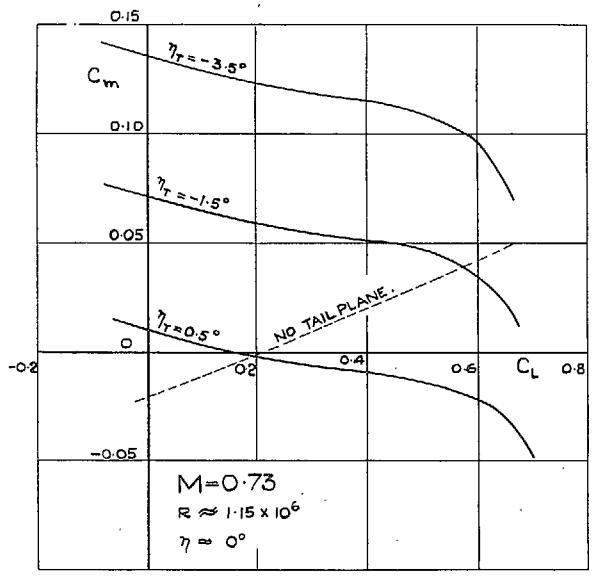

G

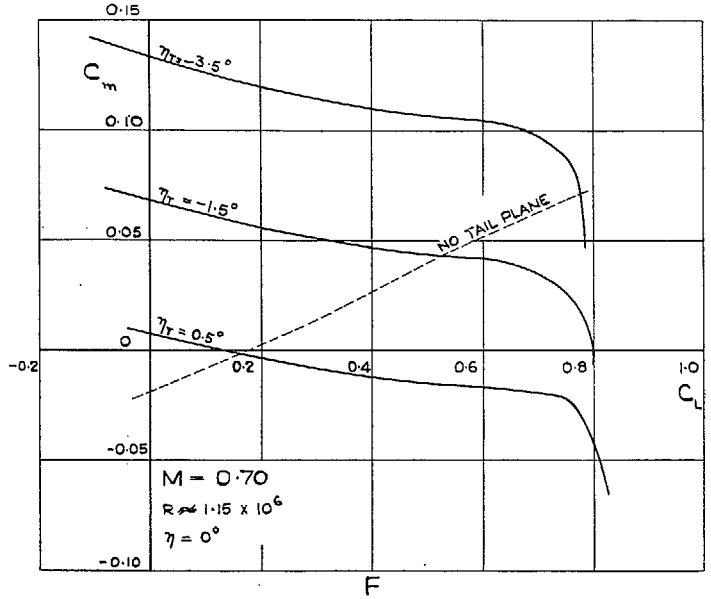

F

FIG. 23. Pitching moment curves (constant elevator angle).

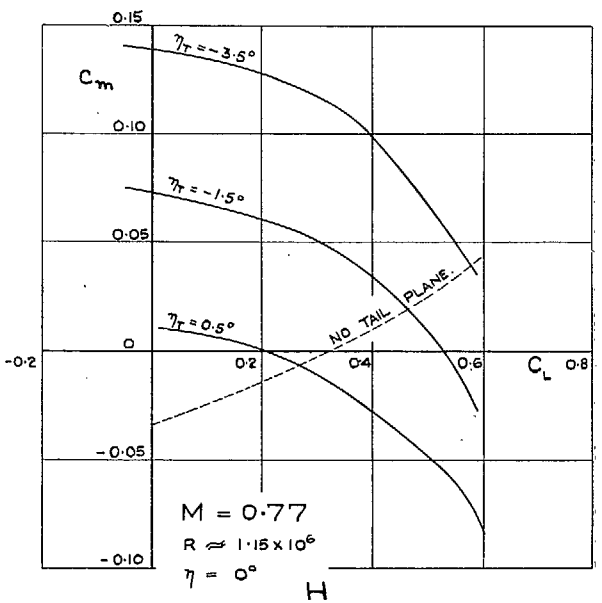

H

FIG. 23. Pitching moment curves (constant elevator angle).

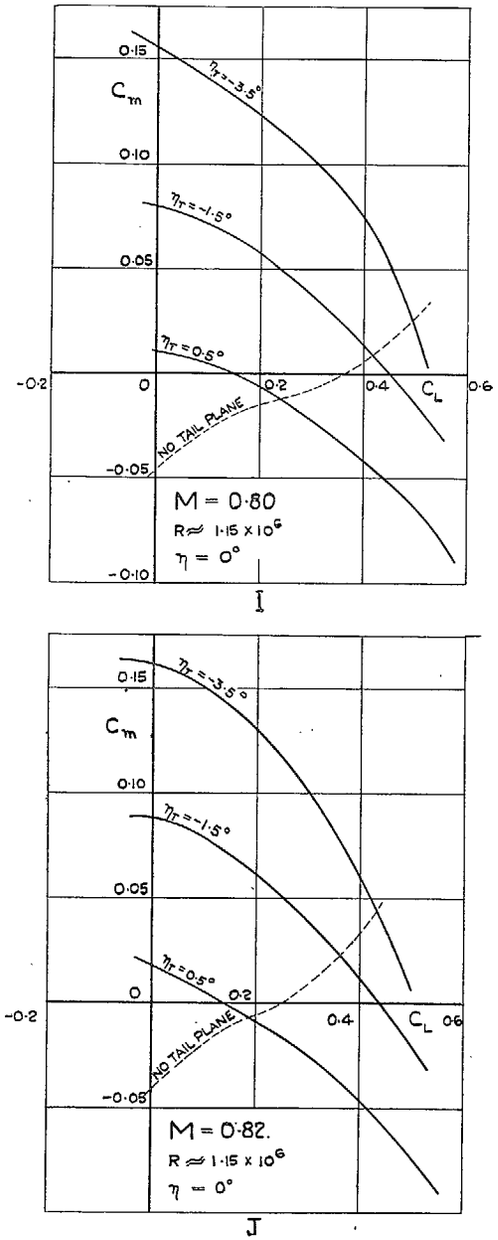

FIG. 23. Pitching moment curves (constant elevator angle).

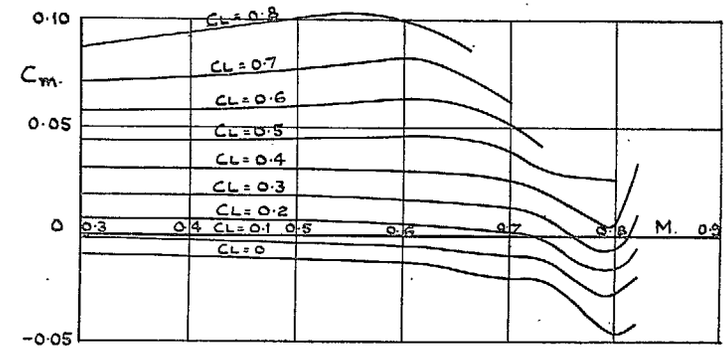

FIG. 24. Pitching moments without tailplane (with radiators).

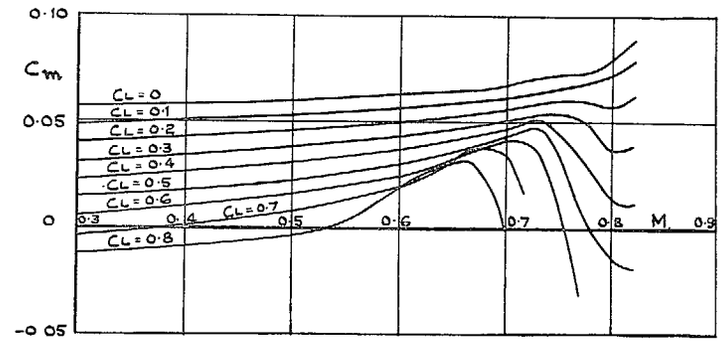

FIG. 25. Pitching moments with tailplane (with radiators, $\eta_T = -1{\cdot}5$ deg, $\eta = 0$ deg).

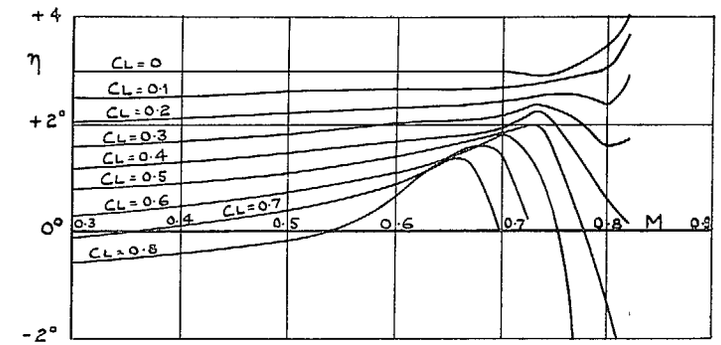

FIG. 26. Effect of Mach number on elevator angle to trim (complete model with radiators, $\eta_T = -1{\cdot}5$ deg).

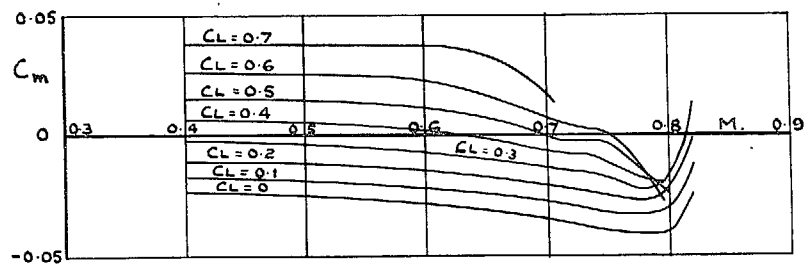

FIG. 27. Effect of Mach number on pitching moment, wing only.

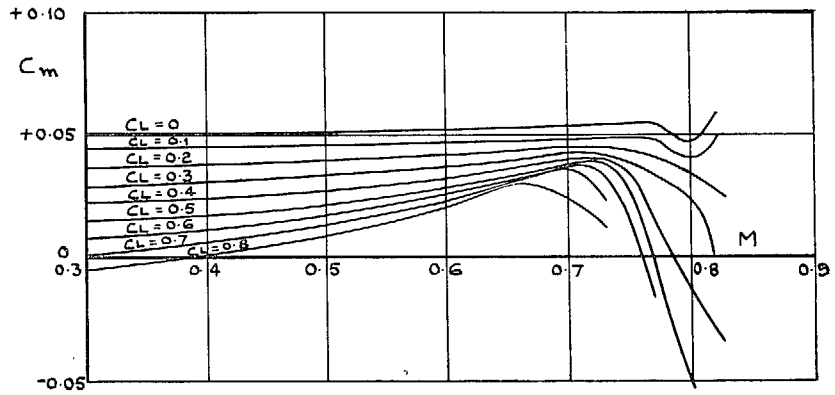

FIG. 29. Effect of Mach number on pitching moment, wing + body + tailplane (no radiators). $\eta_T = -1{\cdot}5$ deg, $\eta = 0$ deg.

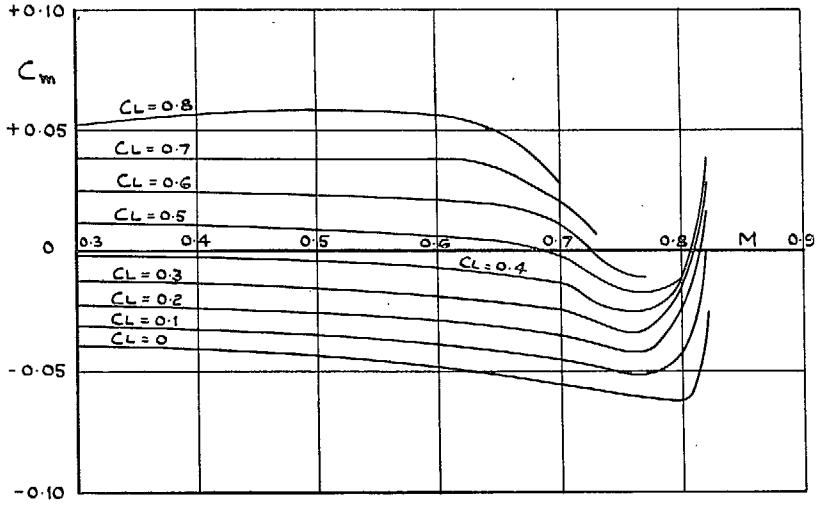

FIG. 28. Effect of Mach number on picthing moment, wing + body (no radiators or tailplane).

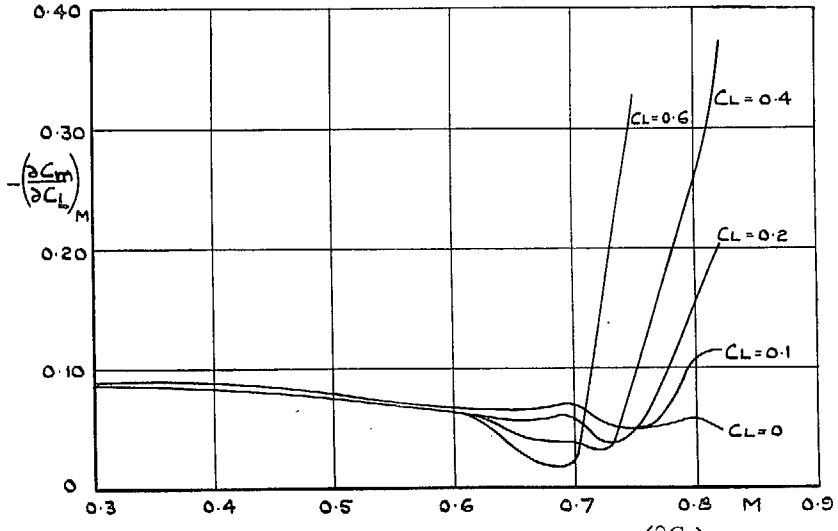

FIG. 30. Effect of Mach number on $-\left(\frac{\partial C_m}{\partial C_L}\right)_M$

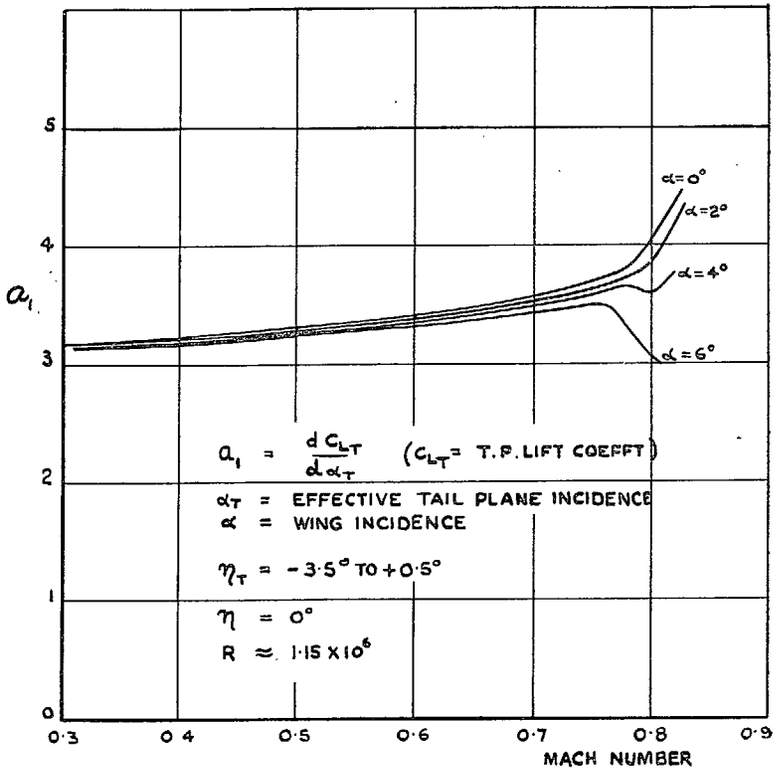

FIG. 31. Effect of Mach number on tailplane lift gradient.

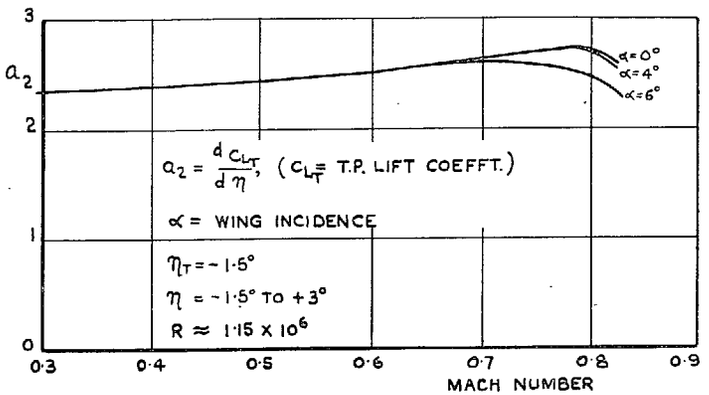

FIG. 32. Effect of Mach number on tailplane lift due to elevator.

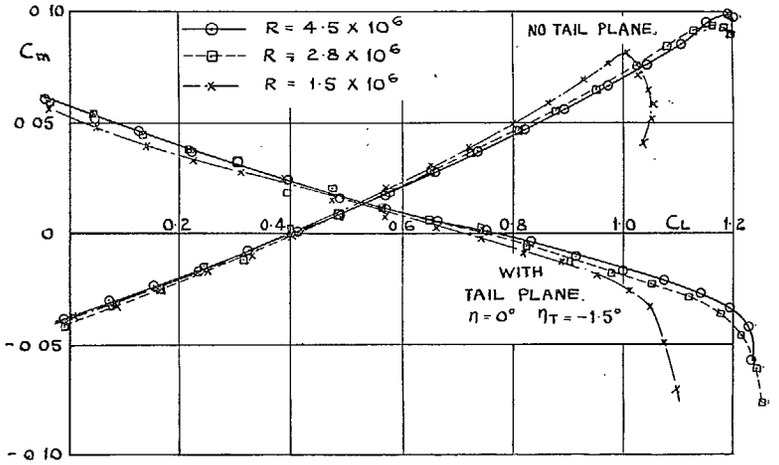

FIG. 33. Pitching moment curves at low speed ($M < 0{\cdot}2$), wing + body (no radiators).

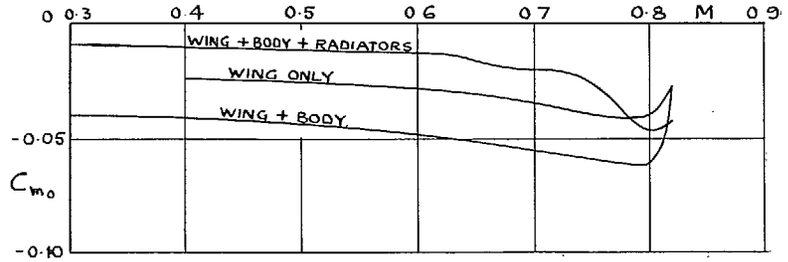

FIG. 34. Effect of Mach number on C_{m0}.

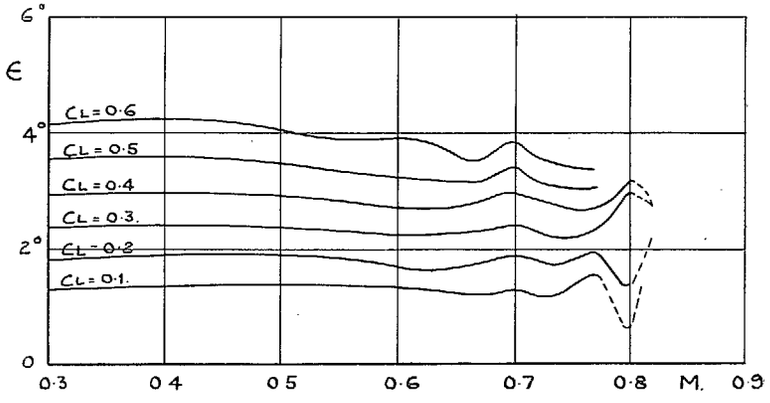

FIG. 35. Effect of Mach number on downwash angle at tail.

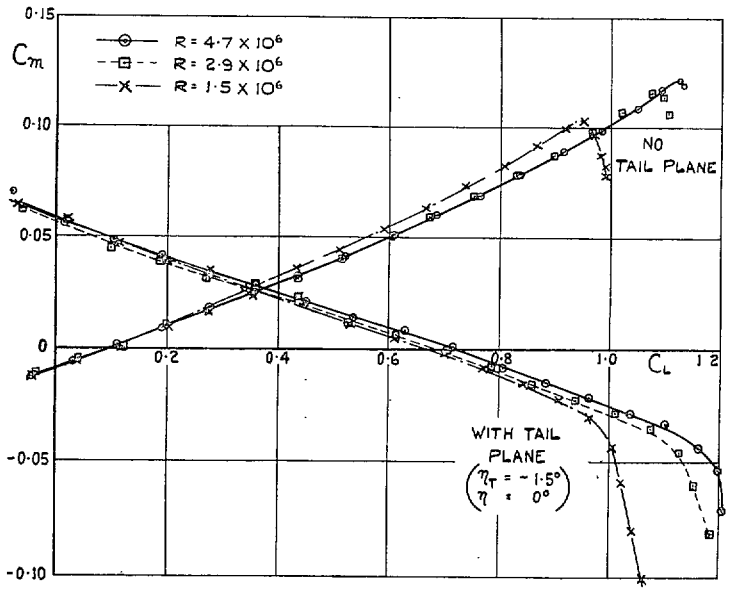

FIG. 36. Pitching moment curves at low speed ($M < 0 \cdot 2$), complete model (flaps up).

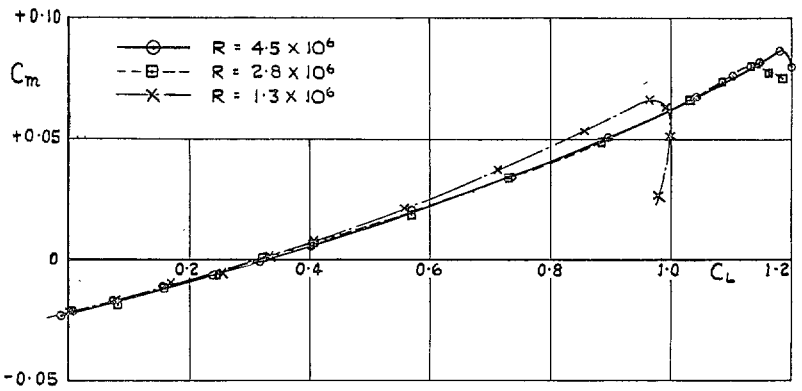

FIG. 37. Pitching moment curves at low speed ($M < 0 \cdot 2$), wing only.

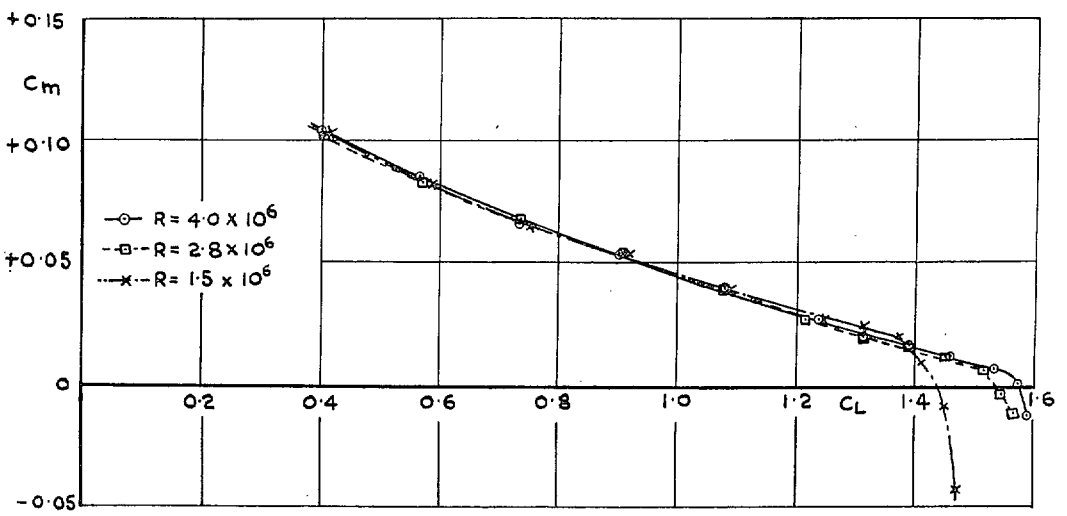

FIG. 38. Pitching moment curves at low speed ($M < 0 \cdot 2$), complete model—landing flaps down.

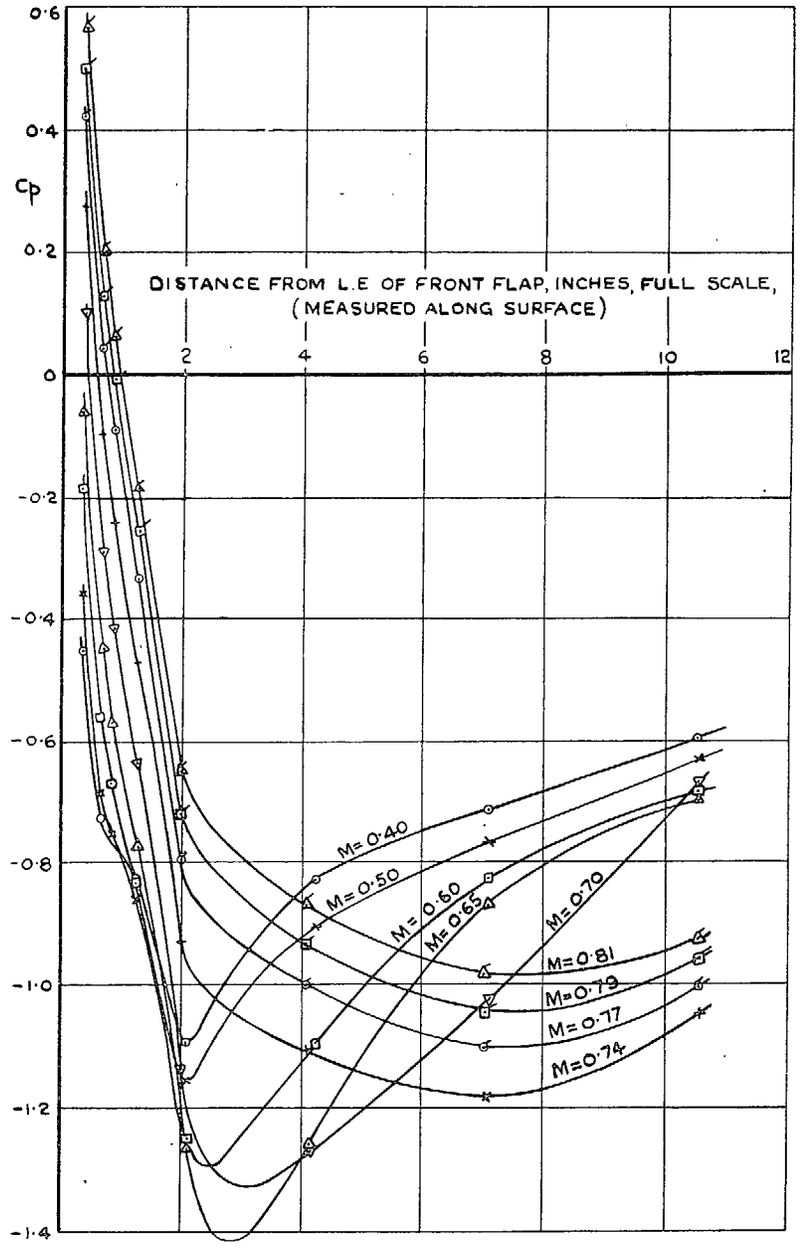

FIG. 39. Pressure distribution on front radiator flap, flap shut, wing incidence = — 0·87 deg.

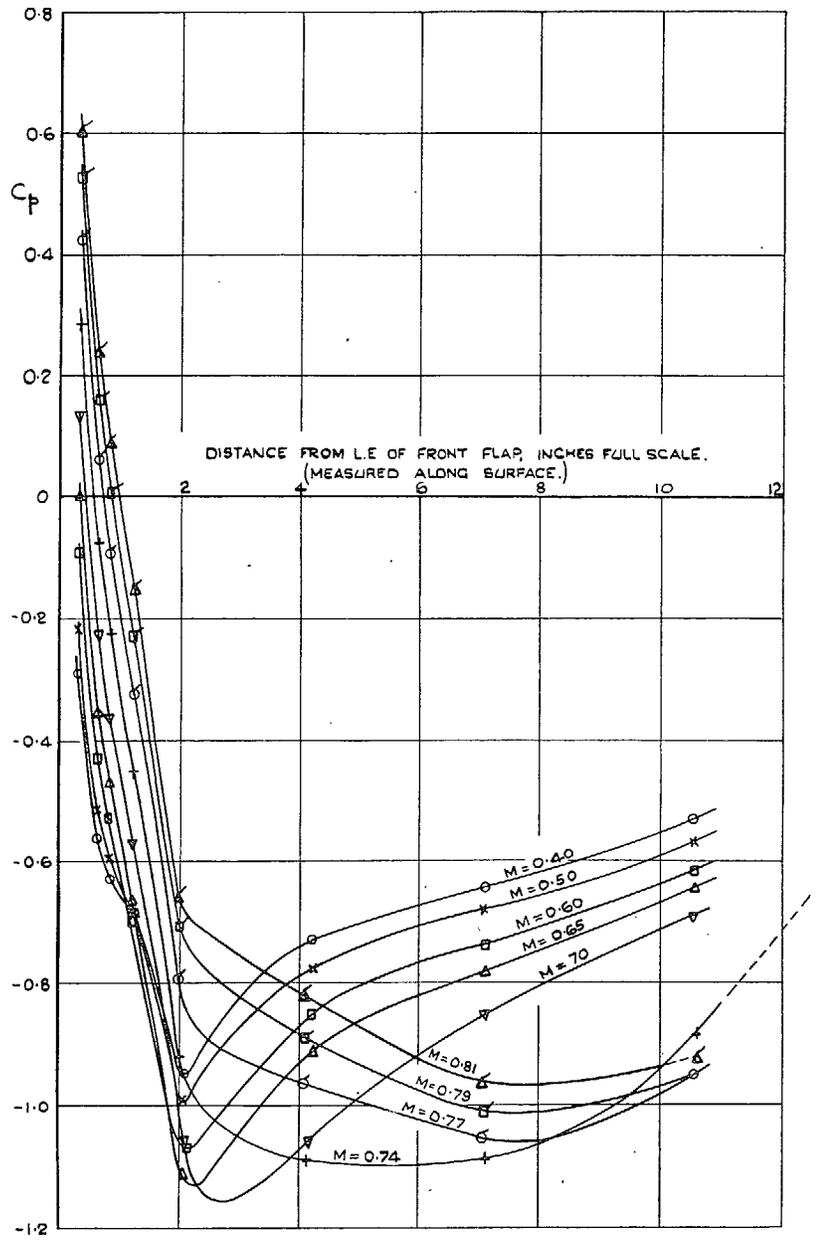

FIG. 40. Pressure distribution on front radiator flap—flap shut, wing incidence = + 1·24 deg.

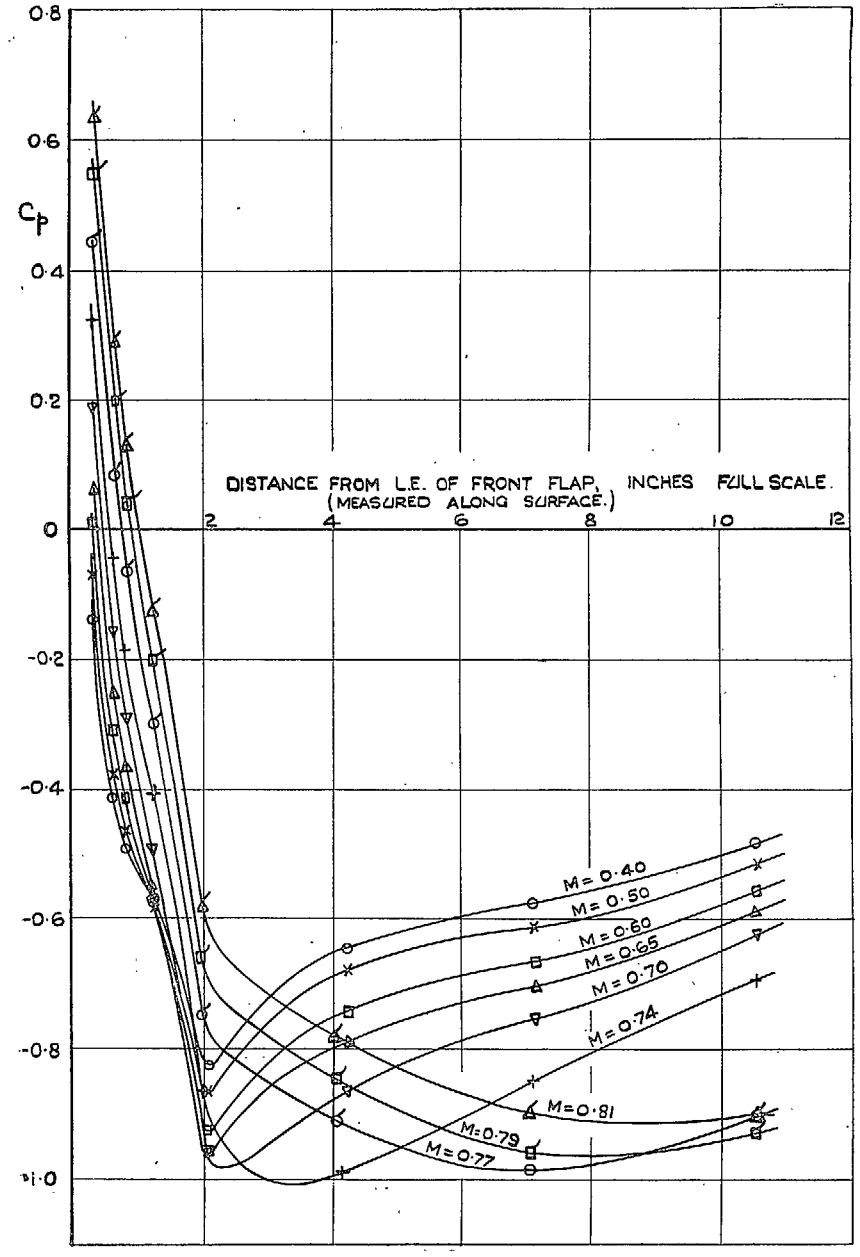

FIG. 41. Pressure distribution on front radiator flap—flap shut, wing incidence = + 3·34 deg.

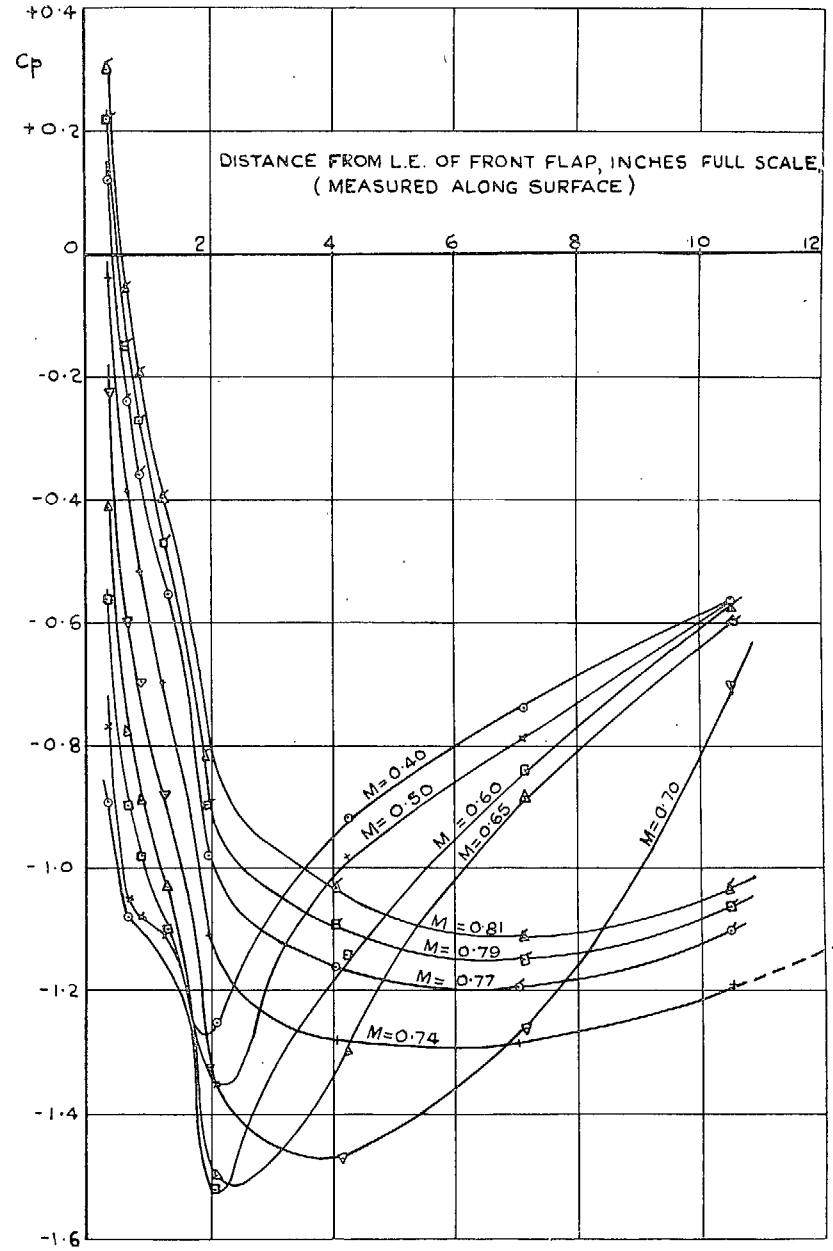

FIG. 42. Pressure distribution on front radiator flap, flap 2 deg. open, wing incidence = — 0·87 deg.

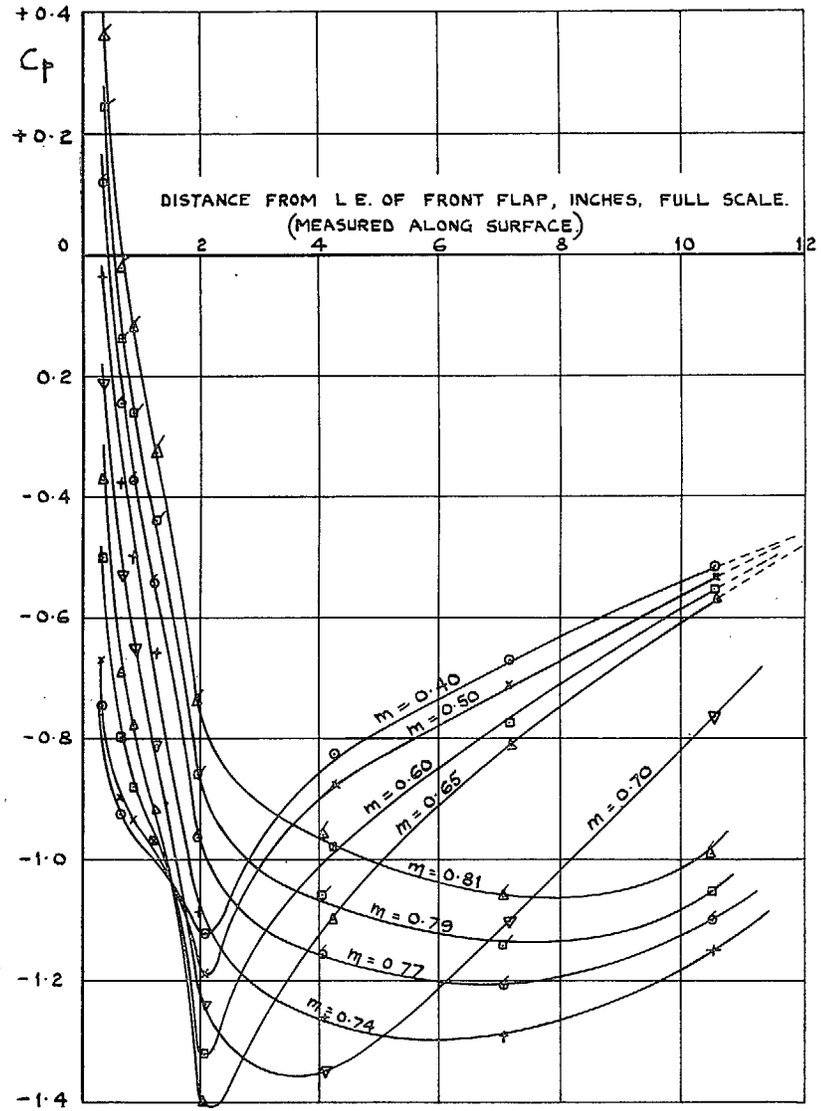

FIG. 43. Pressure distribution on front radiator flap—flap 2 deg open, wing incidence = + 1·24 deg.

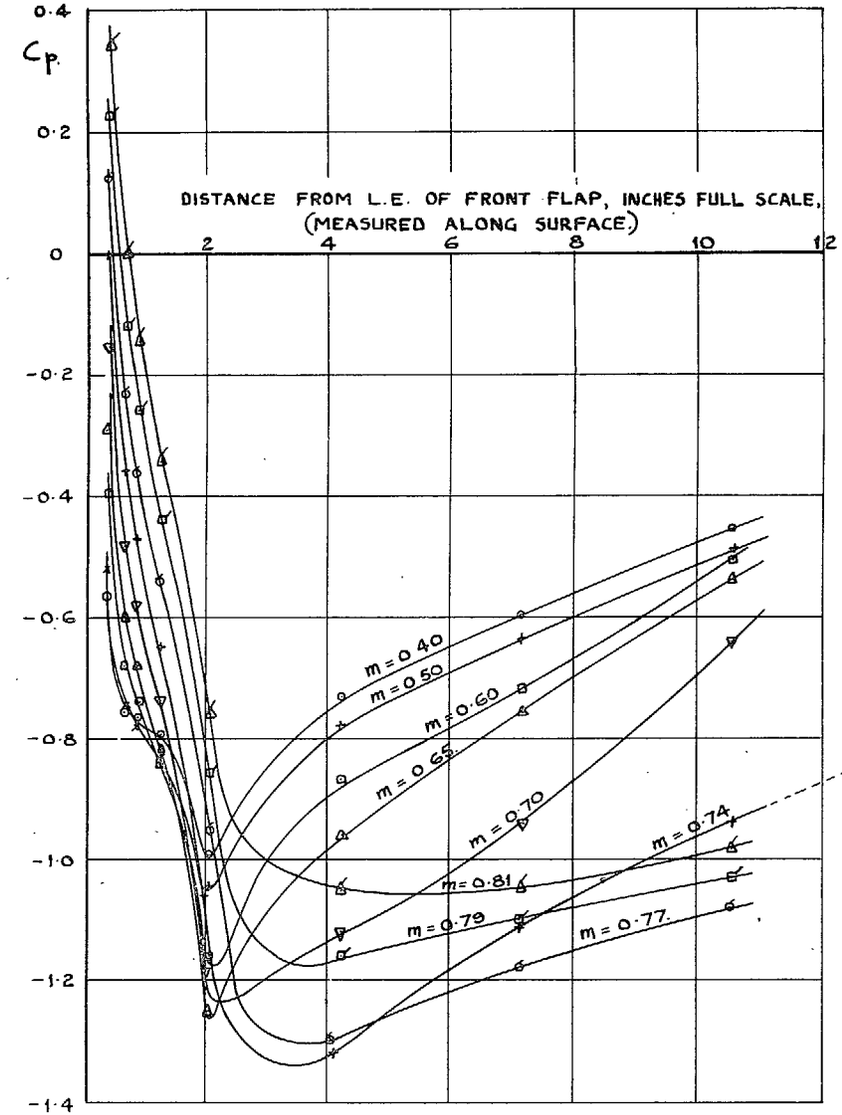

FIG. 44. Pressure distribution on front radiator flap—flap 2 deg open, wing incidence = + 3·34 deg.

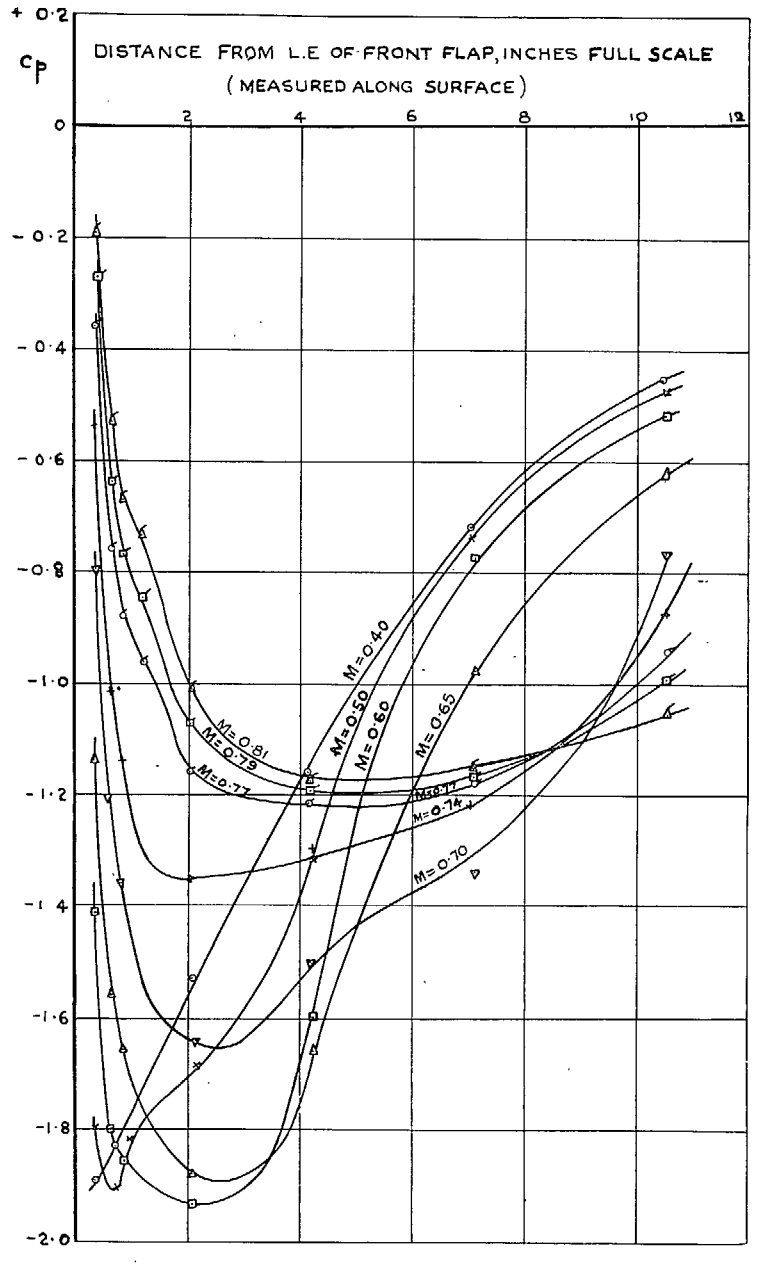

FIG. 45. Pressure distribution on front radiator flap—flap 5 deg open, wing incidence = — 0·87 deg.

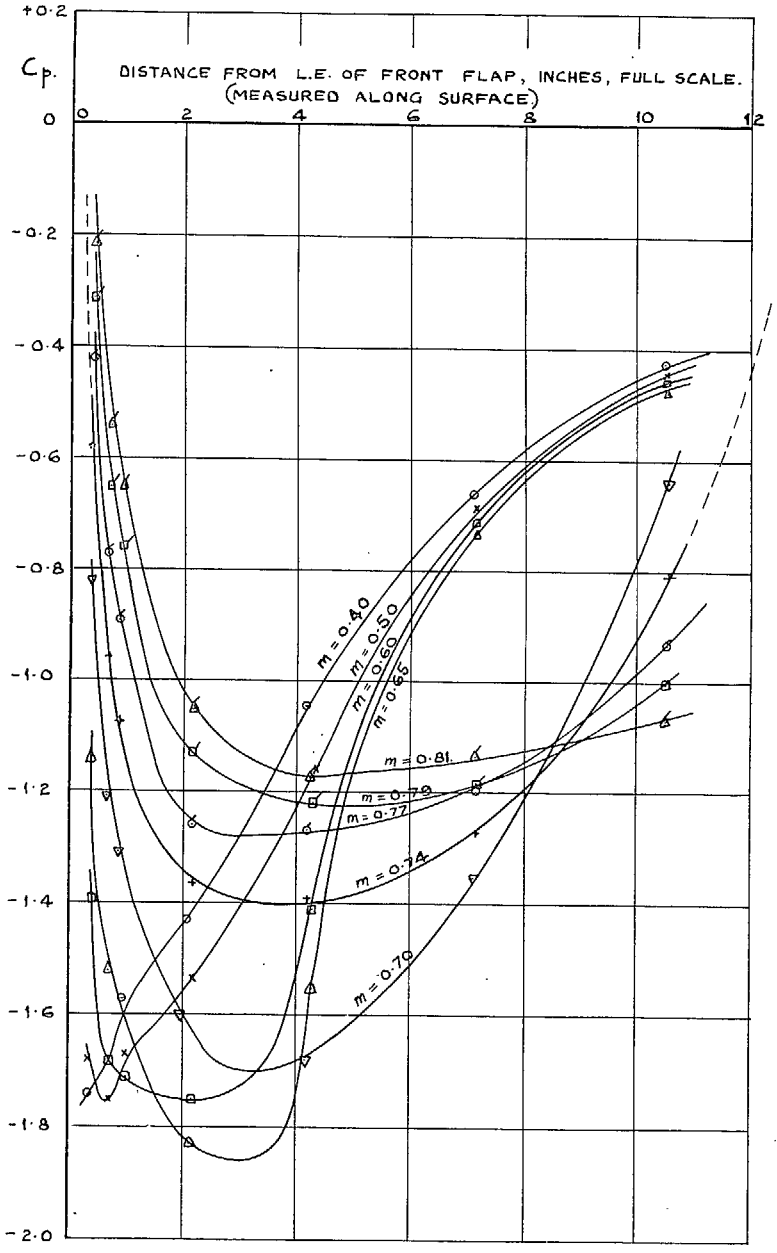

FIG. 46. Pressure distribution on front radiator flap—flap 5 deg open, wing incidence = + 1·24 deg.

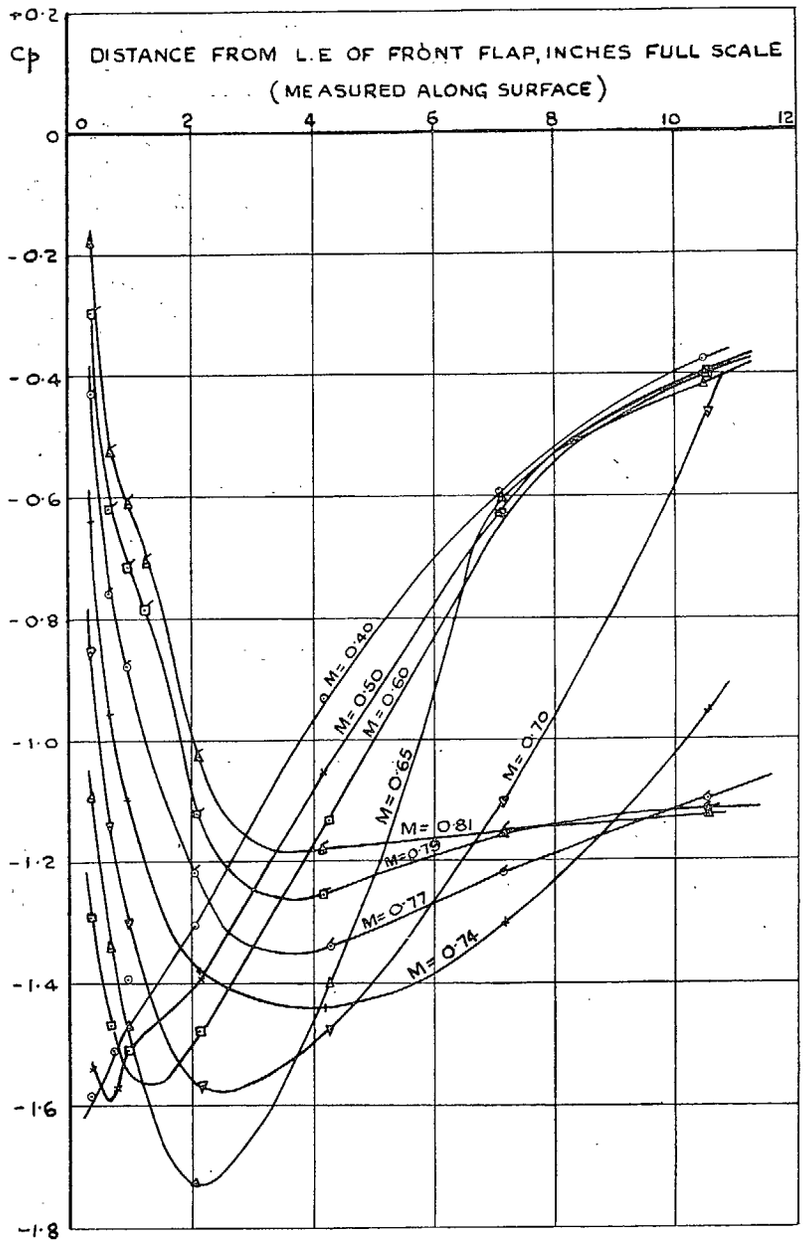

FIG. 47. Pressure distribution on front radiator flap—flap 5 deg open, wing incidence = + 3·34 deg.

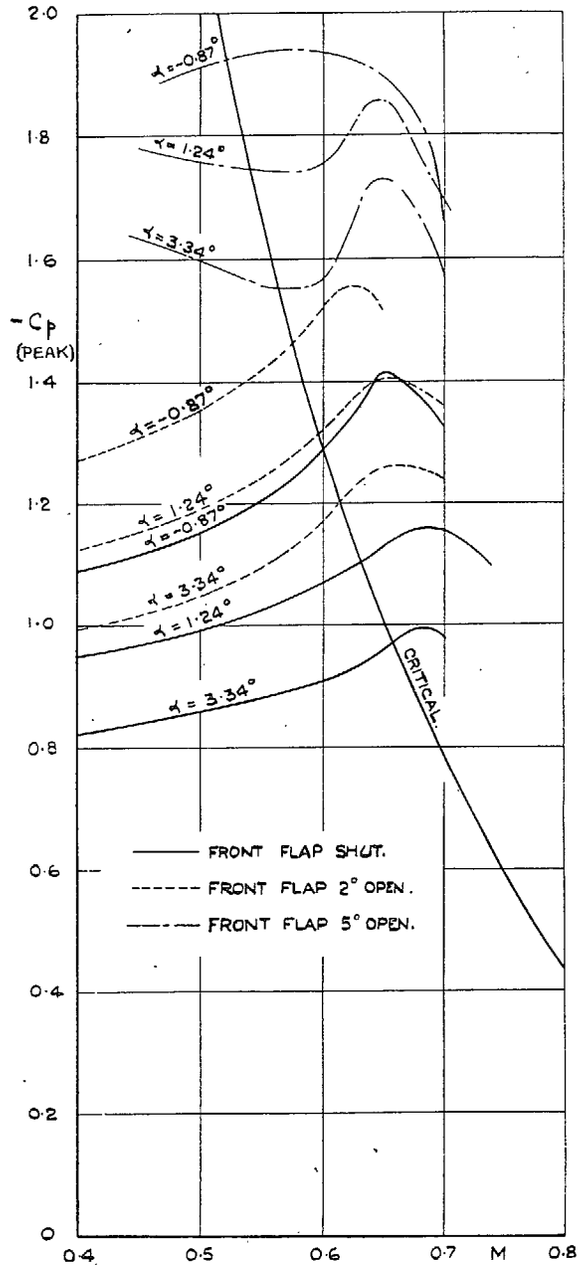

FIG. 48. Radiator front flap, peak suction coefficients.

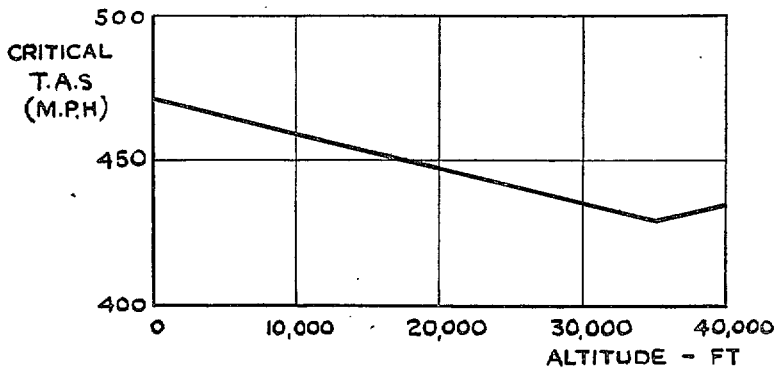

FIG. 49. Critical speed of radiator (front and rear flaps shut).

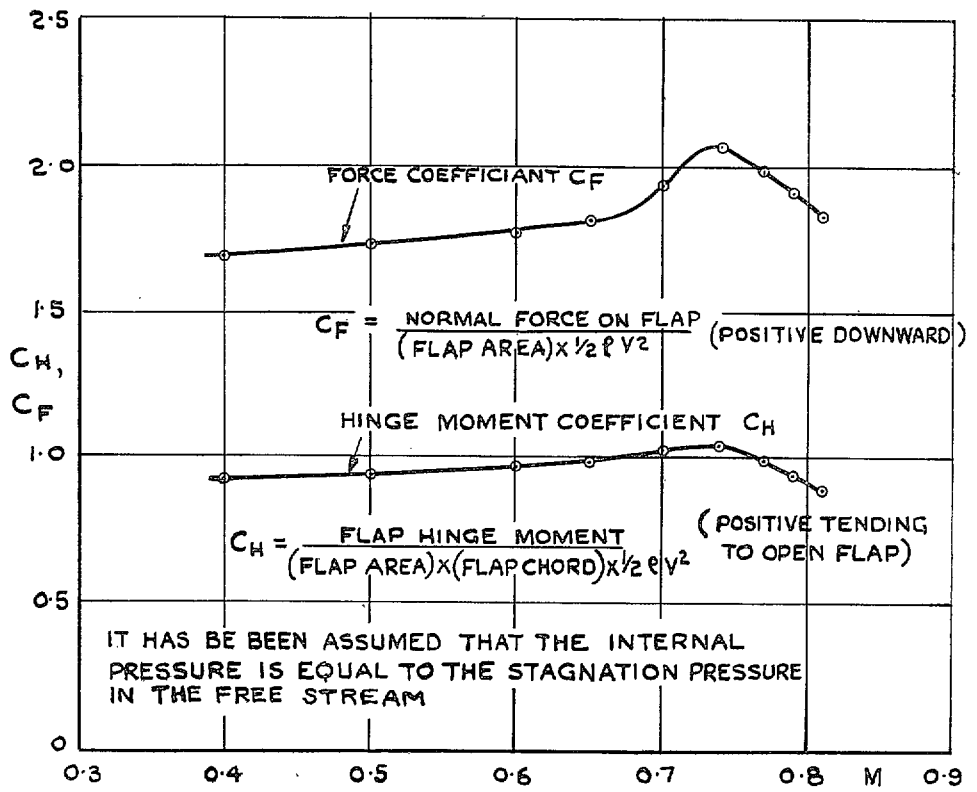

FIG. 50. Effect of Mach number on radiator front flaphinge-moment and force coefficients. Front flap 2 deg open, wing incidence = + 1·24 deg.

PART III

Tests on Cabins for the Spiteful

By

W. A. MAIR, M.A. and S. P. HUTTON, B.Eng.

1. *Introduction.*—Measurements in the 24-ft Wind Tunnel[1] at the Royal Aircraft Establishment have shown that the high peak suction found on the standard Spitfire cabin with sharp corners can be considerably reduced by fitting a curved panel in front of the flat bullet-proof screen. Increasing the radius at the edges of the bullet-proof screen also reduced the peak suction, but neither this modification nor the addition of the curved front panel gave any important reduction of drag at low speeds. However, the change of peak suction suggested that there might be a considerable difference of drag at higher speeds. Measurements made in flight on a Spitfire IX showed that fitting the curved front panel gave a small increase of top speed, and diving tests on the same aircraft showed that the difference of drag between the two alternative cabins increased with Mach number.

Four alternative cabins which have been proposed for the Spiteful were tested in the High Speed Wind Tunnel.

2. *Description of Cabins.*—The four cabins which were tested are shown in Figs. 1, 2 and 3. The cabins were mounted on a $\frac{1}{4}$-scale model of the Spiteful with clipped wings (span 66 in). The wing was set at 3·5 deg to the fuselage datum, which is 2 deg higher than the wing setting on the first prototype, the model having been built before the final wing setting was known. However, the results showed no consistent change of cabin drag with incidence, so that this difference of wing setting is probably not important.

Cabin A, shown in Fig. 1, has a curved panel in front of the windscreen and flat side panels. This cabin is described as cabin L in Ref. 1. Cabin B, shown in Fig. 2, is a modified form of A and also has a curved front panel. Cabin C, shown in Fig 3, has a flat bullet-proof windscreen with flat side panels and no curved front panel. This cabin is described as cabin J in Ref. 1. Cabin D is the same as C except that D has a greater radius at the junction of the side panels with the front windscreen. Cabin D is described as cabin K in Ref. 1.

3. *Results.*—The drags of the four cabins are shown in Fig. 4, plotted against Mach number. Measurements were made at incidences from −1 to +4 deg, at $\frac{1}{2}$-deg intervals. No consistent change of cabin drag with incidence could be observed from the results, but the measurements at incidences from 3 to 4 deg were unreliable, probably on account of the increased wing drag at the higher incidences. Mean values of the cabin drags for incidences from −1 to +2·5 deg were therefore taken, and these mean values are plotted in Fig. 4. The error in the values of the drag probably does not exceed 0·25 lb at any Mach number up to 0·7.

4. *Effect of Cabin Drag on Top Speed.*—In considering the effect of changes of cabin drag on top speed, the effects of compressibility on the drag of the whole aircraft cannot be neglected.

Consider an aircraft which has a top speed V and a drag coefficient C_D at this speed. The drag coefficient at any other speed is not in general equal to C_D, if compressibility effects are appreciable.

Let a small extra drag be added to the aircraft, having a drag coefficient ΔC_D at the same speed V.

Let $\frac{dC_D}{dV} = a$ and $\frac{d(\Delta C_D)}{dV} = b$ at constant height.

Then for constant power, if ΔV is the reduction of top speed due to the extra drag,

$$V^3 C_D = (V - \Delta V)^3 [(C_D + \Delta C_D) - (a + b)\Delta V],$$

and if ΔC_D and ΔV are small,

$$\frac{\Delta V}{V} = \frac{\Delta C_D}{3C_D + (a + b)V}. \quad \ldots \quad \ldots \quad \ldots \quad \ldots \quad \ldots \quad \ldots \quad (1)$$

In considering the effects of cabin drag, b is negligible in comparison with a and the expression reduces to

$$\frac{\Delta V}{V} = \frac{\Delta C_D}{3C_D + aV} \quad \ldots \quad \ldots \quad \ldots \quad \ldots \quad \ldots \quad \ldots \quad \ldots \quad (2)$$

Values of the dimensionless coefficient dC_D/dM, from which the quantity a is derived, are plotted against Mach number in Fig. 5 for the Spitfire and Spiteful. The values for the Spitfire are taken from the results given in Part I, after applying corrections for blockage. The values for the Spiteful are taken from some early tests on the model without radiators. Since the radiators on the Spiteful have a rather low critical Mach number, the values of dC_D/dM given for the higher Mach numbers in Fig. 5 may be too low.

Of the four cabins tested, C has the highest drag at all Mach numbers and A has the lowest drag over the most important part of the speed range. Using the values of cabin drag and dC_D/dM given in Figs. 4 and 5, the increase of top speed of the Spiteful due to a change from cabin C to cabin A has been calculated, and the results are plotted in Fig. 6. It has been assumed that the drag of the full-scale aircraft is 60 lb at 100 ft/sec and that the range of top speed considered (400 to 480 m.p.h.) is obtained by variation of engine power. The calculations have been made for a height of 30,000 ft, but the effect of altitude on the speed increment is small.

5. *Discussion.*—Cabins A, B and D show very little increase of drag with Mach number, for values of M below 0·7, but the drag of cabin C increases by about 1 lb as M increases from 0·6 to 0·7. The peak suction coefficient on cabin C is 1·8 at low speeds (Ref. 1), and the corresponding critical Mach number as calculated from this suction coefficient by Kármán's formula is 0·48. However, pressure measurements on a Frise aileron[2] in the High Speed Wind Tunnel have shown that, on bodies which have high peak suctions at low speeds, the suction may decrease with increase of Mach number, the effect being probably due to separation of the boundary layer near the point of maximum suction. In such a case the critical Mach number, as calculated in the usual way from low-speed pressure measurements, has no meaning. Thus the increase of drag of cabin C is not necessarily the result of the formation of a shock wave, and may be due to a separation of flow at the sharp edges of the front windscreen which becomes more serious as the Mach number increases. Also, the appearance of shock waves on the other cabins may possibly be delayed by local separations which reduce the peak suctions.

The drags of cabins A and D at $M = 0{\cdot}4$, given in Fig. 4, agree fairly well with the values measured in the 24-ft wind tunnel at very low Mach numbers, but the drag of cabin C at $M = 0{\cdot}4$ is considerably greater than the value found from the 24-ft tunnel tests. This suggests that there was some separation at the sharp edges on cabin C at $M = 0{\cdot}4$ which was not present at the very low Mach number of the 24-ft tunnel tests.

Flight tests[3] on a Spitfire IX have shown that changing the windscreen shape from C to cabin A gives an increase of top speed of about 5 m.p.h. at about 420 m.p.h. at 24,000 ft. This is equivalent to a reduction of drag of 2·3 lb due to changing from cabin C to cabin A, at $M = 0{\cdot}6$. This reduction of drag is about 1 lb greater than the reduction shown in Fig. 4.

REFERENCES

No.	*Author*	*Title, etc.*
1	Duddy	Wind Tunnel Tests on Alternative Spitfire Cabins. R.A.E. Technical Note No. Aero 1213. (June, 1943.)
2	Mair, Thompson and Hutton	High Speed Wind Tunnel Tests on a Spitfire Type Wing and Aileron. A.R.C. 7169. (August, 1943.)
3	Stewart	Effect of Conical Windscreen on Performance of a Spitfire IX. R.A.E. Technical Note No. Aero 1284. (1943.)

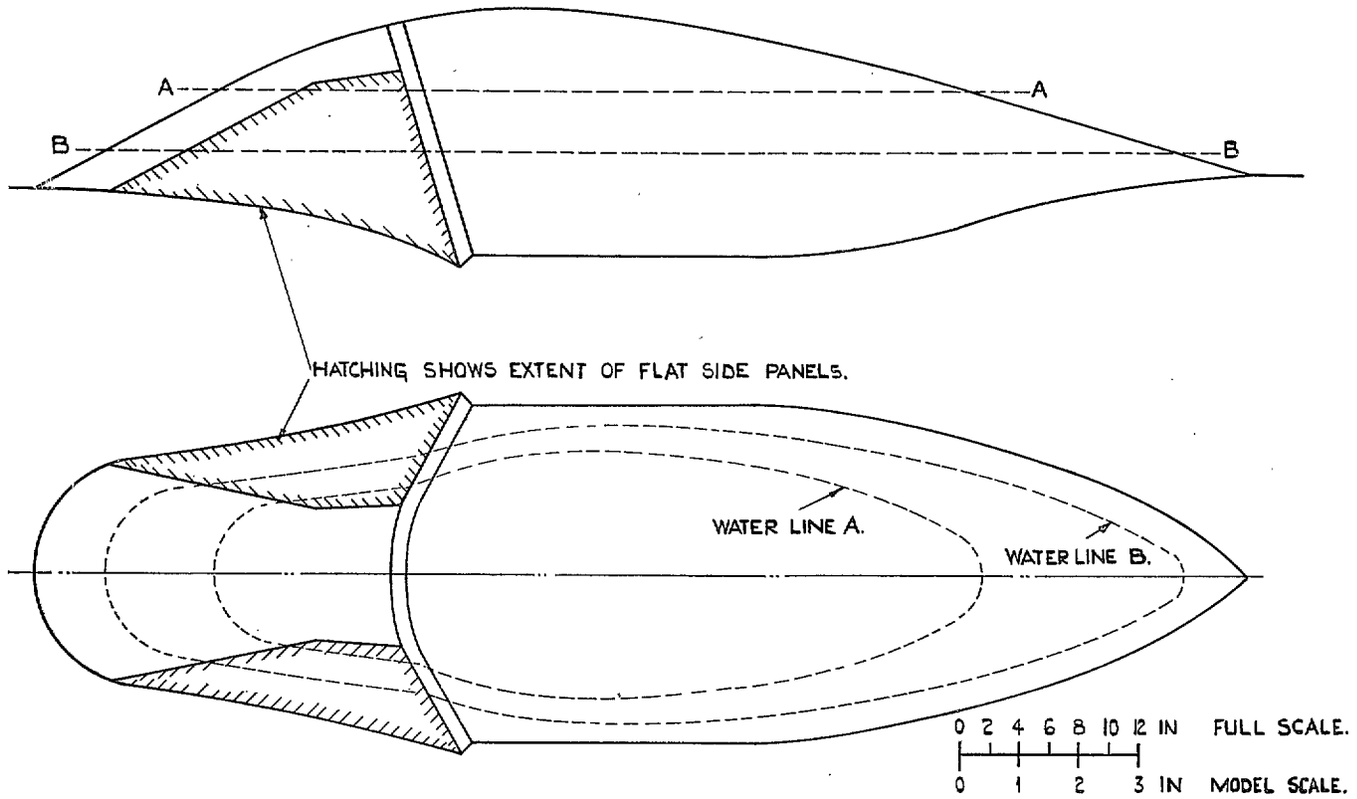

FIG. 1. Cabin A.

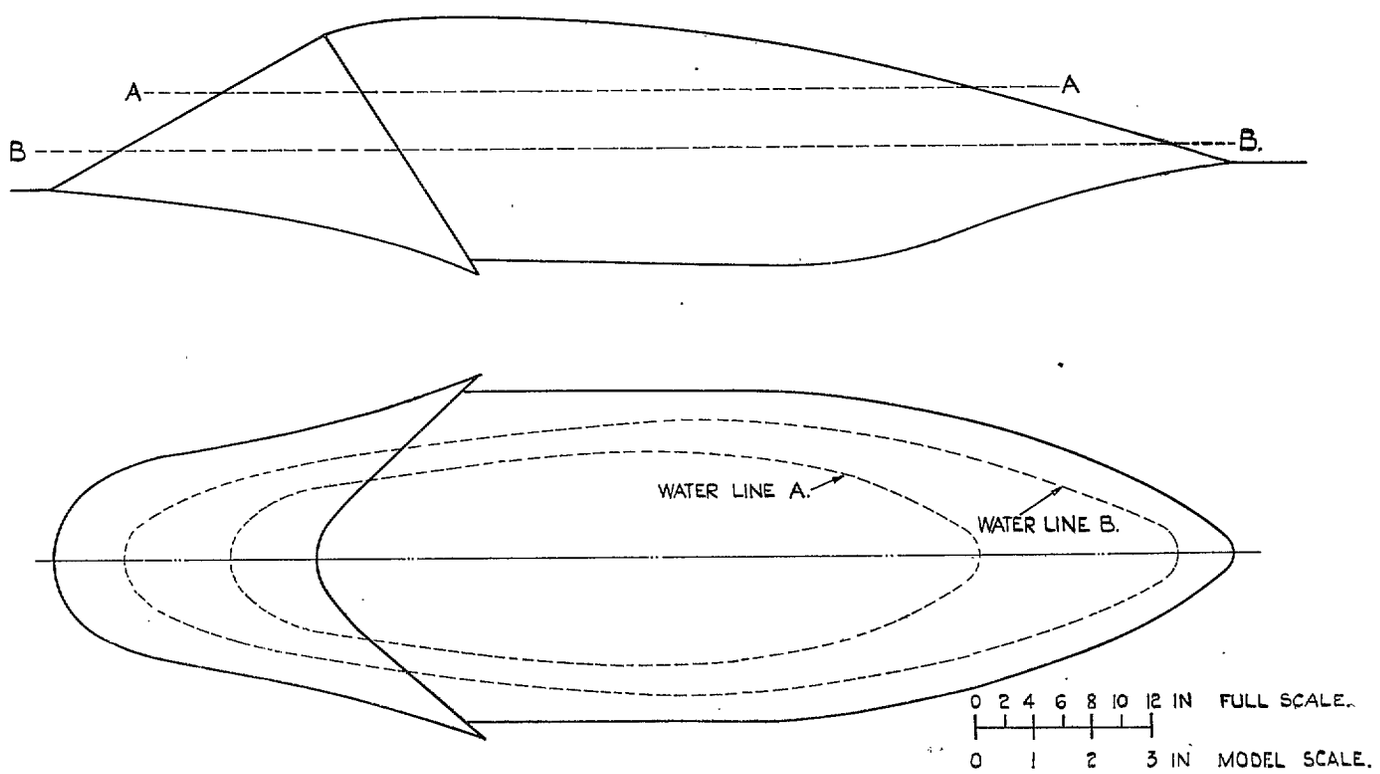

FIG. 2. Cabin B.

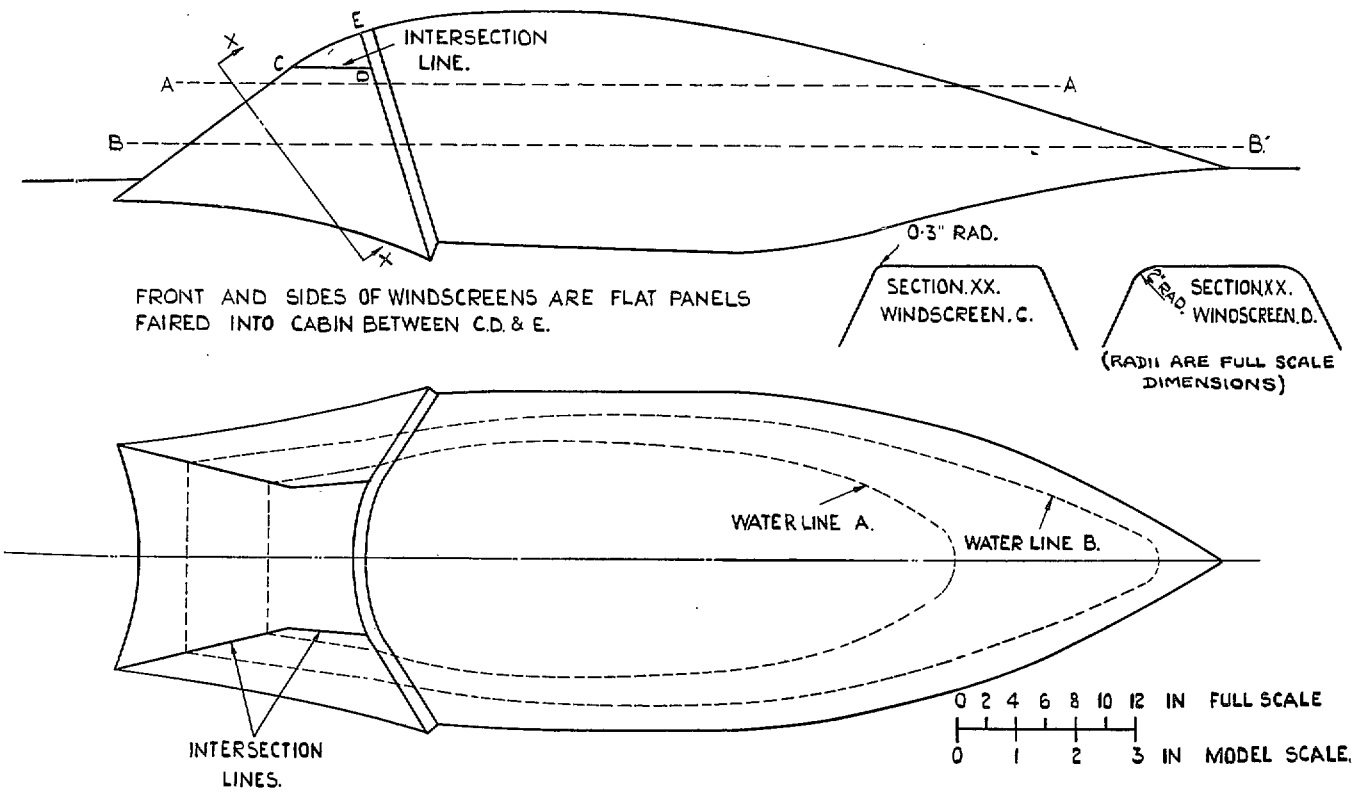

FIG. 3. Cabins C and D.

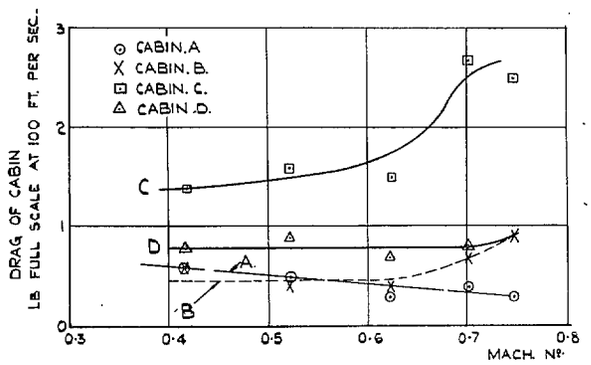

FIG. 4. Drag of alternative cabins.

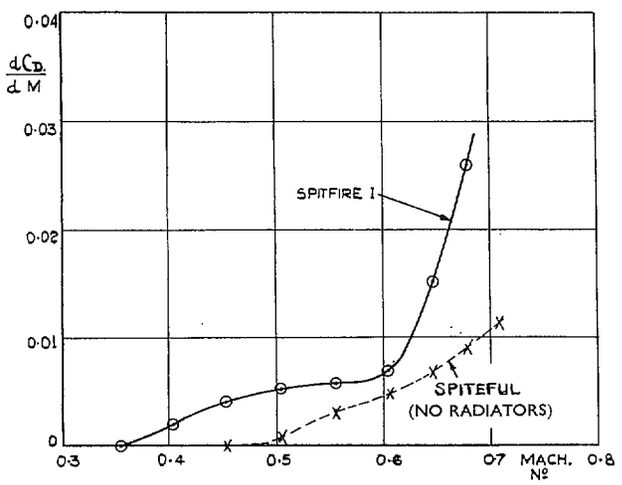

FIG. 5. Rate of increase of drag with Mach number.

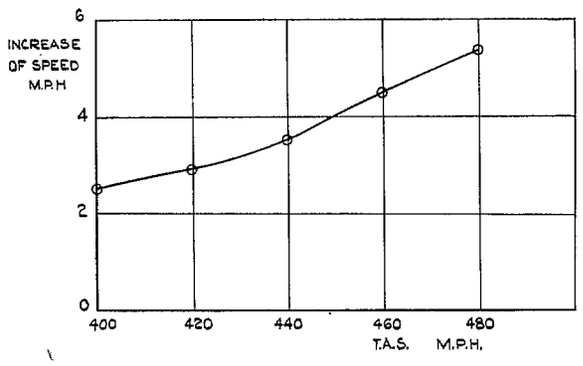

FIG. 6. Increase of top speed at 30,000 ft due to change from cabin C to cabin A.

PART IV

Tests on the Attacker (E. 10/44)

By

S. P. Hutton, M.Eng., D. A. Clarke, B.Sc.(Eng.) A.C.G.I. and D. J. Tremlett, B.Sc.(Eng.) A.C.G.I.

1. *Introduction.*—The Attacker is a single-seat jet-propelled fighter. It was designed around the existing wing structure of the Spiteful (Part II), but the fuselage has been altered to accommodate the new power unit (Rolls Royce Nene). The wing span was increased slightly to fit the wider fuselage. The aircraft was expected to reach a Mach number of about 0·8 in level flight, and wind-tunnel tests were required to investigate stability and trim changes occurring up to the highest Mach number reached by the tunnel.

2. *Description of Model.*—The tests were made on a $\frac{1}{6}$-scale wooden model. Dimensions of the aircraft are given in Table 1 and the general arrangement is shown in Fig. 1.

The crescent-shaped entries to the engine duct are on each side of the fuselage ahead of the wing leading edge. The boundary layer from the front of the fuselage ahead of the entries is led away through by-pass ducts and discharged beneath the fuselage.

In the model the main duct exit area was calculated to give the correct entry conditions for top-speed level flight ($v/V=0{\cdot}650$). Structural difficulties made it necessary to deflect the duct over the wing. No model power unit was incorporated. Fig. 2 shows the ducting as tested.

Tests were also made on reflexed wing-root fillets, designed to reduce the large value of $(-C_{m0})$ found with the original fillets. Details of both types of fillet are given in Fig. 3.

The position of the struts carrying the model made it impossible to test the dive-recovery flaps in the required position on the complete model, so a single flap was tested on the rectangular wing used for determining strut interference. The chord of this wing was almost equal to the required local chord for the flap on the model.

3. *Results.*—The more important results are presented graphically in Figs. 4 to 21.

3.1. *Lift.*—Between $M=0{\cdot}3$ and $0{\cdot}73$ the no-lift angle is almost constant at $-0{\cdot}3$ deg, and between $M=0{\cdot}73$ and $0{\cdot}80$ increases by about $0{\cdot}8$ deg (Fig. 4). The lift-curve slope increases with Mach number up to about $M=0{\cdot}75$, then decreases with further rise of Mach number (Fig. 20).

The low-speed tests with flaps up show a maximum lift coefficient of $1{\cdot}02$ at $R=1{\cdot}2\times10^6$ (Fig. 6). This is to be compared with the value of $0{\cdot}98$ obtained in other low-speed tests[1]. There is a favourable scale effect which increases $C_{L\,\max.}$ to $1{\cdot}25$ at $R=4{\cdot}2\times10^6$ and causes an increase in $dC_L/d\alpha$ from $5{\cdot}11$ to $5{\cdot}35$ over the same range of Reynolds numbers. The body has little effect on $C_{L\,\max.}$

3.2. *Drag.*—Figs. 10 and 11 show that the drag coefficient of the aircraft, and also of the wing alone, is nearly independent of Mach number up to $M=0{\cdot}70$ for all lift coefficients up to $0{\cdot}6$.

For low lift coefficients the drag coefficient for wing and body is about $2\frac{1}{2}$ times that of the wing alone. For the complete model at $C_L=0$ there is no large increase of drag until the Mach number exceeds about $0{\cdot}79$.

3.3. *Longitudinal Stability.*—Changes in stick-fixed manœuvre margin[2] at a given altitude are approximately equal to changes in $(-\partial C_m/\partial C_L)_M$. This assumes that the tail lift-curve slope a_1 is not affected by Mach number. From Fig. 17 it is seen that there is a decrease of $(-\partial C_m/\partial C_L)_M$ with increasing Mach number up to about $M=0{\cdot}73$. The loss for $C_L=0{\cdot}1$ between $M=0{\cdot}3$ and $0{\cdot}73$ is about $0{\cdot}05$.

Figs. 18 and 19 show that downwash and a_1 do not vary much with Mach number. Thus the main reason for the decrease of stability seems to be the large difference beween the changes of tailplane and main plane lift-gradients with Mach number. As the Mach number increases, the wing lift gradient (Fig. 20) rises steadily, whereas a_1 for the tailplane (Fig. 19) is approximately constant up to $M = 0{\cdot}82$. Consequently the stability decreases with increasing speed until $dC_L/d\alpha$ starts to decrease at $M = 0{\cdot}73$; the stability then begins to increase with speed.

A part of the difference between the changes of these two lift gradients with Mach number is accounted for by the difference in aspect ratio. The remainder may be due to wake effects at the tailplane.

Fig. 9 shows that the body has a fairly large destabilizing effect at low speed and shifts the aerodynamic centre forward by about $0{\cdot}06\bar{c}$. As the Reynolds number increases from $1{\cdot}2\times10^6$ to $4{\cdot}2\times10^6$ the neutral point, with or without tail, moves back slightly.

3.4. C_{m0}.—This is numerically large even at low speeds (Fig. 9). Fig. 16 shows that a large part of this is due to the body and that the body contribution is approximately independent of Mach number.

The value of $-C_{m0}$ increases steadily with Mach number from $0{\cdot}05$ at $M = 0{\cdot}3$ to $0{\cdot}09$ at $M = 0{\cdot}82$. The tests do not cover higher Mach numbers, but the curves at higher lift coefficients suggest that the C_{m0} curve will hook over and that C_{m0} will decrease numerically at Mach numbers above about $0{\cdot}83$. As the corresponding maximum numerical value of C_{m0} is very near the factored value assumed for stressing purposes, an attempt was made to reduce it by adding a fillet, reflexed at the trailing edge of the wing root. This is shown in Fig. 3. The only difference between the two fillets is that on the reflexed one the tail of the fillet, aft of the wing trailing edge, was turned up 15 deg. Low speed tests showed that this changed C_{m0} from about $-0{\cdot}055$ to $-0{\cdot}045$. High-speed tunnel tests at $M = 0{\cdot}3$ confirmed this change. The fillet reduces the body increment by about half and the effect on C_{m0} is nearly independent of Mach number up to $M = 0{\cdot}82$ (Fig. 16). At $M = 0{\cdot}80$ the reduction of $-C_{m0}$ due to the reflexed fillet is 10 per cent.

3.5. *Trim Changes at High Mach Numbers.*—Fig. 21 shows that at Mach numbers above $0{\cdot}75$ the elevator angle to trim decreases rapidly. This effect is also shown in Figs. 14(*a*) and (*b*), which give the unbalanced pitching moment at zero elevator angle. A comparison with Figs. 15(*a*) and (*b*) shows that the effect is due to an increase of tail lift coefficient at high Mach number. A small part of this is caused by change of downwash angle at the tail with Mach number, for constant C_L (Fig. 18), but most of it is due to increase of incidence for a constant wing C_L (Fig. 4).

3.6. *Dive-recovery Flaps.*—The tests on the dive-recovery flaps could not be made on the complete model, because the supporting struts were very near the position of the flaps. Accordingly, a flap was tested on a rectangular wing of the appropriate section. Details of the flap are given at the end of Table 1 and the correct position of the flaps on the complete aircraft is shown in Fig. 1.

The effect of a pair of flaps has been estimated by doubling the pitching moment and lift increments on the single flap. In applying these increments to the complete aircraft it has been assumed that the downwash for a given total lift coefficient is unaffected by the flaps. This is equivalent to assuming that the flaps have no effect on the spanwise distribution of lift. This assumption cannot be exactly correct, although the flaps are not in front of any part of the tailplane, but the calculations based on this assumption will probably give an upper limit to the recovery effect of the flaps.

For the complete aircraft the estimated increase of C_m due to the flaps, at a constant lift coefficient of $+0{\cdot}05$, is about $0{\cdot}12$ for Mach numbers between $0{\cdot}76$ and $0{\cdot}80$. This nose-up trim change is equivalent to an elevator movement of about $4\frac{1}{2}$ deg. The nose-down trim change due

to compressibility effects, on the aircraft without flaps, is equivalent to a change of elevator angle of about 2 deg at $M = 0{\cdot}80$, but of course this may be greater at higher Mach numbers. Thus the nose-down tendency at $M = 0{\cdot}8$ could probably be counteracted by flaps of about half the span tested.

4. *Conclusions.*—There is a considerable loss of static longitudinal stability with increase of Mach number up to 0·73. This is due mainly to the increase of wing lift gradient with Mach number while the tailplane lift gradient is almost constant. Similar effects have been found in tests on other fighters, *e.g.*, Spitfire and Spiteful (Parts I and II).

The wings of the Spiteful and Attacker are almost identical, and the lift and pitching-moment curves for the wing-alone cases show good agreement up to $M = 0{\cdot}76$. Above this the pitching-moment curves differ to some extent, but this can be accounted for by the different methods used for strut correction in the two series of tests.

The value of C_{m0} is $-0{\cdot}05$ at low Mach numbers, changing to $-0{\cdot}09$ at $M = 0{\cdot}82$. A large part of this is due to the body, the effect of which can be reduced by half by the use of reflexed fillets at the wing root. This corresponds to a total reduction in the maximum numerical value of C_{m0} of about 10 per cent. The large difference in C_{m0} between the tests on the Spiteful and the Attacker is almost entirely due to the large body of the latter compared with the original Spiteful fuselage.

Between $M = 0{\cdot}75$ and $M = 0{\cdot}80$ there is a large nose-down trim change, caused mainly by the increase of incidence required to maintain a constant lift coefficient on the wing after the shock stall. The maximum lift coefficient at $R = 4{\cdot}2 \times 10^6$ is about 1·25 (without flaps), but the value may be greater at higher Reynolds numbers.

The drag coefficient does not increase rapidly until a Mach number of about 0·79 is exceeded.

REFERENCES

No.	*Author*	*Title, etc.*
1	Morgan and Aiton	Low Speed Wind Tunnel Tests on the Supermarine E.10/44 (Single Jet Fighter). R.A.E. Report No. Aero 2059. (July, 1945.)
2	Gates and Lyon	A Continuation of Longitudinal Stability and Control Analysis. Part I—General Theory. R. & M. 2027. (February, 1944.)

TABLE 1

Leading Dimensions, Full Scale

(Model Scale = 1/6th)

Wing:	
Gross area	226 sq ft
Span	37·0 ft
Standard mean chord	6·11 ft
Aspect ratio	6·1
Straight taper between :—	
Chord at 1·02 ft from centre-line (inside fuselage)	8·34 ft
Chord at 6·00 ft from centre-line (at ' break ')	7·08 ft
Straight taper between :—	
Chord at 6·00 ft from centre-line (at ' break ')	7·08 ft
Chord at 17·00 ft from centre-line (start of tip)	3·34 ft
Position of maximum camber	47·5 per cent
Maximum camber	0·93 per cent
Position of maximum thickness	40 per cent
Thickness ratio :	
From centre-line to ' break '	13 per cent
At 12·00 ft from centre-line	11·3 per cent
At 17·00 ft from centre-line	8·4 per cent
Dihedral	3 deg
Twist	0
Angle of chord line to fuselage datum	+2·50 deg
Sweepback of quarter-chord line :	
From centre-line to ' break '	2·00 deg
From ' break ' to 17·00 ft from centre-line	2·50 deg
Distance of mean quarter-chord point in front of 39 per cent chord line	0·91 ft
Distance of mean quarter-chord point below fuselage datum	1·09 ft
Tailplane :	
Gross area	59·0 sq ft
Span	13·7 ft
Standard mean chord	4·30 ft
Arm (distance of mean quarter-chord point of tailplane from c.g. of aircraft)	17·4 ft
Aspect ratio	3·2
Volume coefficient	0·742
Ratio of gross tailplane area to gross wing area	0·261
Normal setting relative to wing chord	—0·25 deg
Dihedral	10 deg
Height of mean quarter-chord point above c.g. (measured perpendicular to s.m.c.)	2·21 ft
Thickness ratio	9 per cent
Position of maximum thickness	40 per cent
Elevators :	
Type of balance	Horn
Area aft of hinge line	17·4 sq ft
Area of horn	1·4 sq ft
C.G. position :	
Distance behind leading edge of standard mean chord	0·390$\bar{c}$
Distance above standard mean chord	0·123$\bar{c}$
Distance behind leading edge of wing root chord	0·506$\bar{c}$
Distance above wing root chord	0·173$\bar{c}$
Weight :	
Assumed all-up weight	10,500 lb
Dive-recovery flaps :	
Angle of flap	40 deg
Chord	0·5 ft
Span	2·5 ft
Position of hinge line	28 per cent of local chord

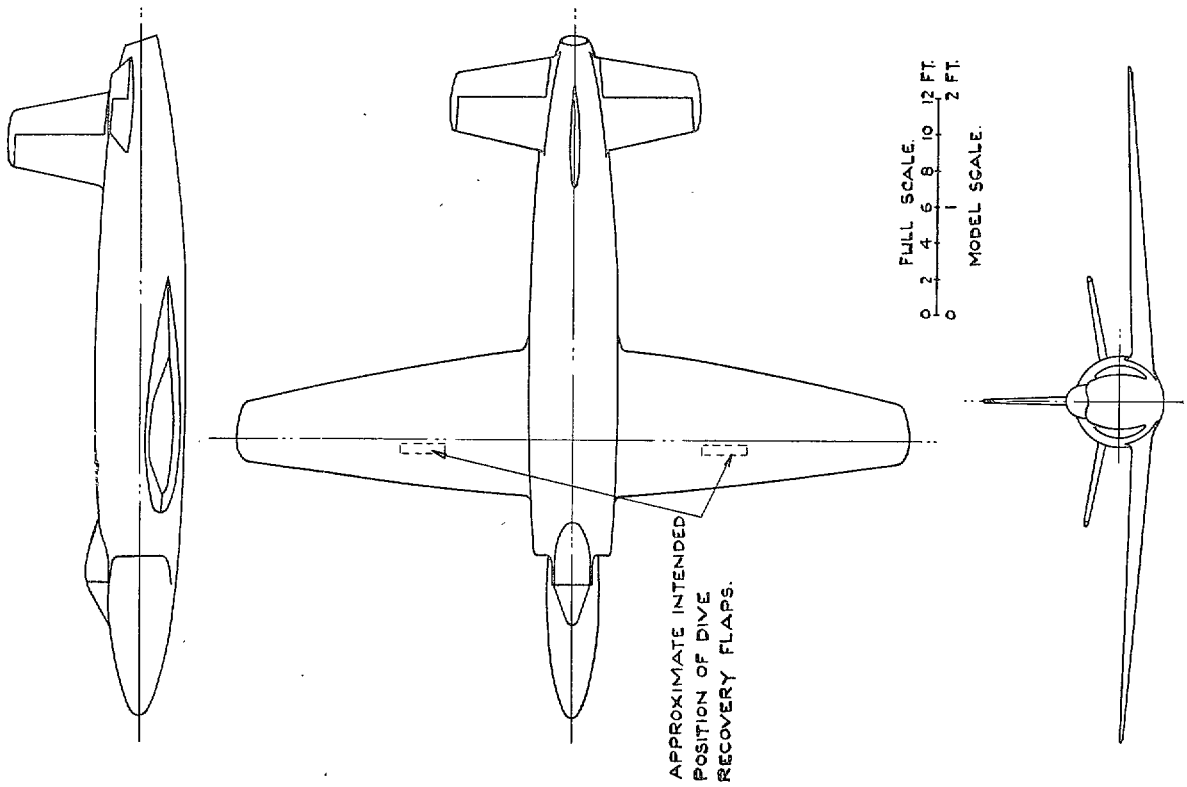

FIG. 1. Attacker (E.10/44).

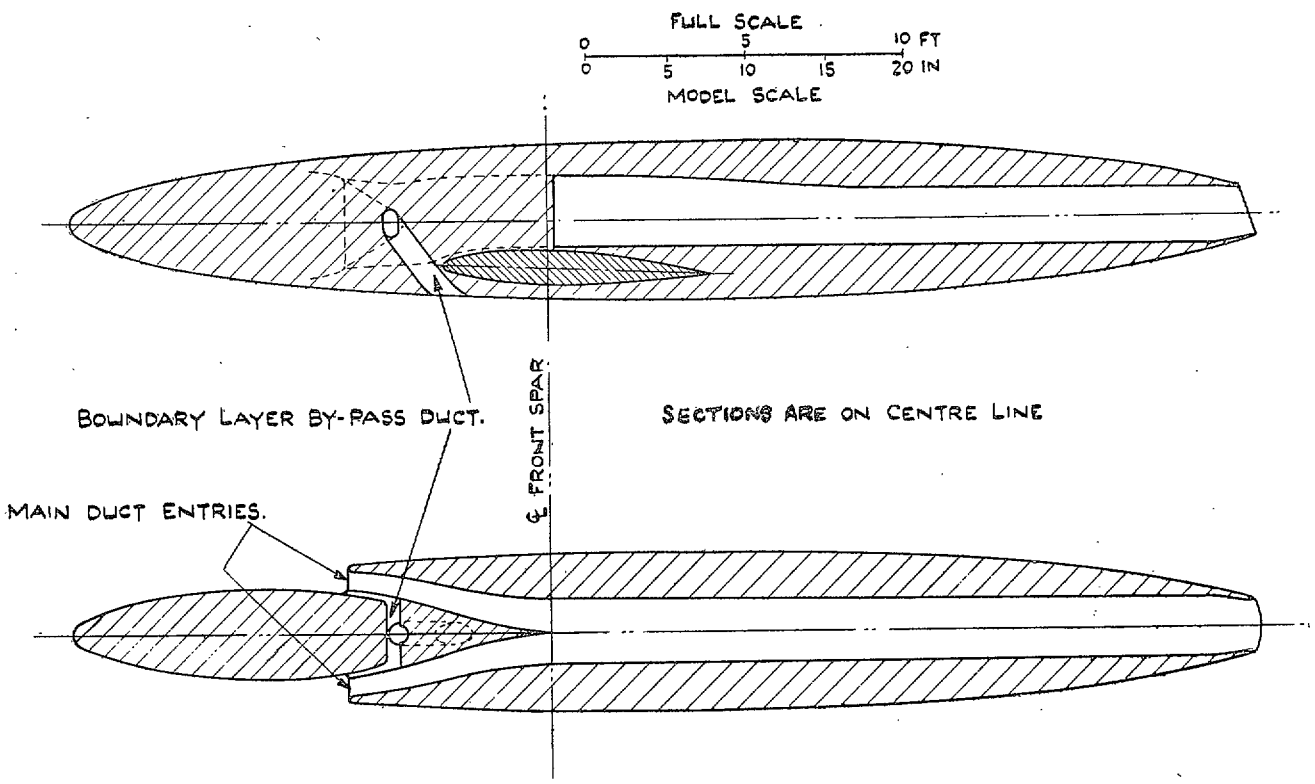

FIG. 2. Ducting on $\frac{1}{6}$-scale model of Attacker.

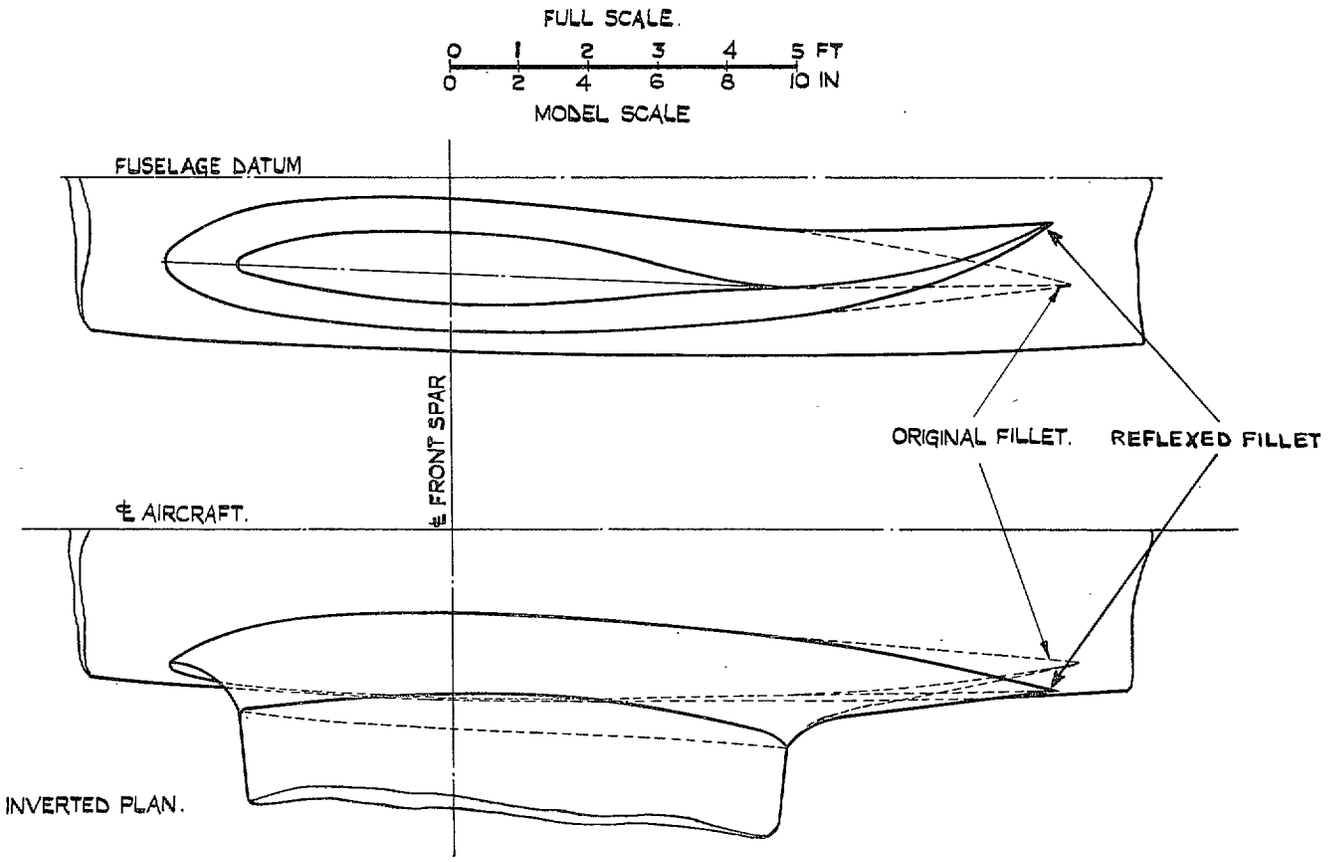

FIG. 3. Original and reflexed fillets.

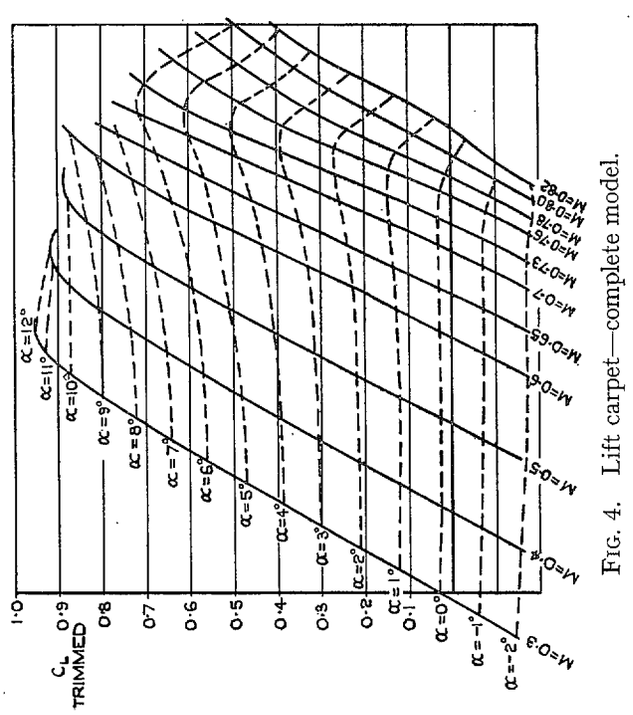

FIG. 4. Lift carpet—complete model.

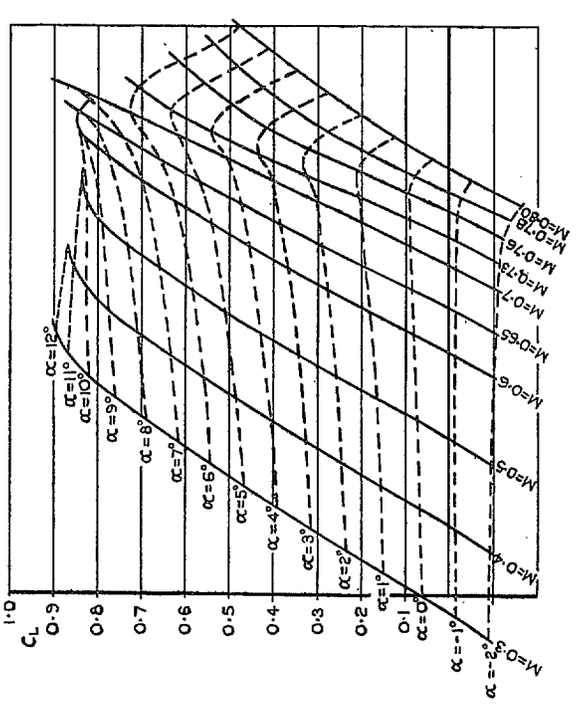

FIG. 5. Lift carpet—wing only.

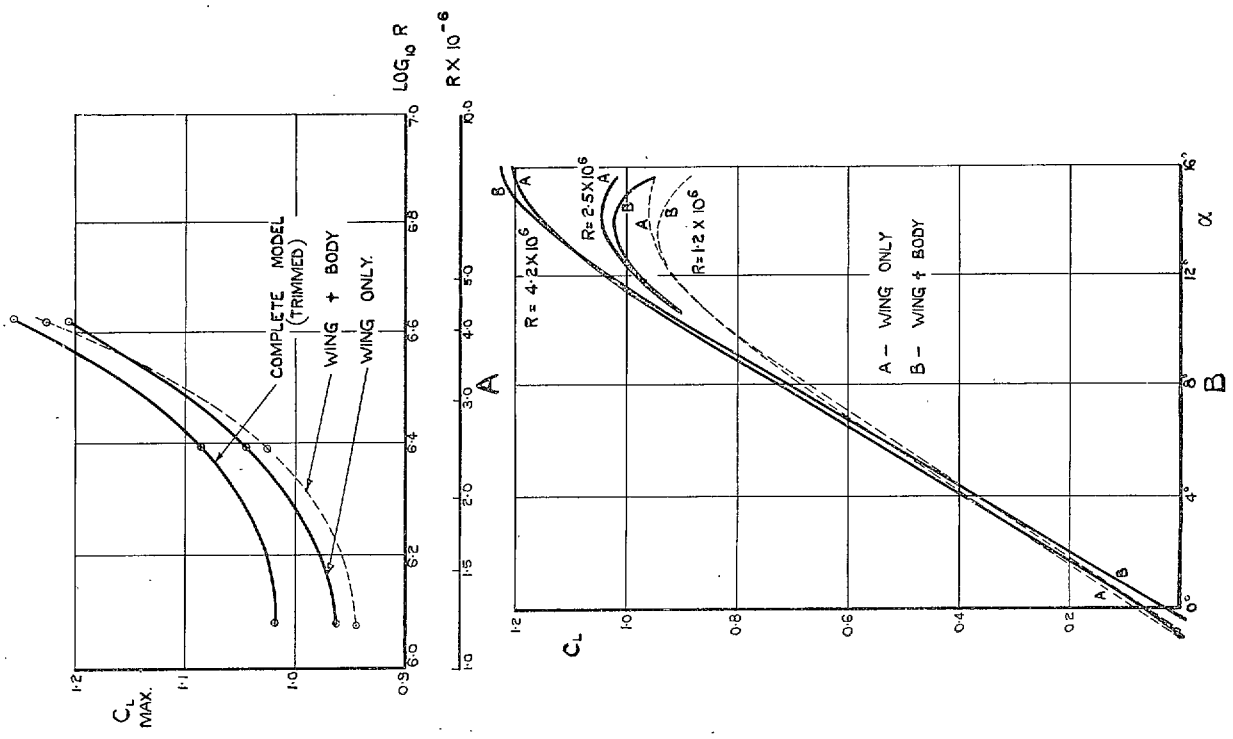

FIG. 6. Lift curves at low speeds ($M < 0 \cdot 2$).

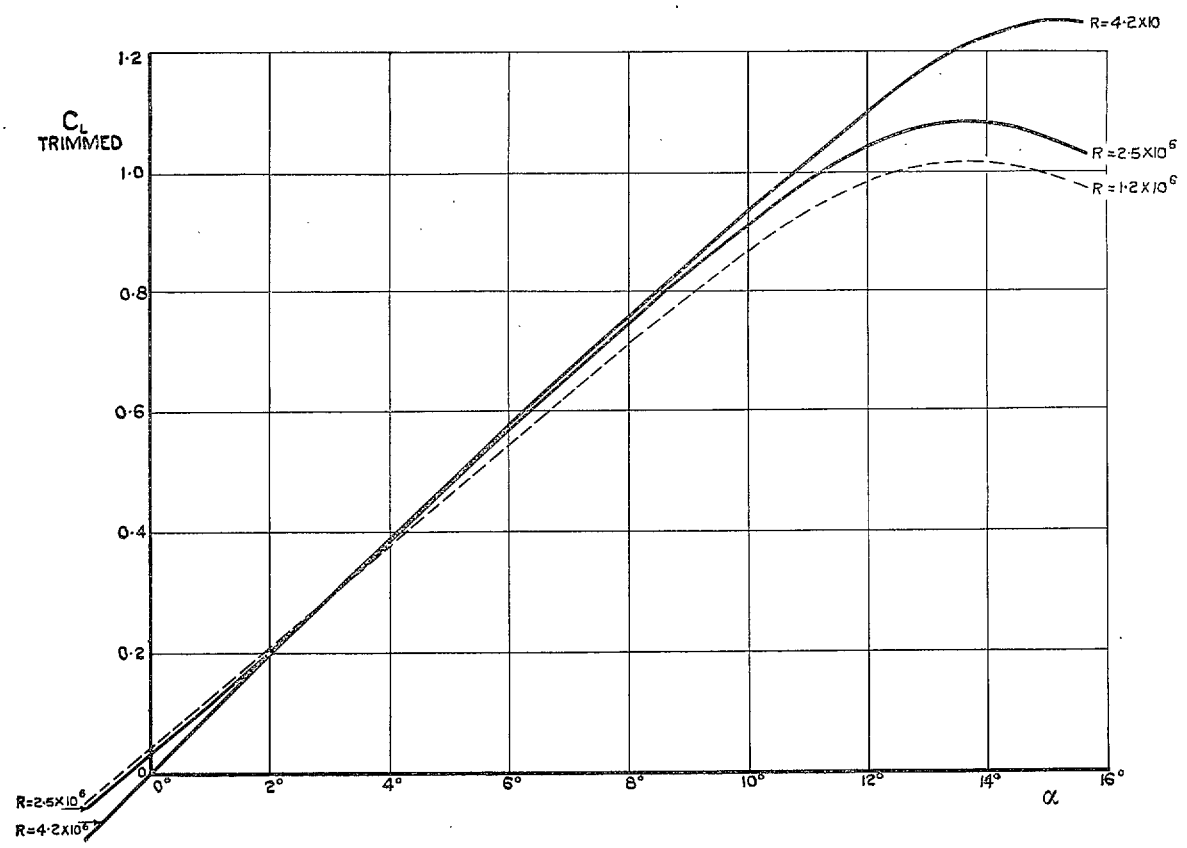

FIG. 7. Complete model—lift curves at low speeds ($M < 0 \cdot 2$).

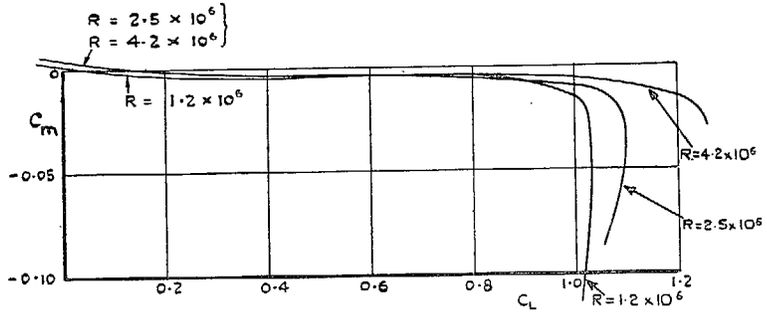

FIG. 8. Pitching-moment curves at low speeds ($M < 0{\cdot}2$)—model with tail ($\eta_T = -\frac{1}{4}$ deg, $\eta = 0$ deg.)

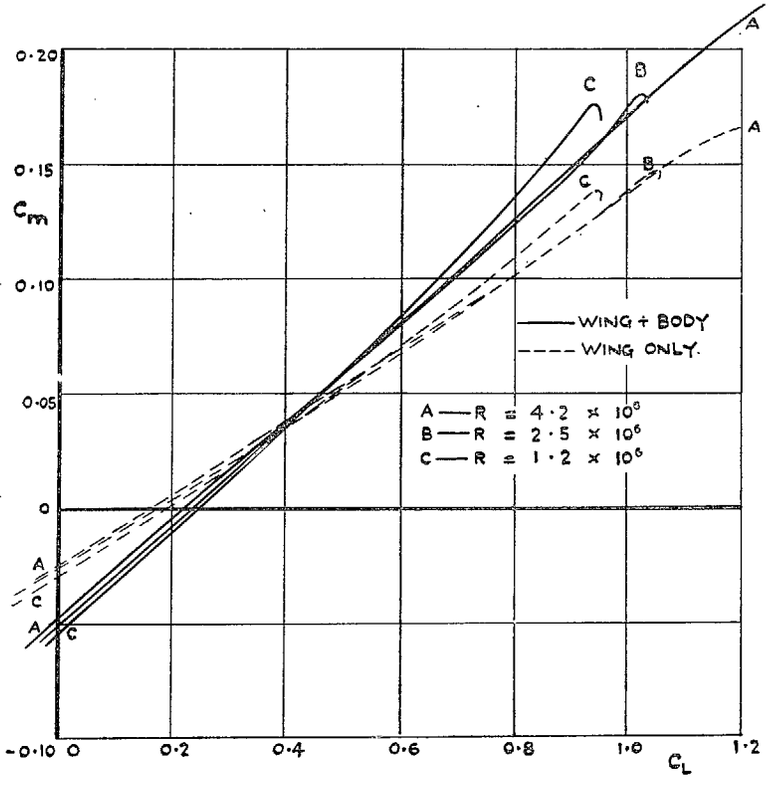

FIG. 9. Pitching-moment curves at low speeds ($M < 0{\cdot}2$)—model without tail.

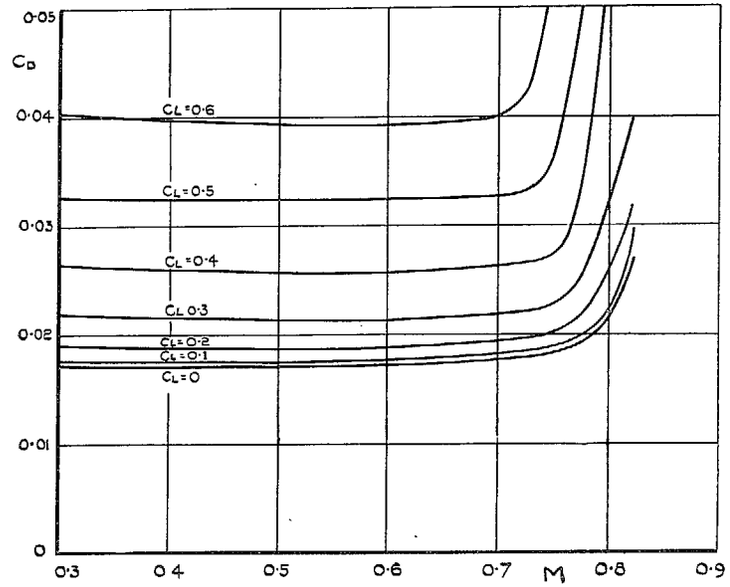

FIG. 10. Effect of Mach number on drag—complete model.

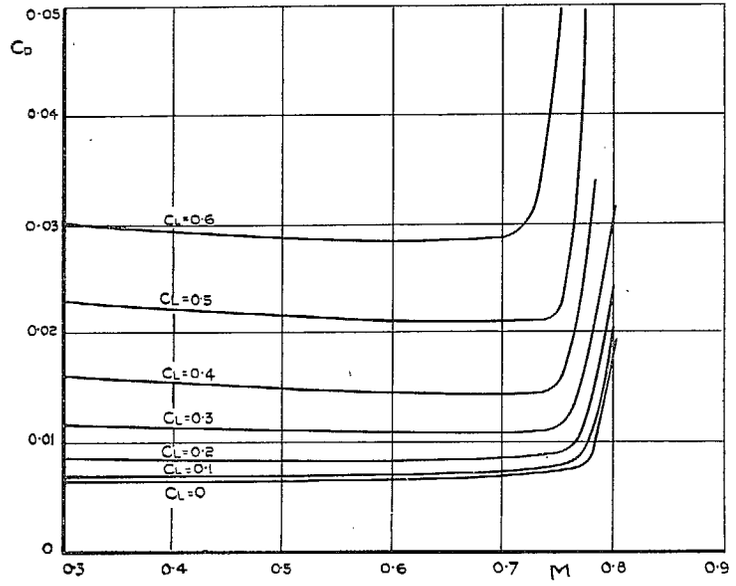

FIG. 11. Effect of Mach number on drag—wing only.

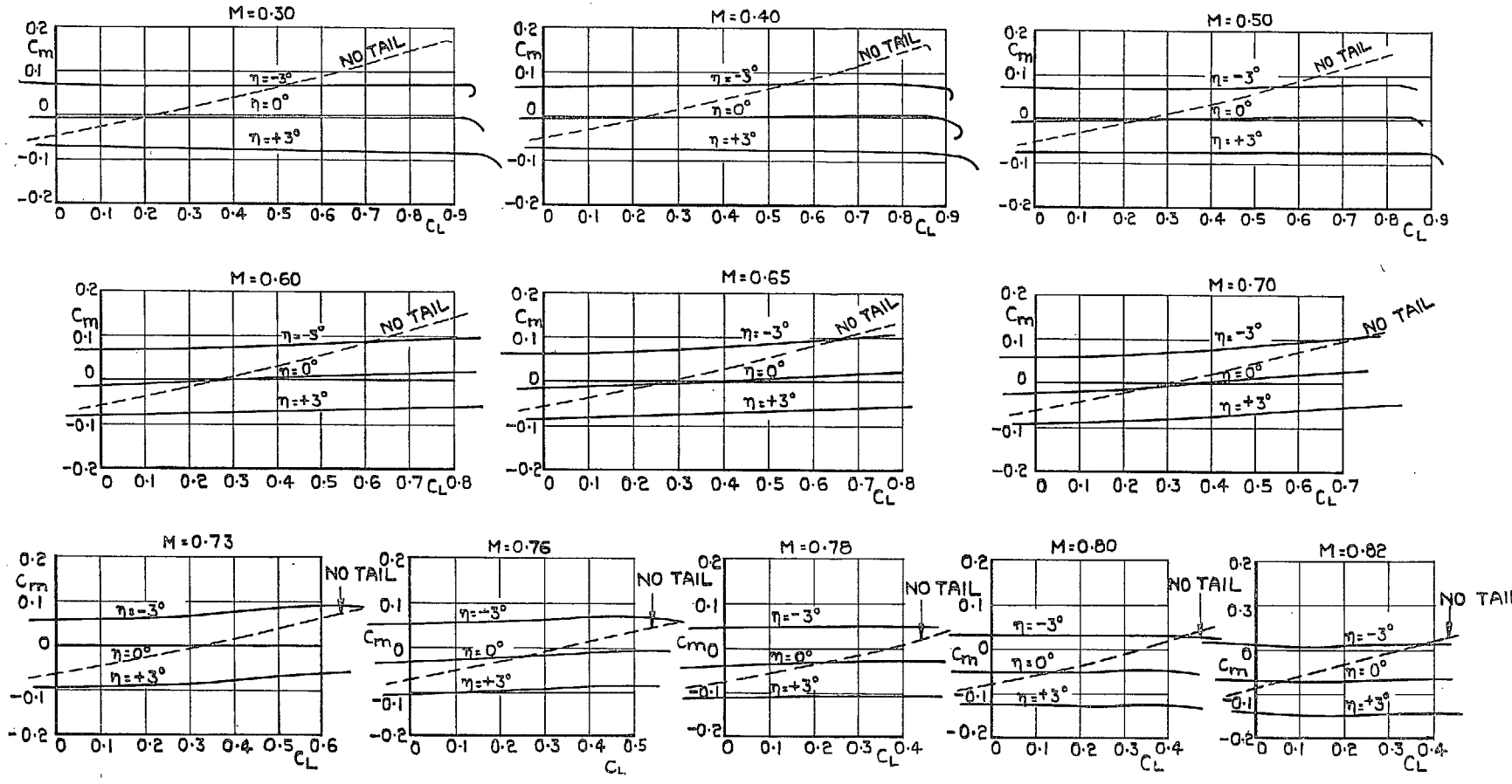

FIG. 12. Pitching-moment curves—complete model, $\eta_T = -\frac{1}{4}$ deg.

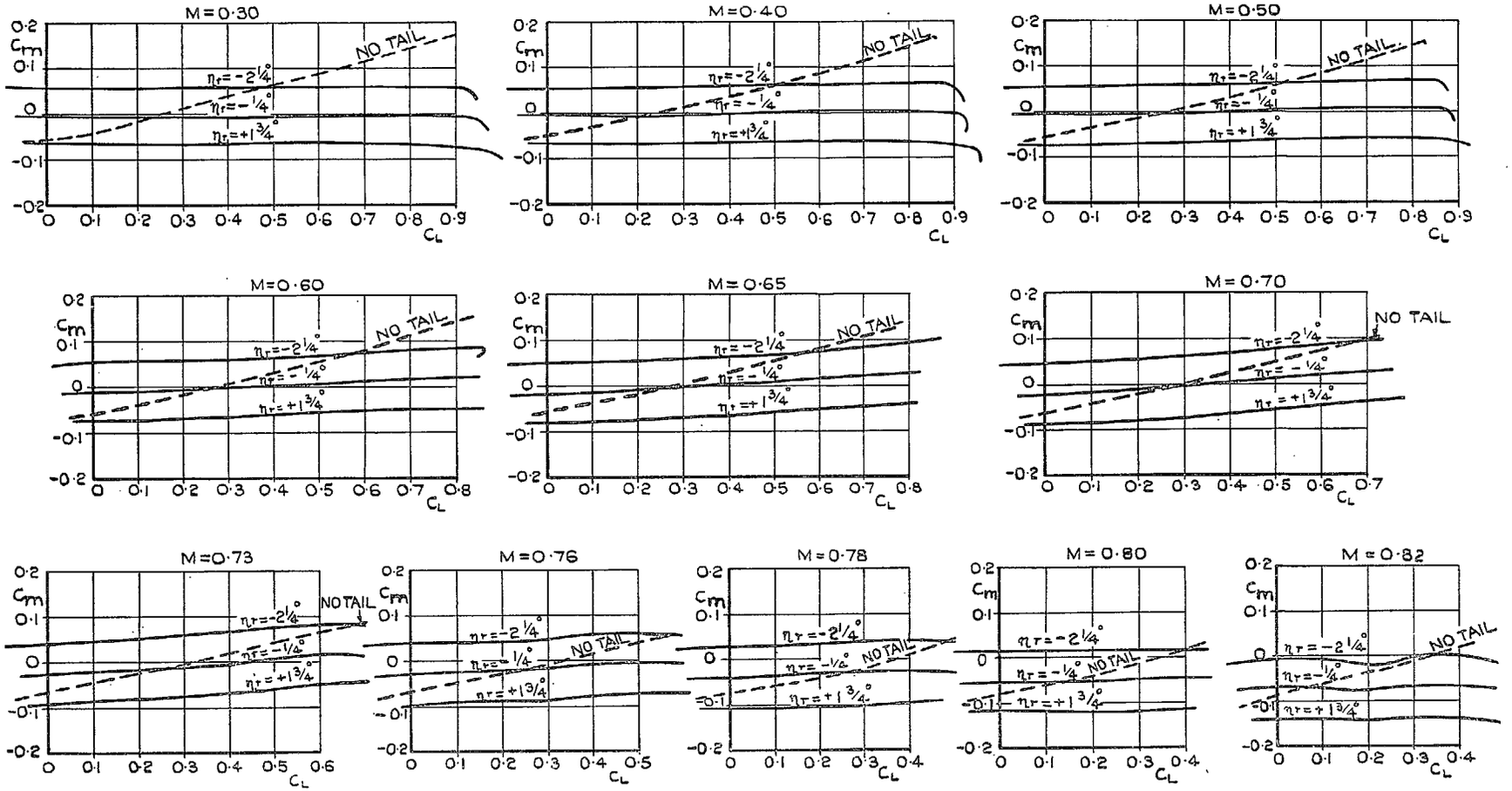

FIG. 13. Pitching-moment curves—complete model, $\eta = 0$.

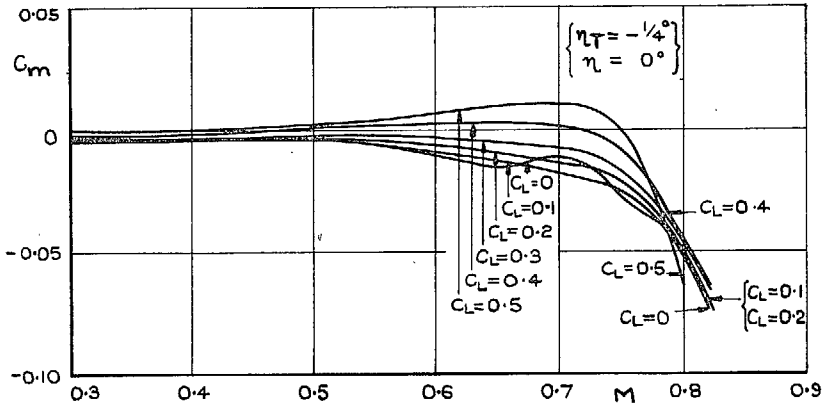

A. EFFECT OF MACH Nº ON PITCHING MOMENT
COMPLETE MODEL, ORIGINAL FILLETS.

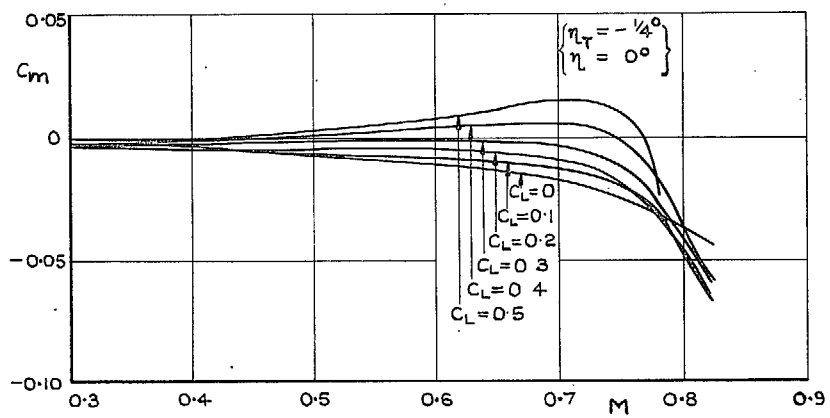

B. EFFECT OF MACH Nº ON PITCHING MOMENT
COMPLETE MODEL, REFLEXED FILLETS.

FIG. 14.

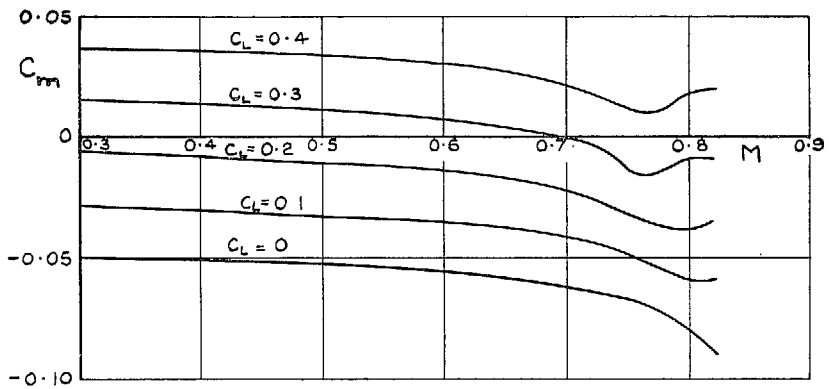

A. EFFECT OF MACH Nº ON PITCHING MOMENT
ORIGINAL FILLETS
MODEL COMPLETE EXCEPT FOR TAIL.

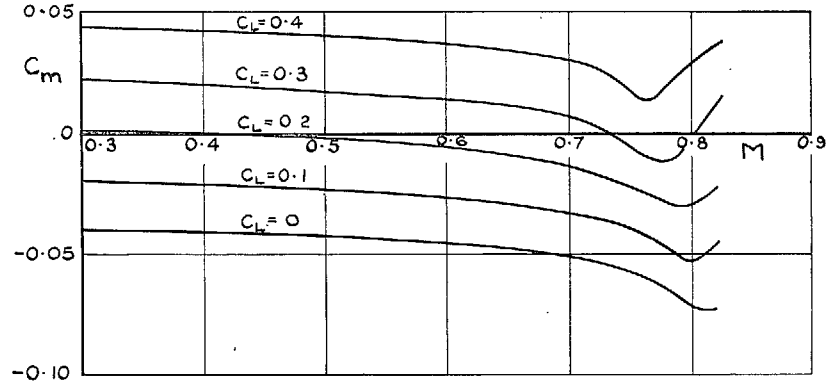

B. EFFECT OF MACH Nº ON PITCHING MOMENT
REFLEXED WING ROOT FILLETS
MODEL COMPLETE EXCEPT FOR TAIL

FIG. 15.

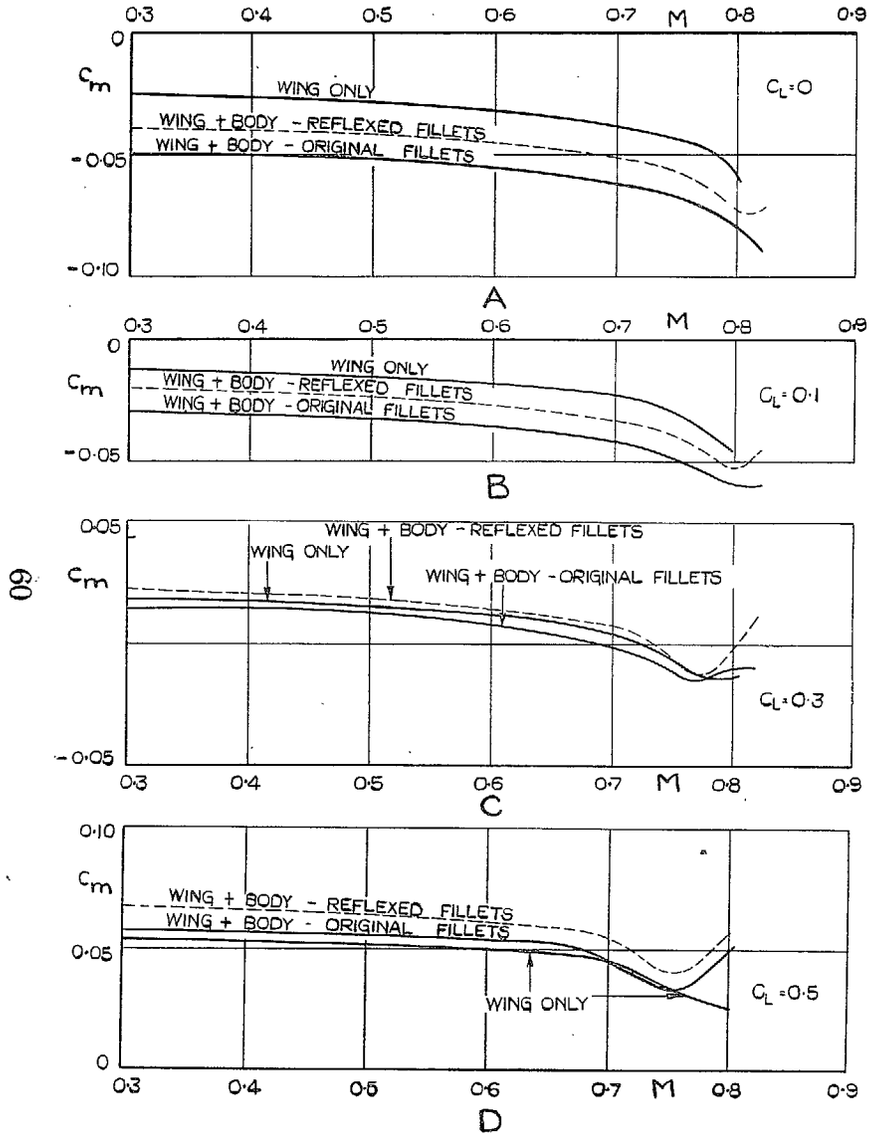

FIG. 16. Effect of fillets and body on pitching moment.

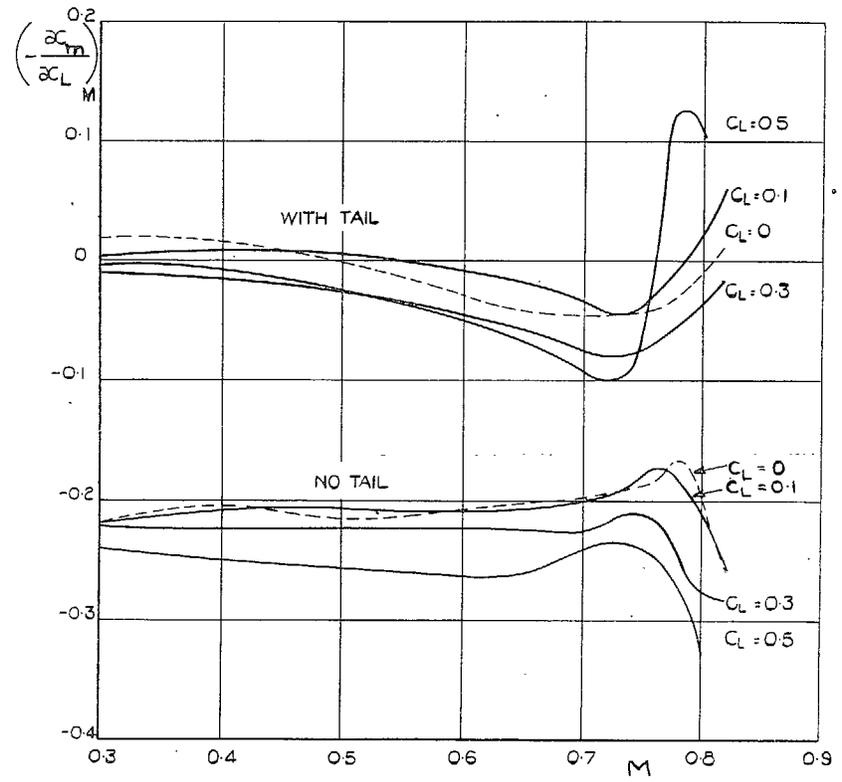

FIG. 17. Effect of Mach number on $(-\partial C_m/\partial C_L)_M$, complete model, original fillets.

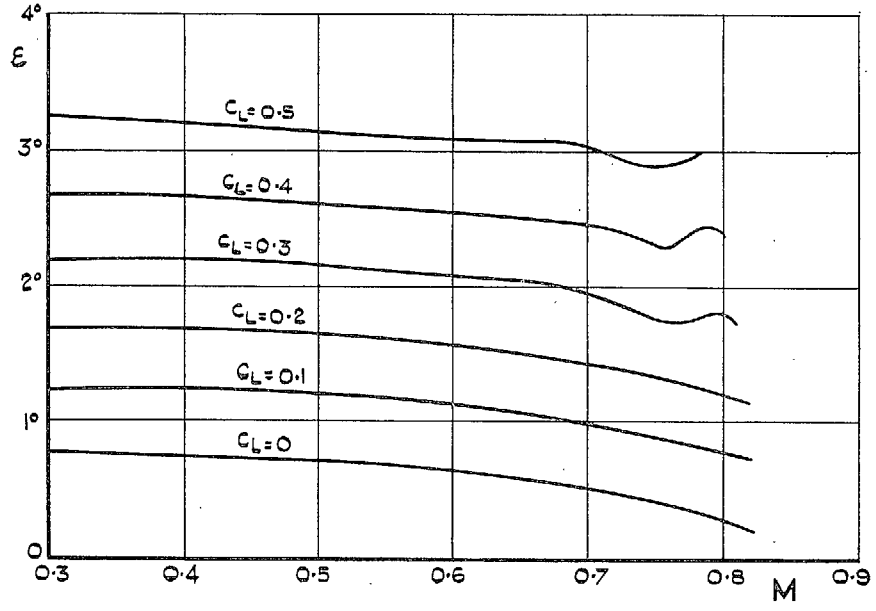

FIG. 18. Effect of Mach number on downwash angle at tail.

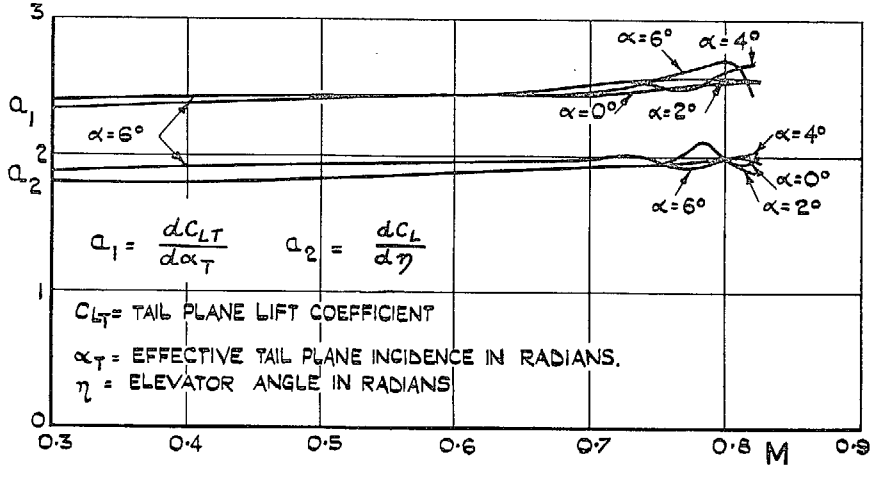

FIG. 19. Effect of Mach number on tailplane lift gradients.

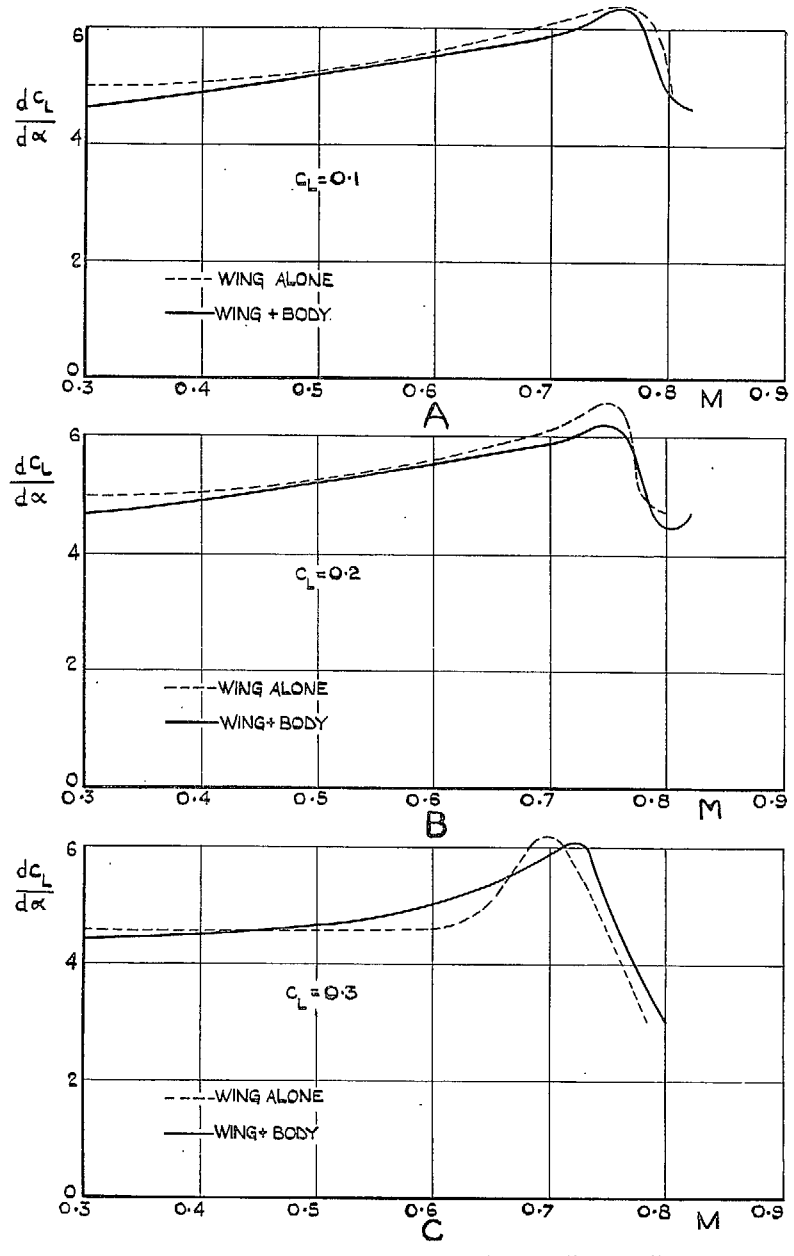

FIG. 20. Effect of Mach number on lift gradients.

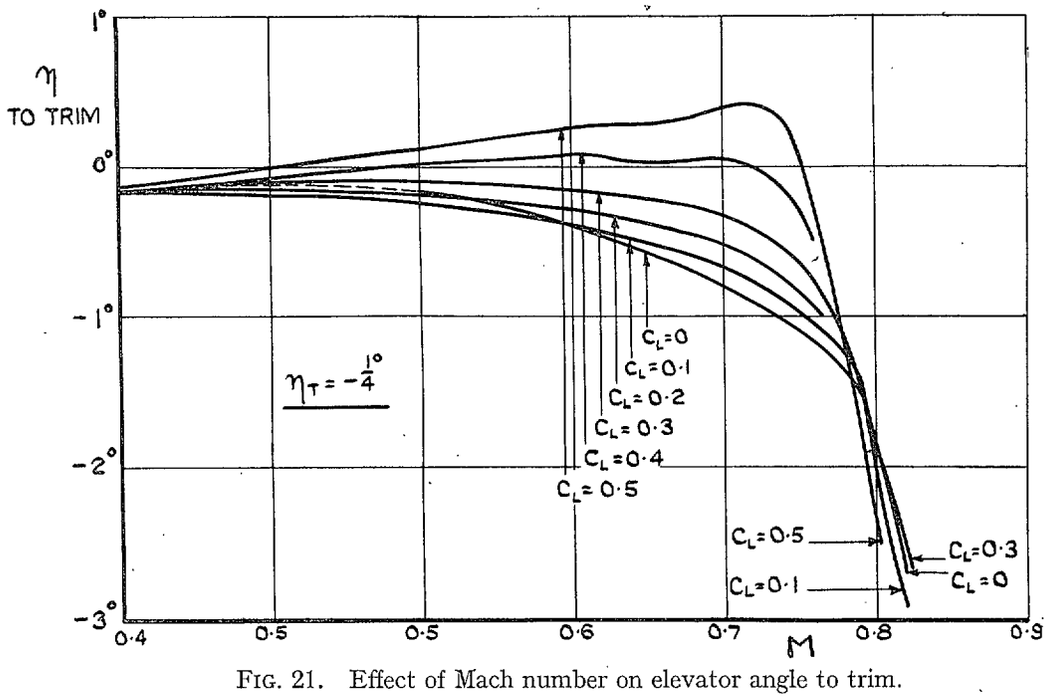

FIG. 21. Effect of Mach number on elevator angle to trim.

PART V

Tests on the Mustang I

By

J. Y. G. Evans, B.Sc., J. Caldwell, B.Sc., Wh.Sch., A.M.I.Mech.E. and C. M. Britland

1. *Introduction.*—The Mustang I is a low-wing, single-engine fighter aircraft of U.S.A. design. Leading dimensions are given in Table 1. Fig. 1 shows the general arrangement of the aircraft and Figs. 2 and 3 give sections of the wing and tailplane.

Tests were made on a $\frac{1}{6}$-scale model for comparison with measurements in flight[1] and in another high-speed wind-tunnel in the U.S.A.

2. *Experimental Details.*—The model was made of wood, except that the radiator flap and baffle plate were of metal. The baffle was a slotted plate at the position of the radiator matrix, designed to give a baffle constant* of 4·9. In all tests the radiator flap was set at a position corresponding roughly to conditions in level flight at top speed. The air intake was represented on the model, without internal flow, but other excrescences such as the exhausts, guns, etc., were omitted. Control surface gaps were all sealed and the ailerons and rudder were at zero setting. The tests were made without a propeller.

The model for the tests on the wing alone had a centre-section formed by extrapolation of the wing surface near the root. This gave a considerable portion of the wing a poor aerodynamic shape for high-speed flow, the section at the centre being 15 per cent thick with 2·9 per cent camber. This should be borne in mind when interpreting the wing results.

3. *Results.*—The results are given in Figs. 4 to 21.

3.1. *Lift.*—The lift gradient begins to decrease as the Mach number exceeds about 0·68, but the decrease is fairly gradual and even at $M = 0{\cdot}8$ the lift gradient is not much less than at low speed (Figs. 4, 5 and 13).

For a given incidence, there is a considerable loss of lift at high Mach numbers (Figs. 4 and 5). The zero-lift incidence is about 2 deg greater at $M = 0{\cdot}8$ than at low speed. This is a greater change of no-lift angle than is usually found in high-speed tunnel tests on conventional fighter aircraft, and may be due to the relatively large camber of the inboard sections of the wing.

Fig. 18 shows that the maximum lift coefficient increases with Reynolds number, reaching a value for the trimmed aircraft of 1·35 at $R = 4 \times 10^6$. There is some scale effect on lift gradient at Reynolds numbers between 1×10^6 and $2{\cdot}5 \times 10^6$.

The effects of Mach number and Reynolds number on the lift coefficient of the wing are generally similar to the effects found on the complete model.

3.2. *Drag.*—Fig. 6 shows a gradual increase of drag coefficient with Mach number up to $M = 0{\cdot}7$, both for the complete model and for the wing. This gradual increase may be due to movement of transition point with increasing tunnel speed and thus may not be applicable to full-scale conditions.

The drag coefficient of the complete model at zero lift increases rapidly with Mach number above about $M = 0{\cdot}73$.

---

* *See* footnote on page 15.

3.3. *Pitching Moment.*—The pitching moment without tail (Fig. 10) is proportional to the force on the tailplane required to trim. With increasing Mach number, up to the limit of the present tests, there is no very large increase of tail load in steady flight, the compressibility rise up to $M = 0{\cdot}75$ being followed by a decrease, and the load may even fall to zero at a Mach number a little above $M = 0{\cdot}8$.

Fig. 12 shows the elevator angles required to trim, plotted against Mach number. A comparison of Figs. 9 and 10 at the lower lift coefficients shows that with increasing Mach number up to the lift critical an increase in nose-down moment for the wing plus body is balanced by a decrease in tailplane lift, giving no resultant change of trim with Mach number. Above the critical, the wing incidence increases rapidly to maintain constant C_L, thus decreasing the downward load on the still efficient tailplane (there is very little change of downwash with Mach number (Fig. 14)). The nose-up moment of the wing and body is insufficient to balance this nose-down change of trim due to increased tailplane lift ; hence negative elevator setting is required to trim.

3.4. *Stability.*—For C_L values below $0{\cdot}4$ the tailplane and elevator are fully effective up to Mach numbers above $0{\cdot}8$ (Figs. 15 and 16).

The manoeuvre margin[2] H_m is given by

$$H_m = -\left(\frac{\partial C_m}{\partial C_L}\right)_M + K\rho a_1,$$

where K is a constant for any aircraft. The tailplane lift-curve slope a_1 has been shown to change very little with Mach number, hence at any given altitude the variation of H_m with Mach number is given by that of $(-\partial C_m/\partial C_L)_M$. This derivative (Fig. 17) decreases gradually up to about $M = 0{\cdot}68$ and then increases rapidly, *i.e.* the aircraft requires more ' stick movement per g ' at very high Mach numbers.

4. *Comparison of Flight and Tunnel Tests.*—4.1. *Drag.*—Drag curves obtained from N.A.C.A. and R.A.E. flight and tunnel tests have been plotted together in Fig. 22. The N.A.C.A. tunnel tests were made in the 16-ft. diameter atmospheric tunnel at the Ames Aeronautical Laboratory.

The Reynolds number and turbulence differ considerably between the various tests, so that no exact agreement can be expected. Also it was found in the R.A.E. flight tests that the lowering of a small spoiler flap immediately ahead of the radiator, intended to block the radiator entry during glides and dives, greatly decreased the drag at the higher Mach numbers. The flight results with and without this flap lowered have been given in Fig. 26. It is not known at the time of writing whether the N.A.C.A. tunnel tests were made with the flap up or down, or if any such drag differences have been observed in the U.S.A. The R.A.E. tunnel tests were all made with the flap in the normal (raised) position.

At sub-critical Mach numbers the drag coefficient of the R.A.E. tunnel model is about $0{\cdot}004$ lower than that found in the other tests. This difference may possibly be attributed to excrescences on the full-scale aircraft and on the N.A.C.A. tunnel model which were omitted in the present tests. Further, although the turbulence in the R.A.E. high-speed tunnel is fairly high, the Reynolds number is low and it is possible that the transition point was further back in the R.A.E. tunnel than in the other tests. The N.A.C.A. flight and tunnel results agree regarding the Mach number at which the drag rise starts, but this is about $0{\cdot}03$ lower than that shown by the R.A.E. flight and tunnel results. At Mach numbers above the critical value, the R.A.E. results show a steeper drag rise than the N.A.C.A. ones.

In general, the agreement is good over the Mach number range considered.

4.2. *Elevator Angle to Trim.*—Fig. 23 gives elevator angles to trim plotted against Mach number from the N.A.C.A. and R.A.E. wind tunnels and from the R.A.E. flight tests (with spoiler flap closed). The lift coefficients differ slightly between the tests and no exact comparison can be expected but there is a common tendency for a nose-down change of pitching moment at the higher Mach numbers. The R.A.E. flight and tunnel curves are in good agreement, but the trim change occurs rather later and is less severe in the N.A.C.A. tunnel results.

5. *Conclusions.*—The measurements of drag and elevator angle to trim at high Mach numbers agree fairly well with measurements made in flight at the R.A.E., but the agreement with flight and tunnel tests by the N.A.C.A. is not as good.

TABLE 1

Leading Dimensions, Full Scale

(Model scale = $\frac{1}{6}$)

Wing:		
Gross area S		237·0 sq ft
Span b		37·15 ft
Standard mean chord $\bar{c}$		6·39 ft
Aspect ratio A		5·8
Root chord (0·040 b outboard from aircraft centre-line)		8·71 ft
Tip chord (0·482 b outboard from aircraft centre-line)		4·17 ft
Station	*Thickness ratio*	*Camber*
Root	15·1 per cent at 39 per cent c.	3·0 per cent at 42 per cent c.
Tip	11·4 per cent at 50 per cent c.	0·8 per cent at 51 per cent c.
Dihedral (of quarter-chord line)		5·0 deg
Sweepback (of quarter-chord line)		0·0 deg
Angle of twist from root to tip		0·19 deg
Angle of mean chord to root chord		1·04 deg
Distance of mean quarter-chord point behind leading edge root chord		2·42 ft
Distance of mean quarter-chord point above root chord		0·67 ft
Tail plane:		
Gross area S_T		41·8 sq ft
Span b_T		13·2 ft
Mean chord $\bar{c}_T$		3·17 ft
Arm (C.G. to quarter-chord point of tail) l_T		15·85 ft.
Volume coefficient V_T		0·438
Setting to wing mean chord η_T		2·00 deg
Height of mean quarter-chord point above wing root chord		2·98 ft
Maximum thickness		10 per cent at 40 per cent c.
Elevators:		
Area aft of hinge		12·86 sq ft
Area ahead of hinge		1·44 sq ft
C.G. position:		
Distance behind leading edge root chord		2·61 ft
Distance above root chord		1·10 ft
Distance behind leading edge mean chord		0·280$\bar{c}$
Distance above mean chord		0·068$\bar{c}$

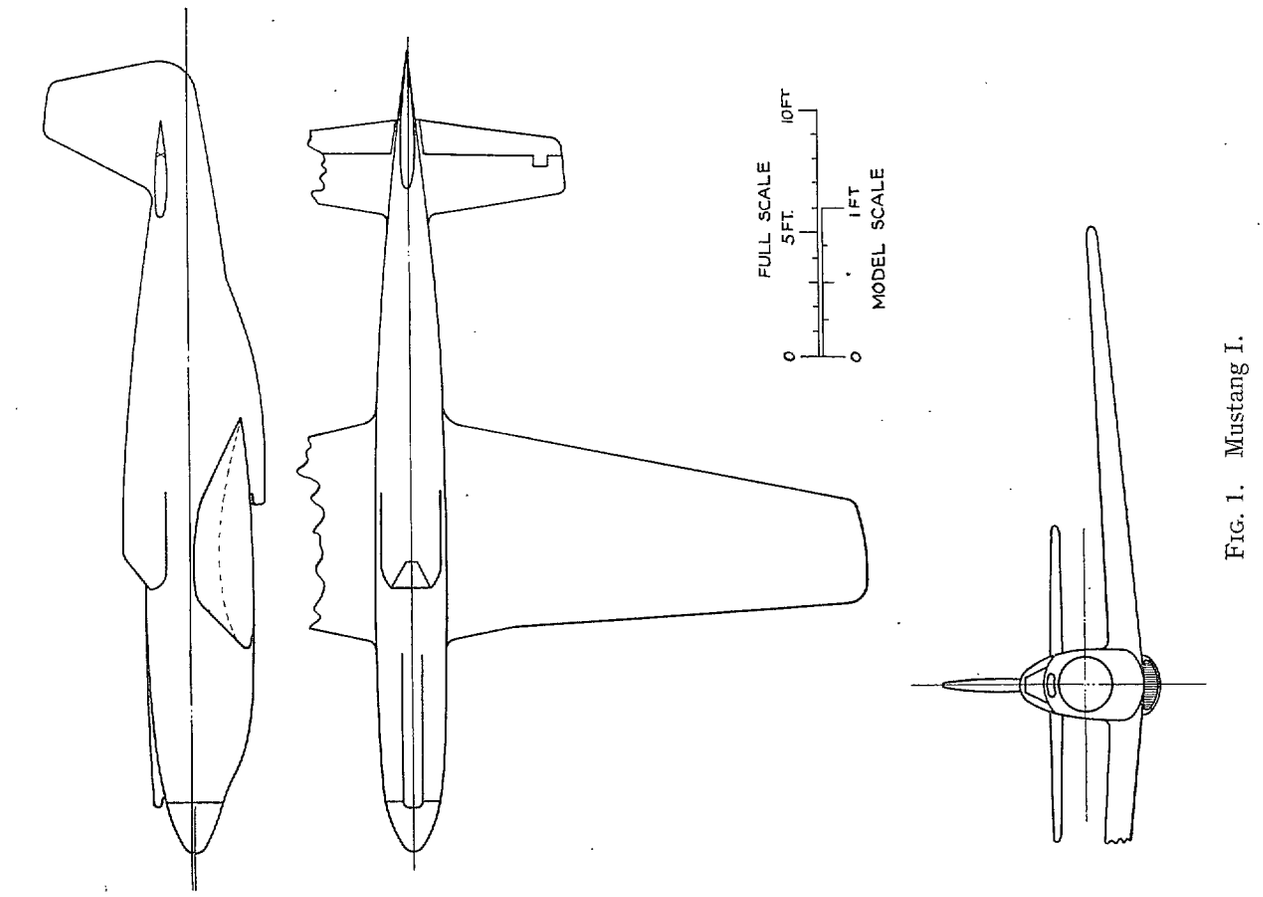

FIG. 1. Mustang I.

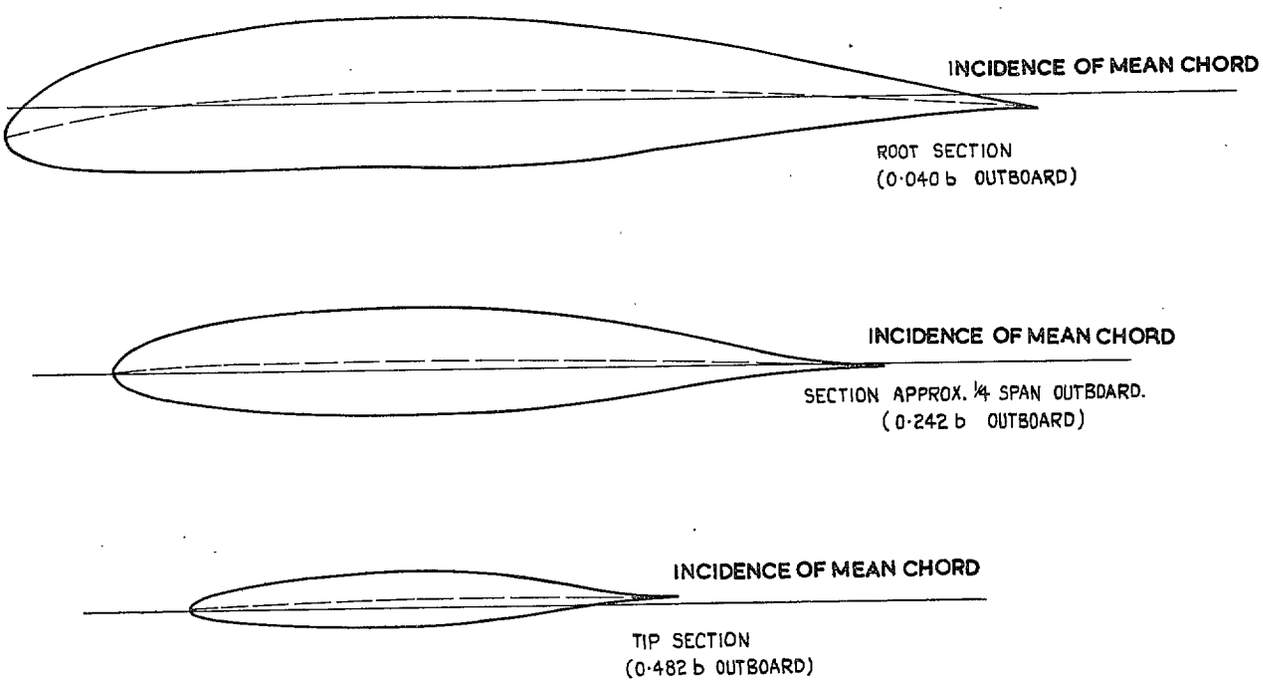

FIG. 2. Wing sections.

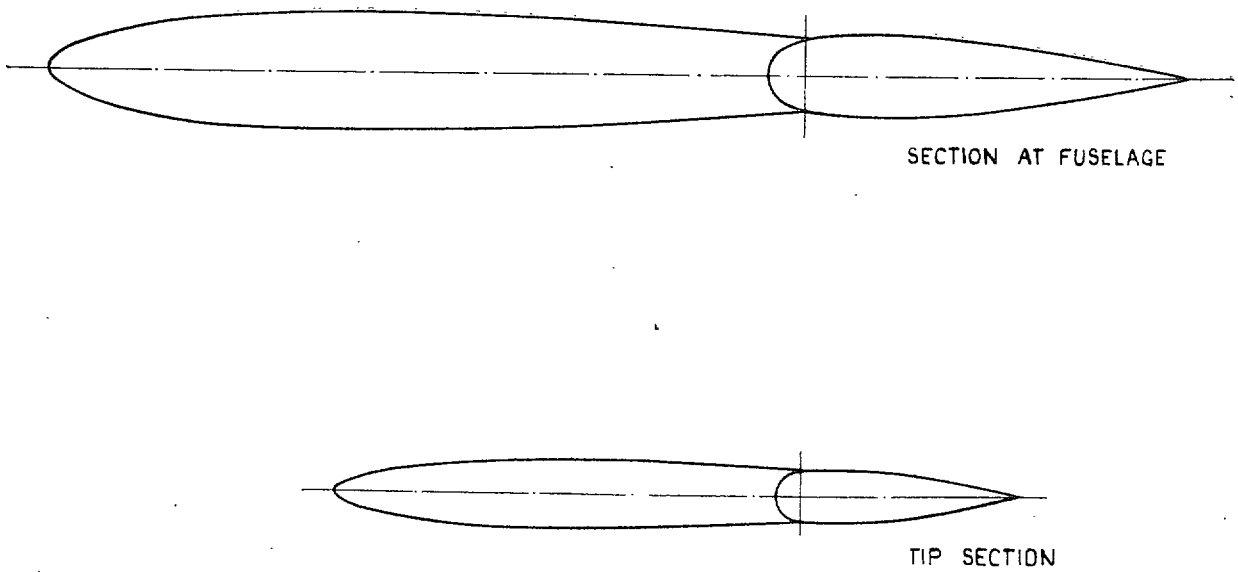

FIG. 3. Tailplane sections.

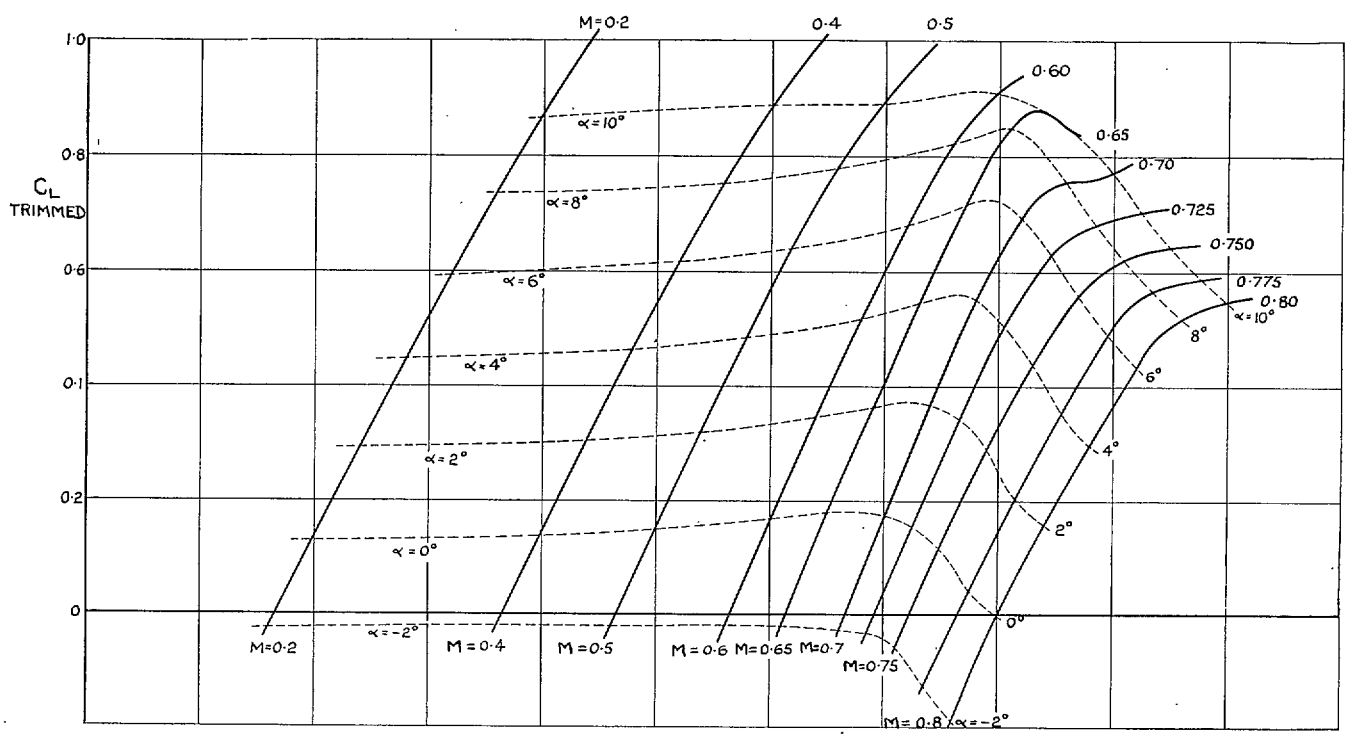

FIG. 4. Lift carpet—complete model ($R = 1 \times 10^6$).

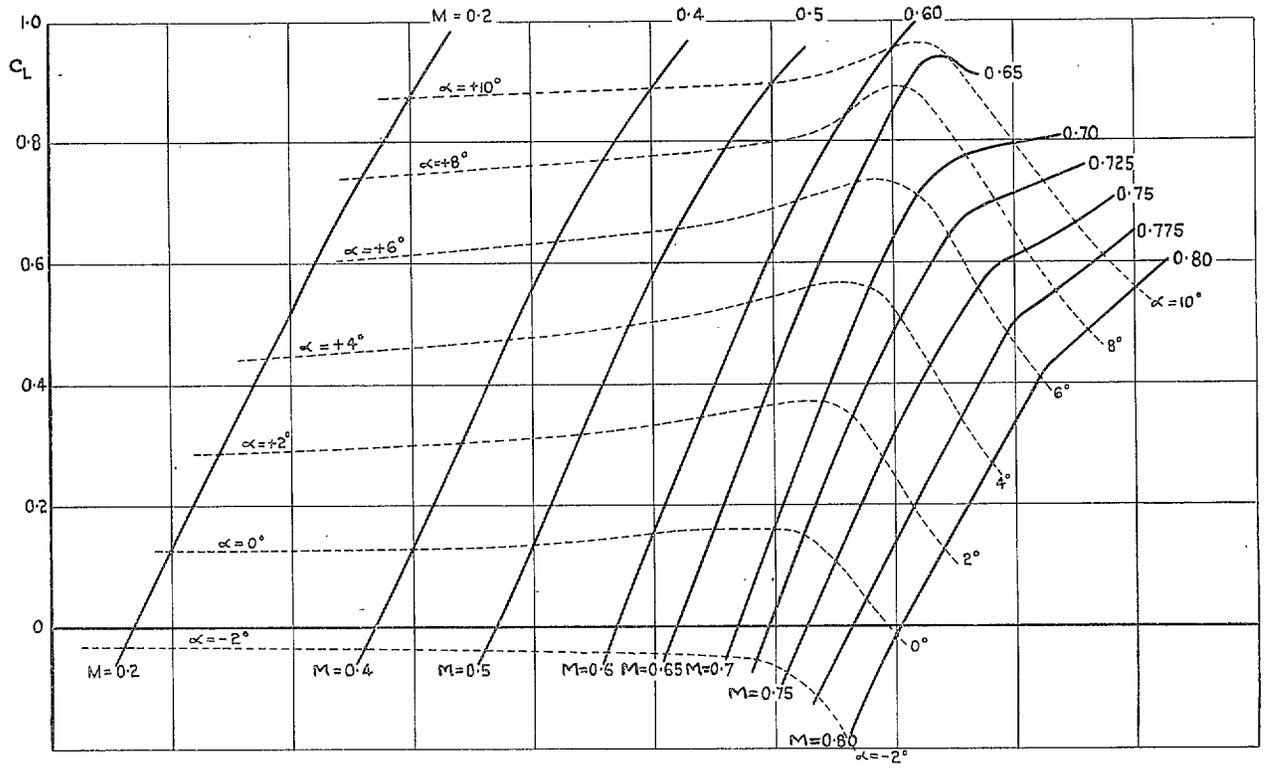

FIG. 5. Lift carpet—wing alone ($R = 1 \times 10^6$).

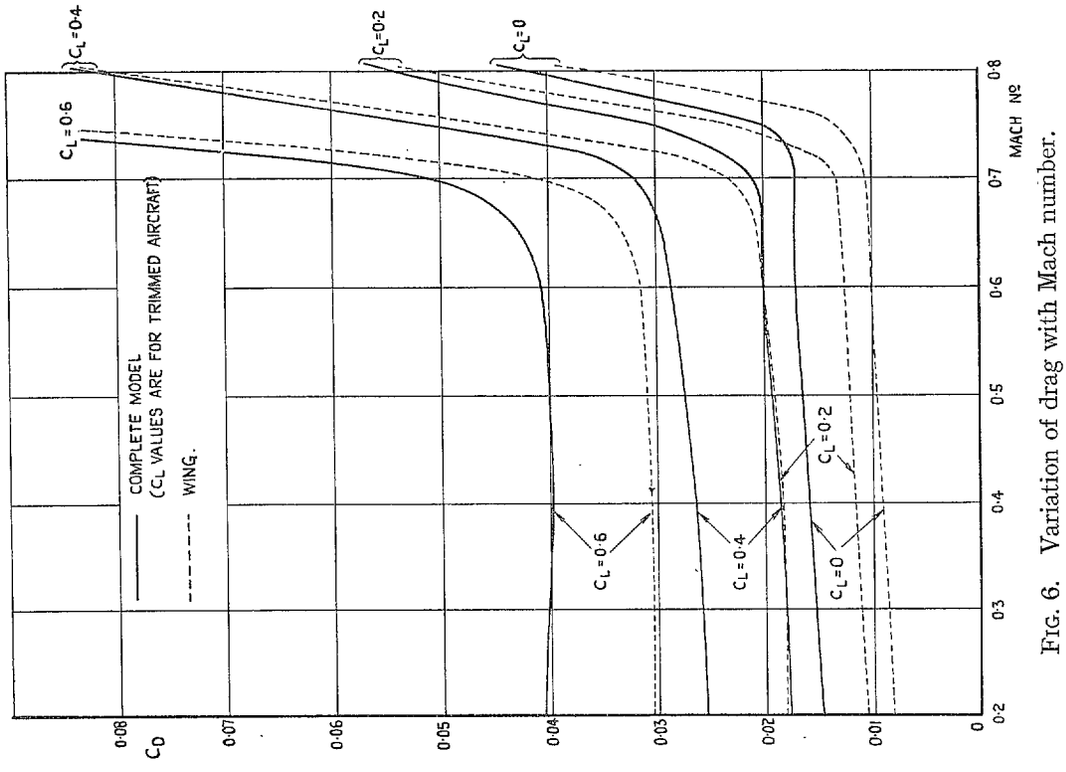

FIG. 6. Variation of drag with Mach number.

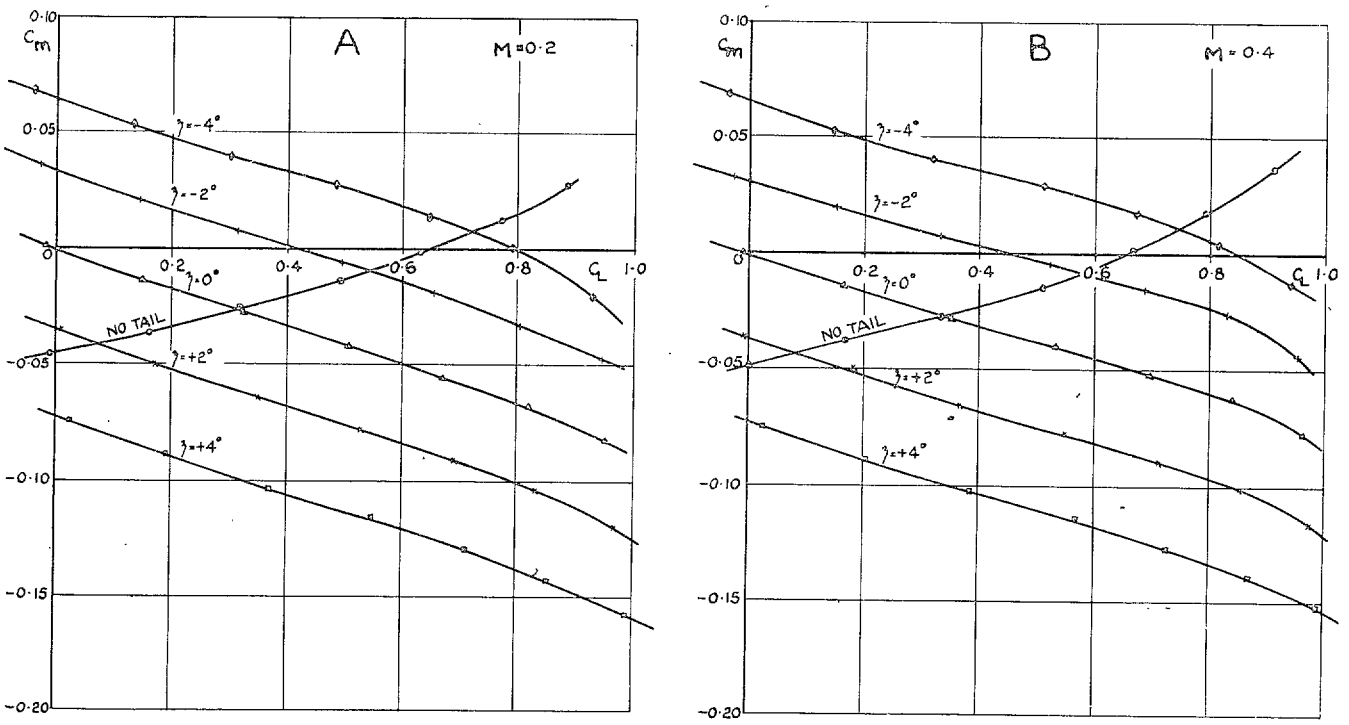

FIG. 7. Pitching moments on complete model, for constant tailplane setting ($\eta_T = 2$ deg).

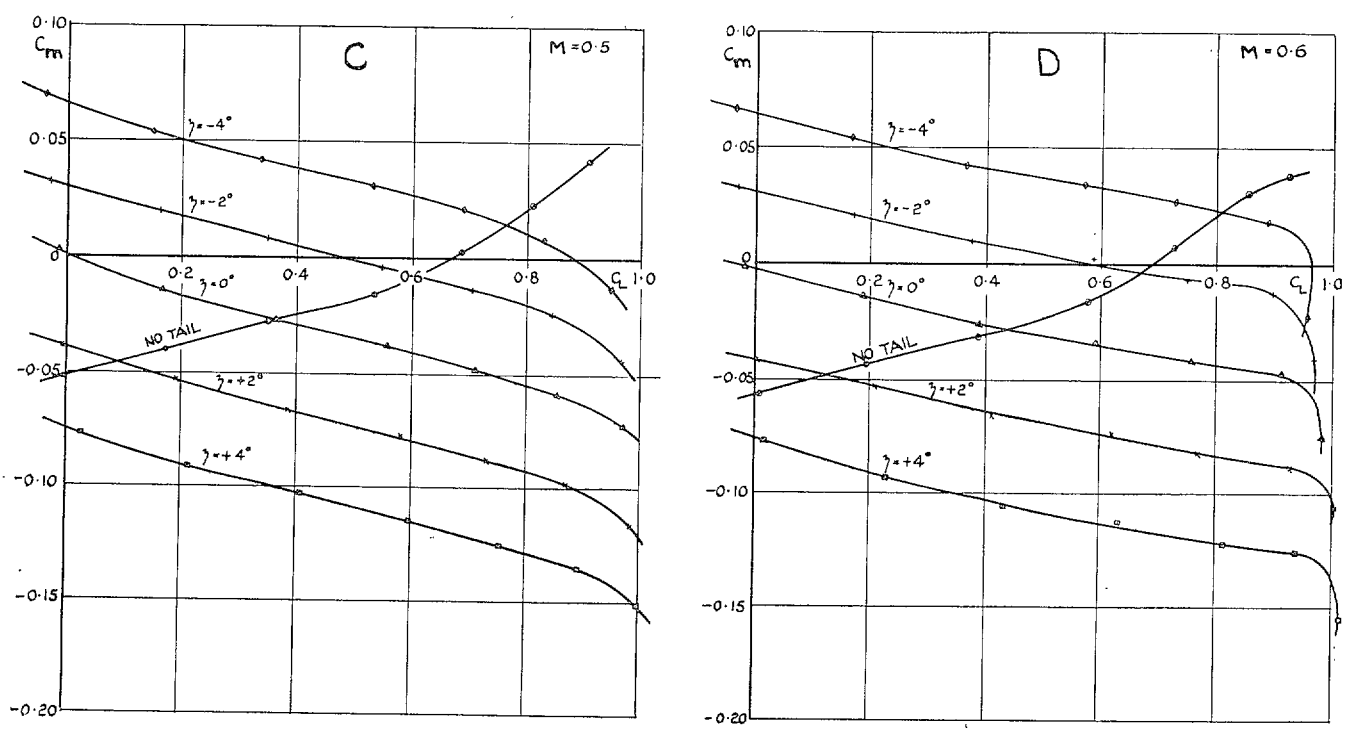

FIG. 7. Pitching moments on complete model, for constant tailplane setting ($\eta_T = 2$ deg).

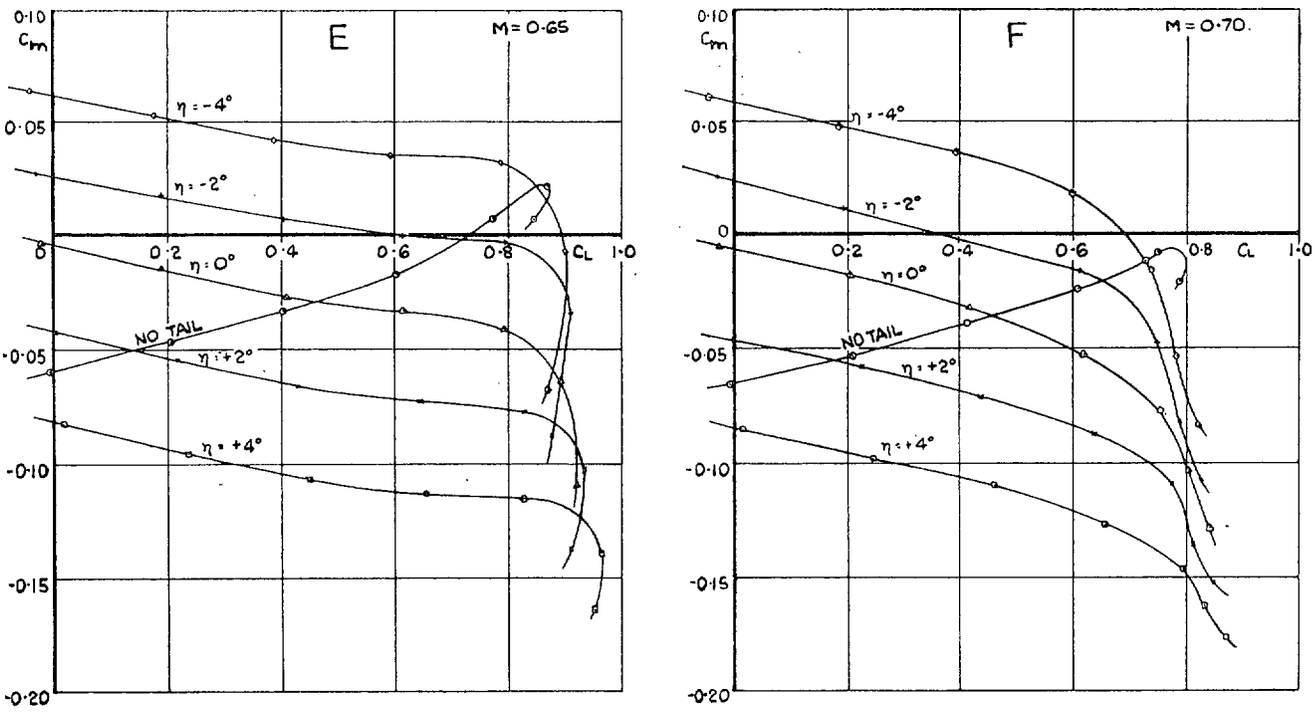

FIG. 7. Pitching moments on complete model, for constant tailplane setting ($\eta_T = 2$ deg).

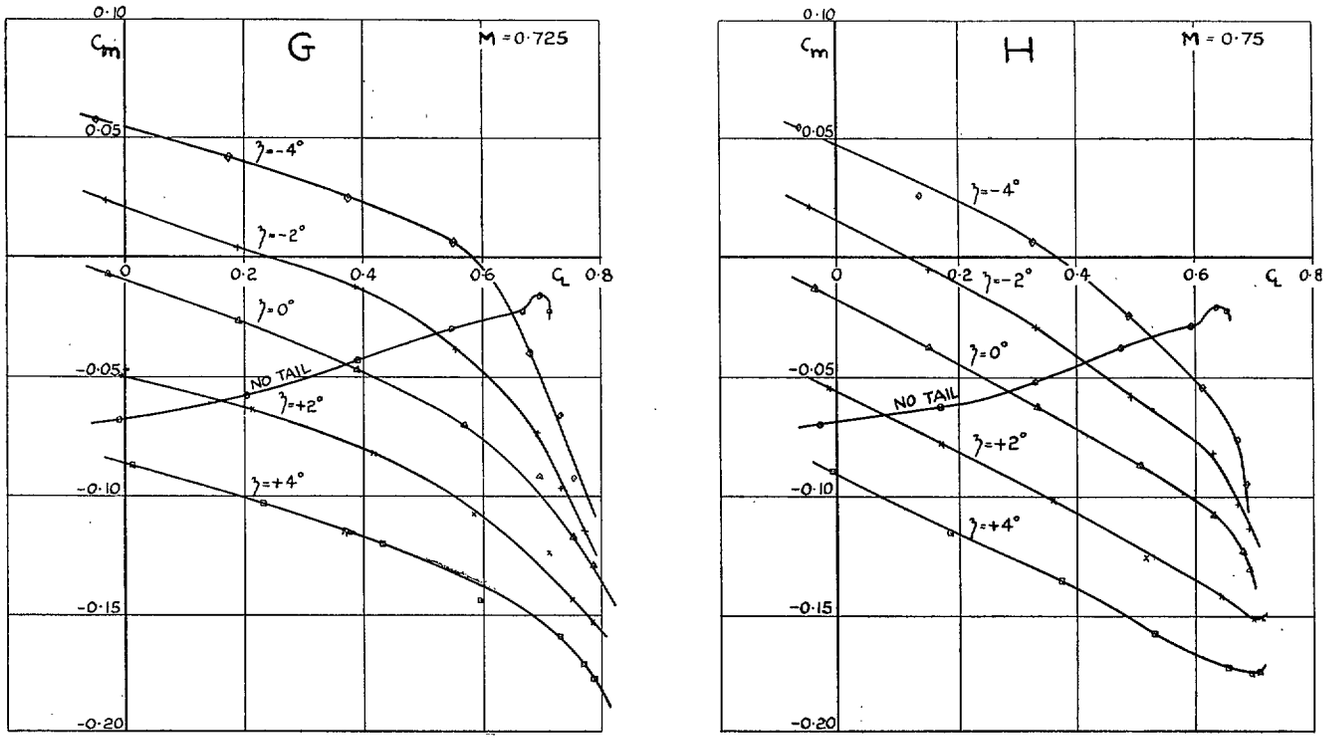

FIG. 7. Pitching moments on complete model, for constant tailplane setting ($\eta_T = 2$ deg).

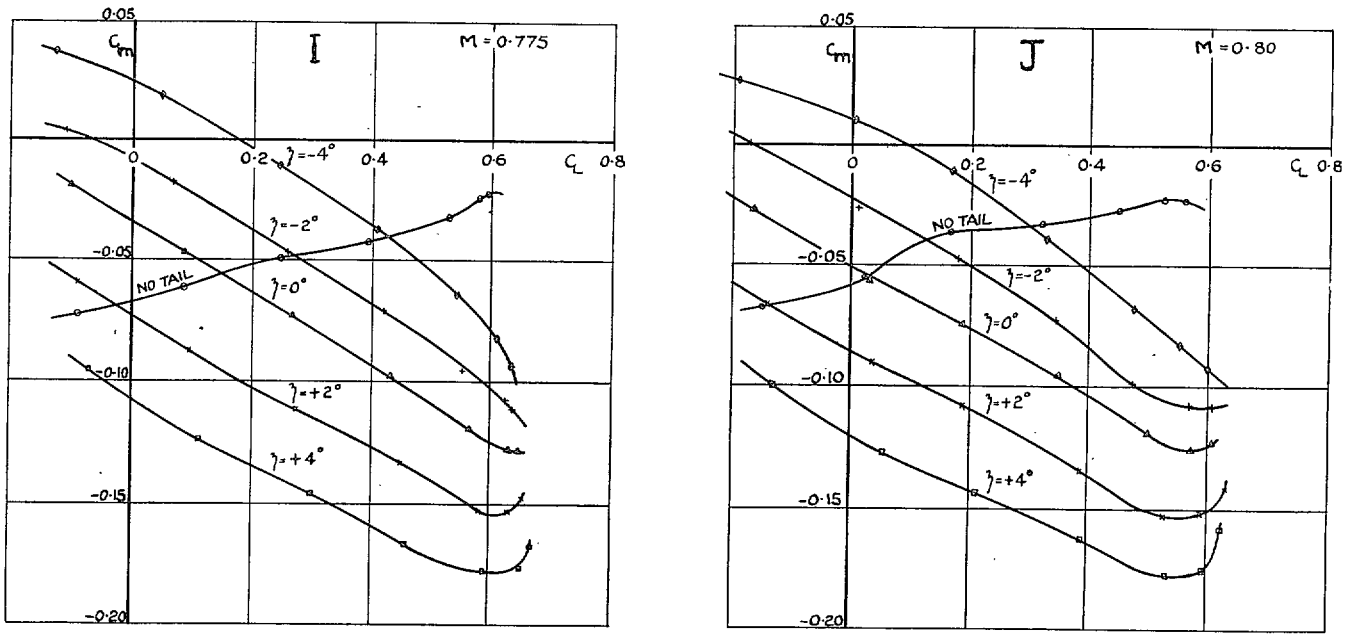

FIG 7. Pitching moments on complete model, for constant tailplane setting ($\eta_T = 2$ deg).

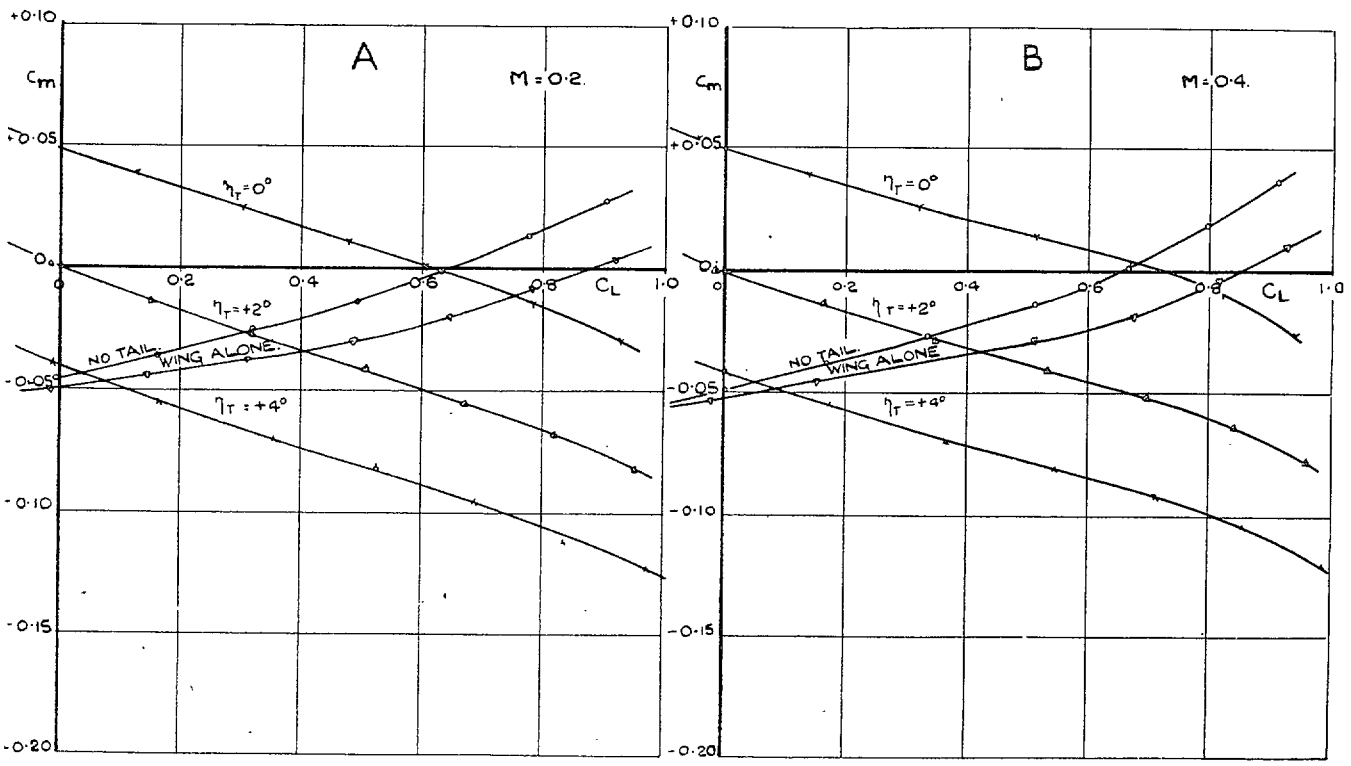

FIG. 8. Pitching moments on complete model, for constant elevator setting ($\eta = 0$ deg).

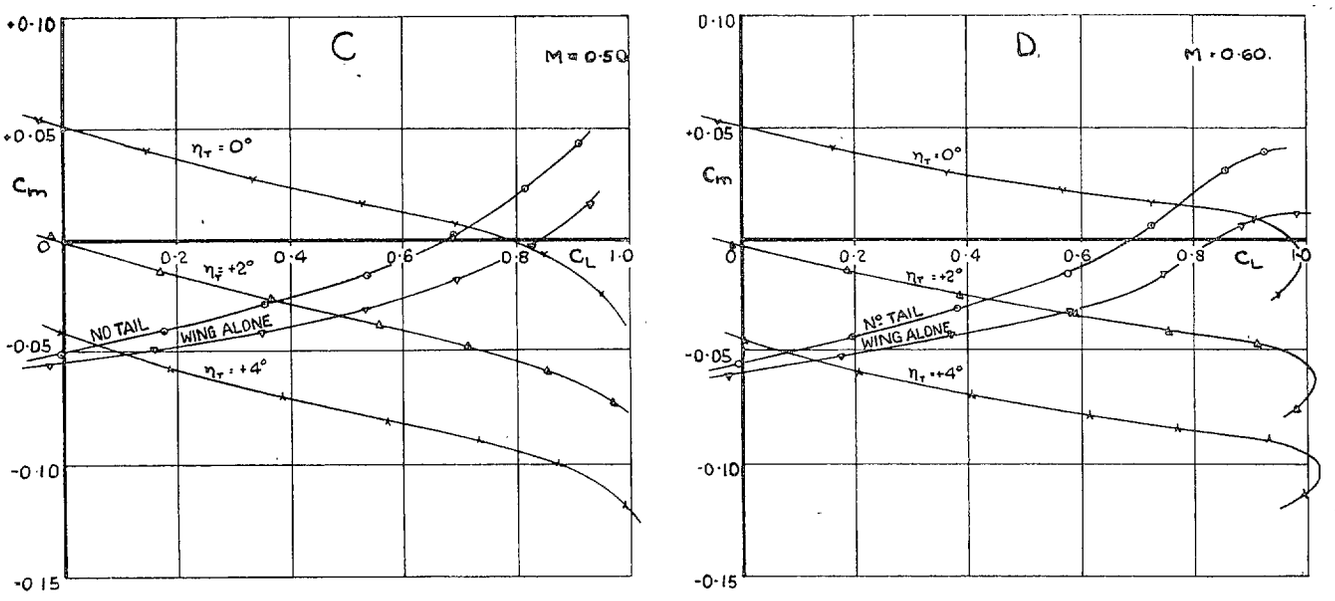

FIG. 8. Pitching moments on complete model, for constant elevator setting ($\eta = 0$ deg).

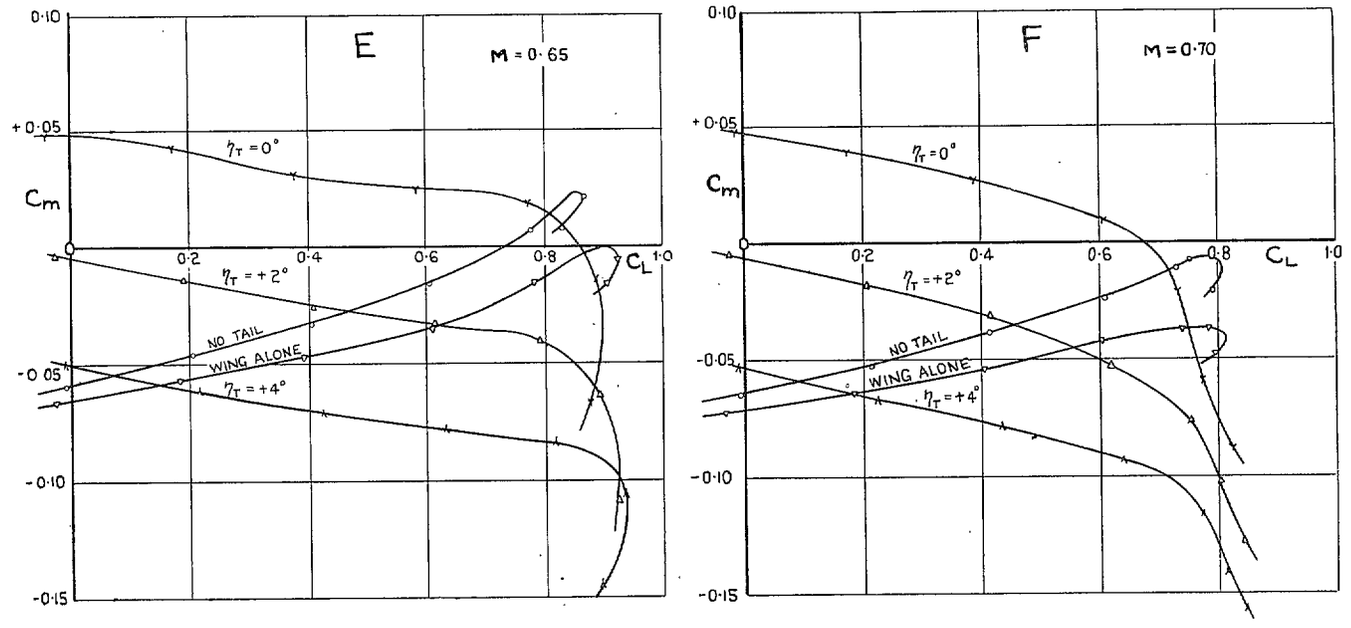

FIG. 8. Pitching moments on complete model, for constant elevator setting ($\eta = 0$ deg).

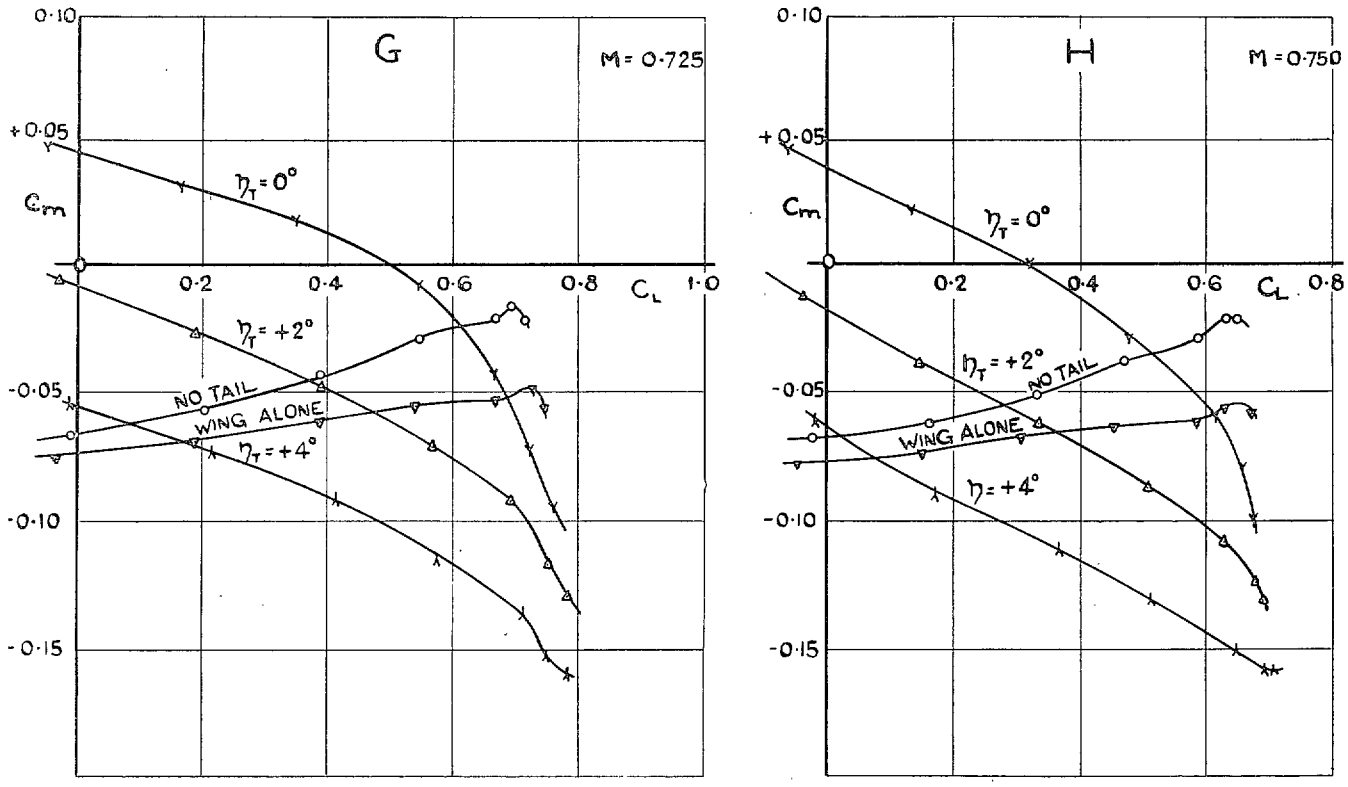

FIG. 8. Pitching moments on complete model, for constant elevator setting ($\eta = 0$ deg).

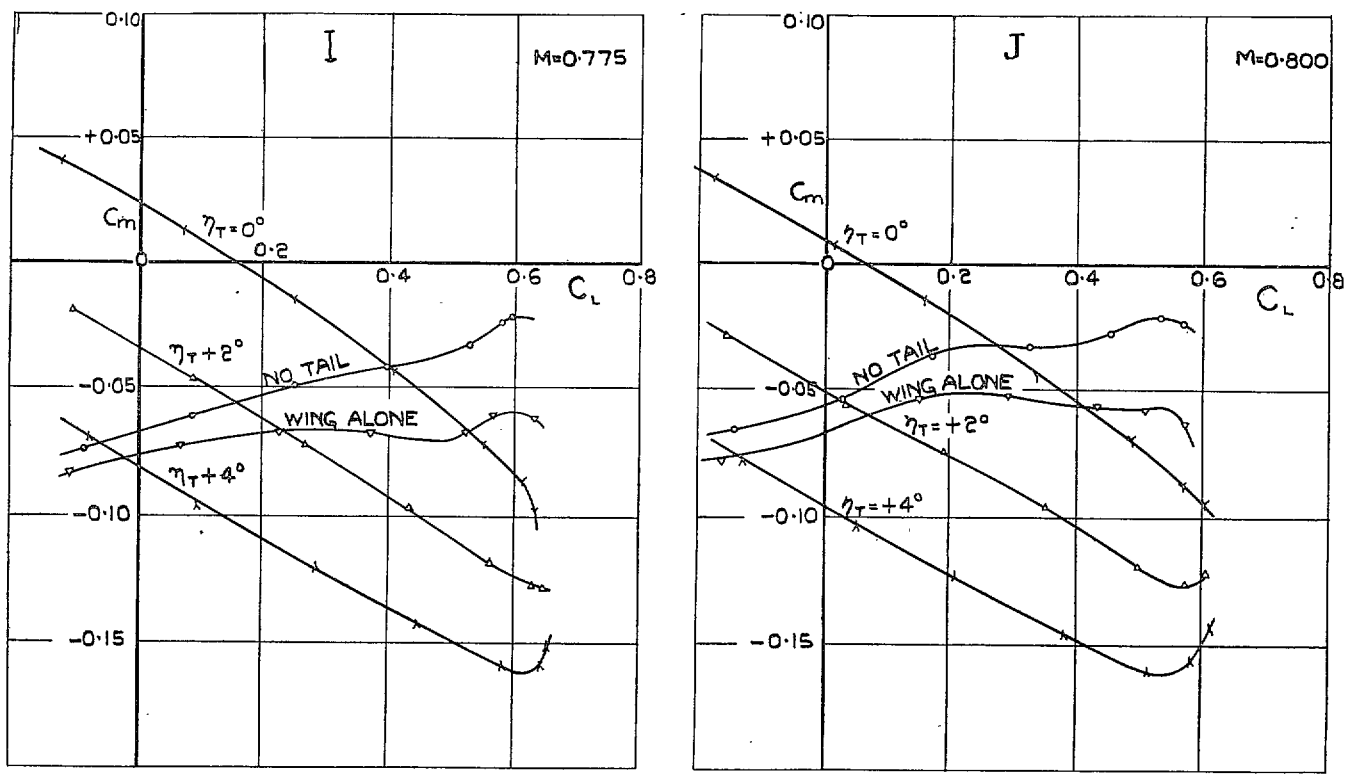

FIG. 8. Pitching moments on complete model, for constant elevator setting ($\eta = 0$ deg).

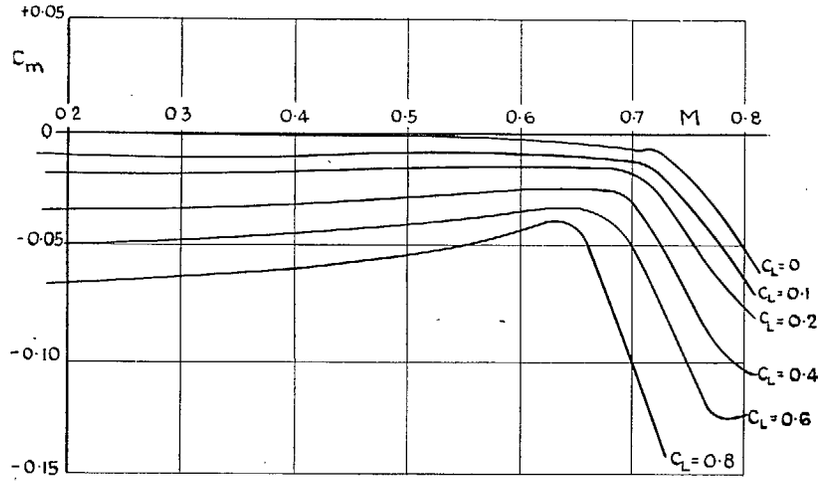

FIG. 9. Variation of pitching moment with Mach number—complete model ($\eta_T = 2$ deg, $\eta = 0$ deg).

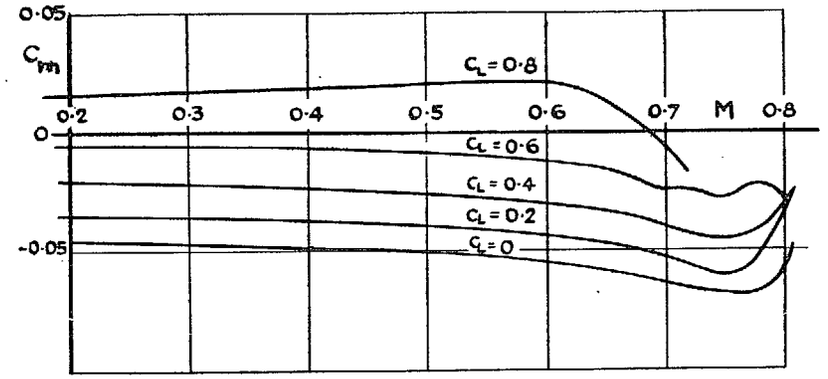

FIG. 10. Variation of pitching moment with Mach number—model without tail.

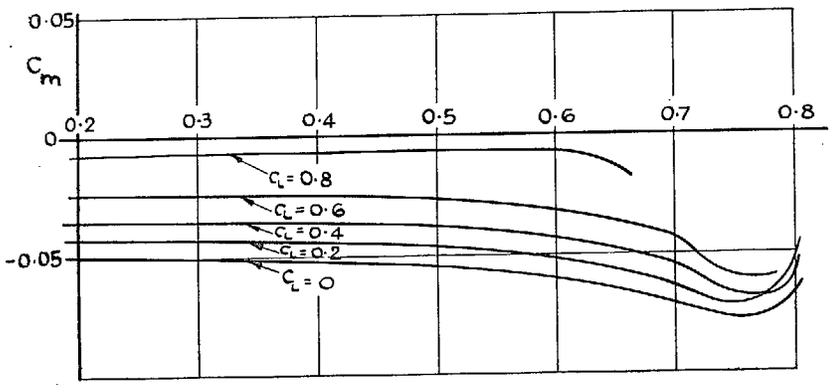

FIG. 11. Variation of pitching moment with Mach number—wing alone.

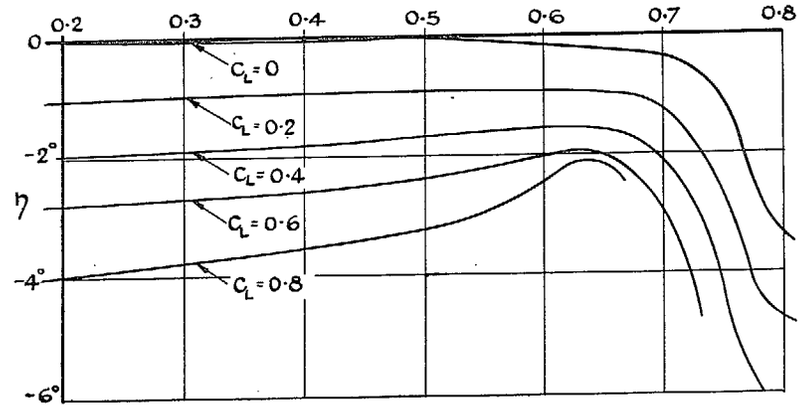

FIG. 12. Variation with Mach number of elevator angle to trim at constant C_L ($\eta_T = 2$ deg).

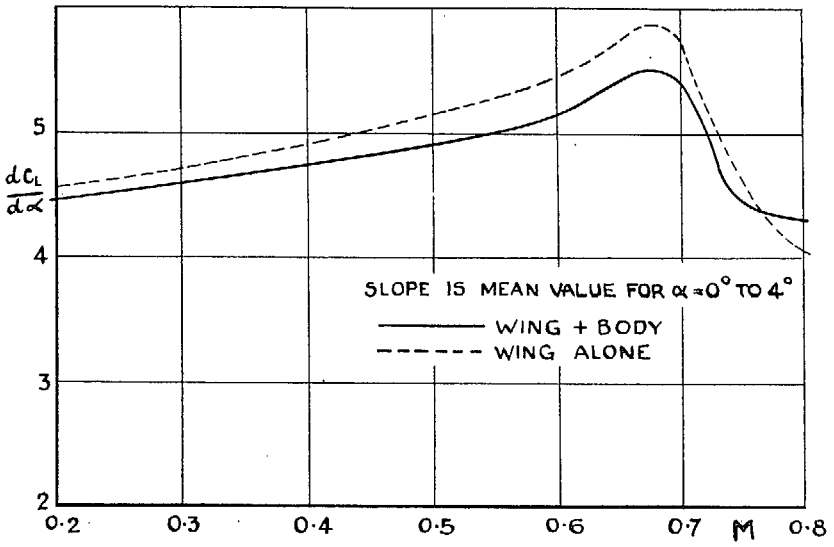

FIG. 13. Variation of $\partial C_L/\partial\alpha$ with Mach number ($R = 1 \times 10^6$).

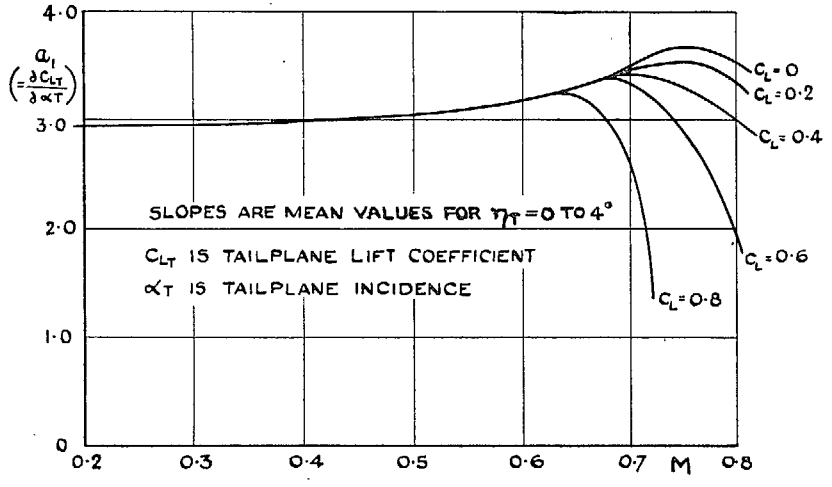

FIG. 15. Variation of a_1 with Mach number.

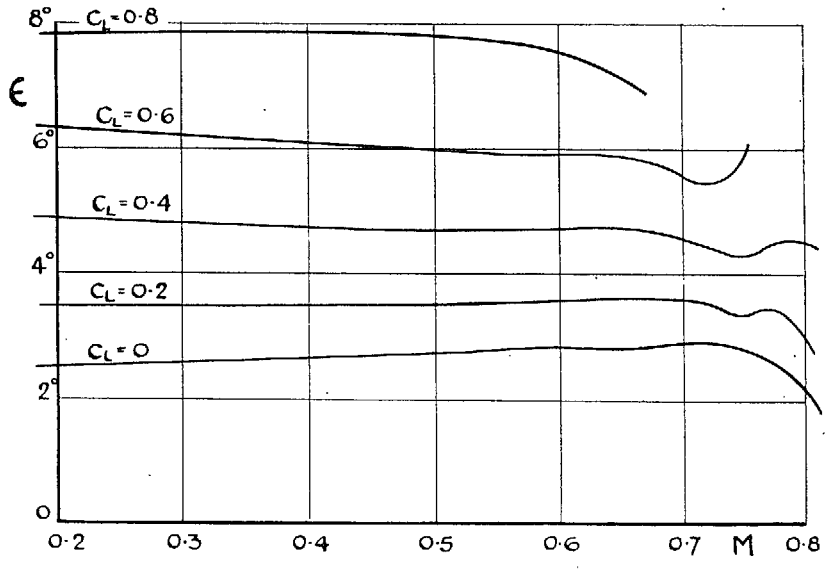

FIG. 14. Variation of downwash angle at tail with Mach number.

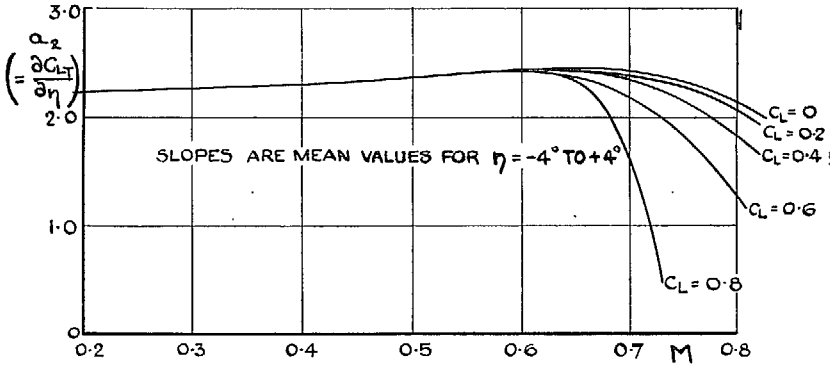

FIG. 16. Variation of a_2 with Mach number.

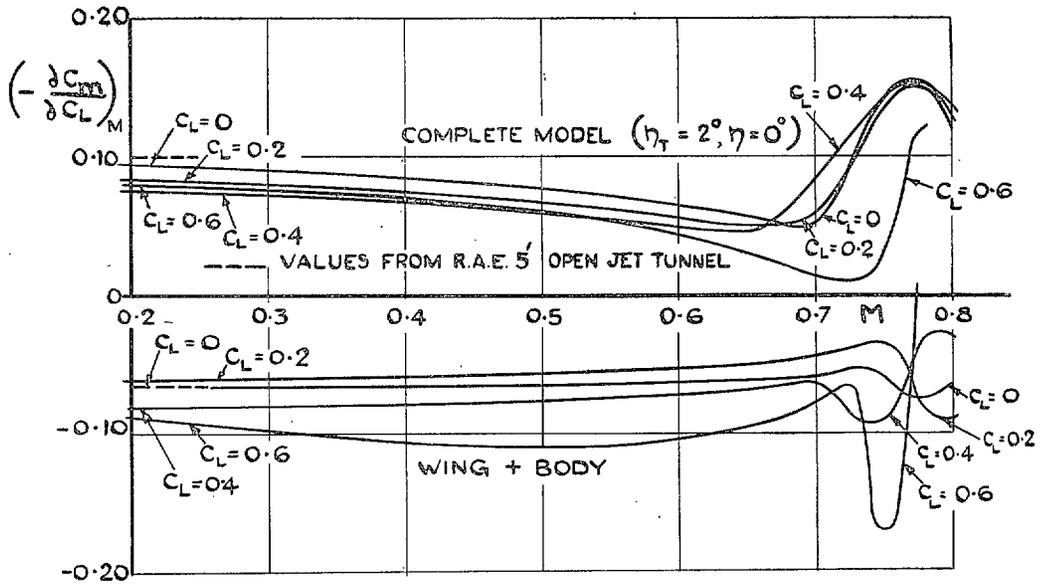

FIG. 17. Variation of $(-\partial C_m/\partial C_L)_M$ with Mach number at constant C_L.

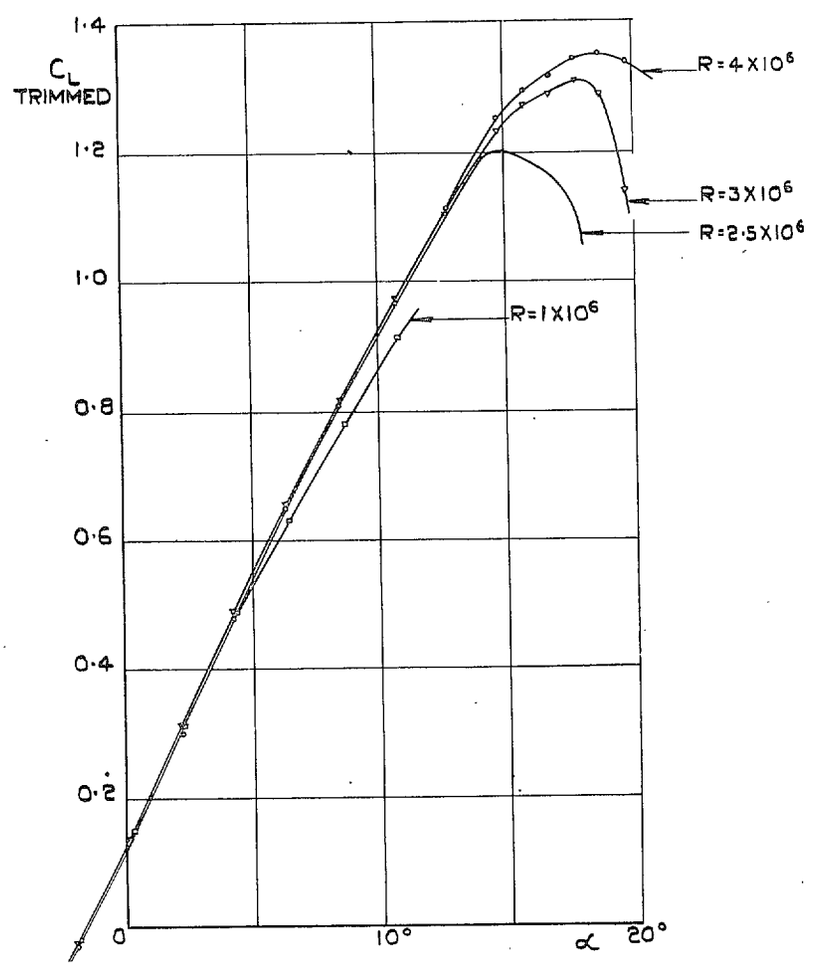

FIG. 18. Low-speed lift curves—complete model ($M < 0·2$).

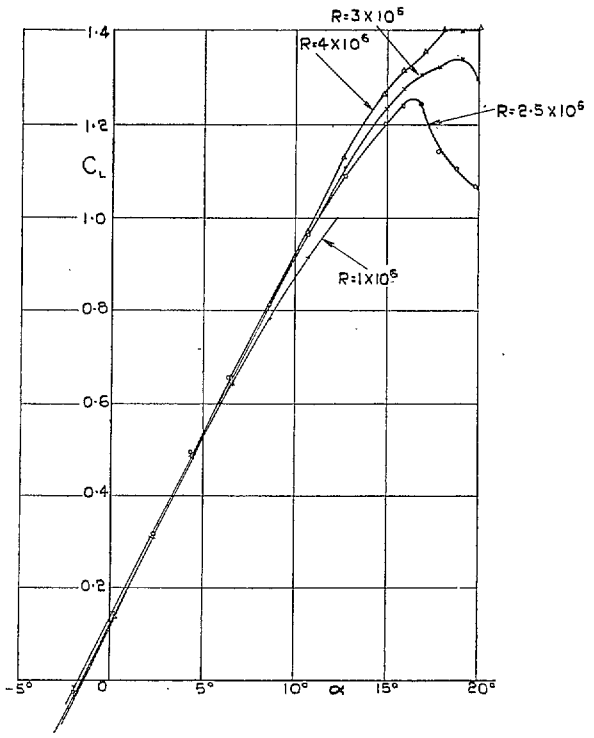

FIG. 19. Low-speed lift curves—wing ($M < 0 \cdot 2$).

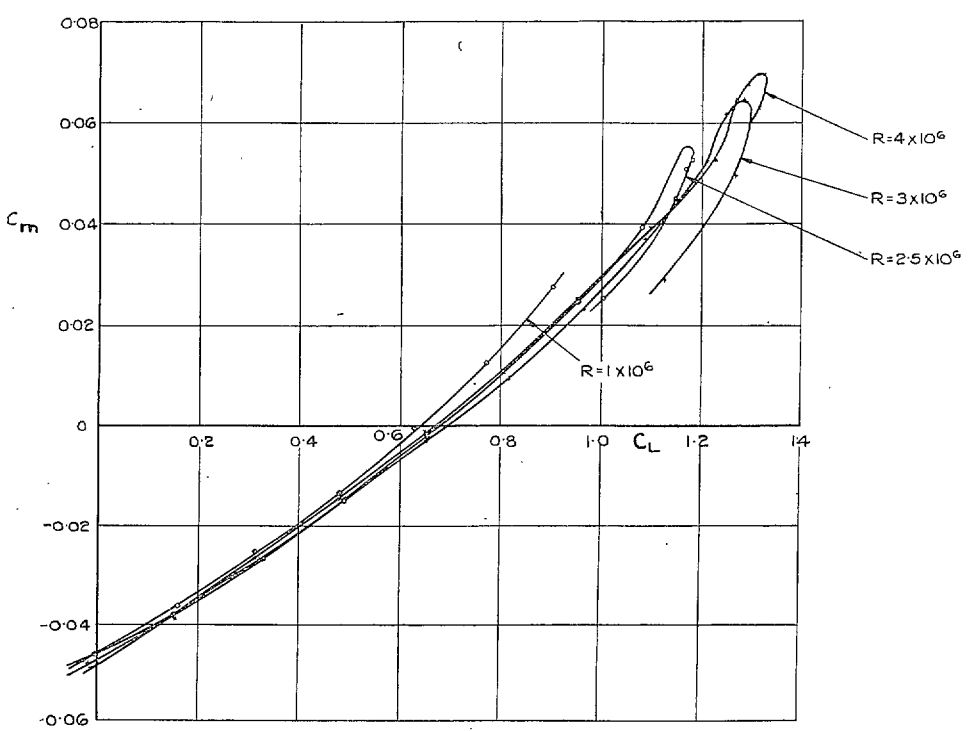

FIG. 20. Scale effect on pitching moment—model without tail ($M < 0 \cdot 2$).

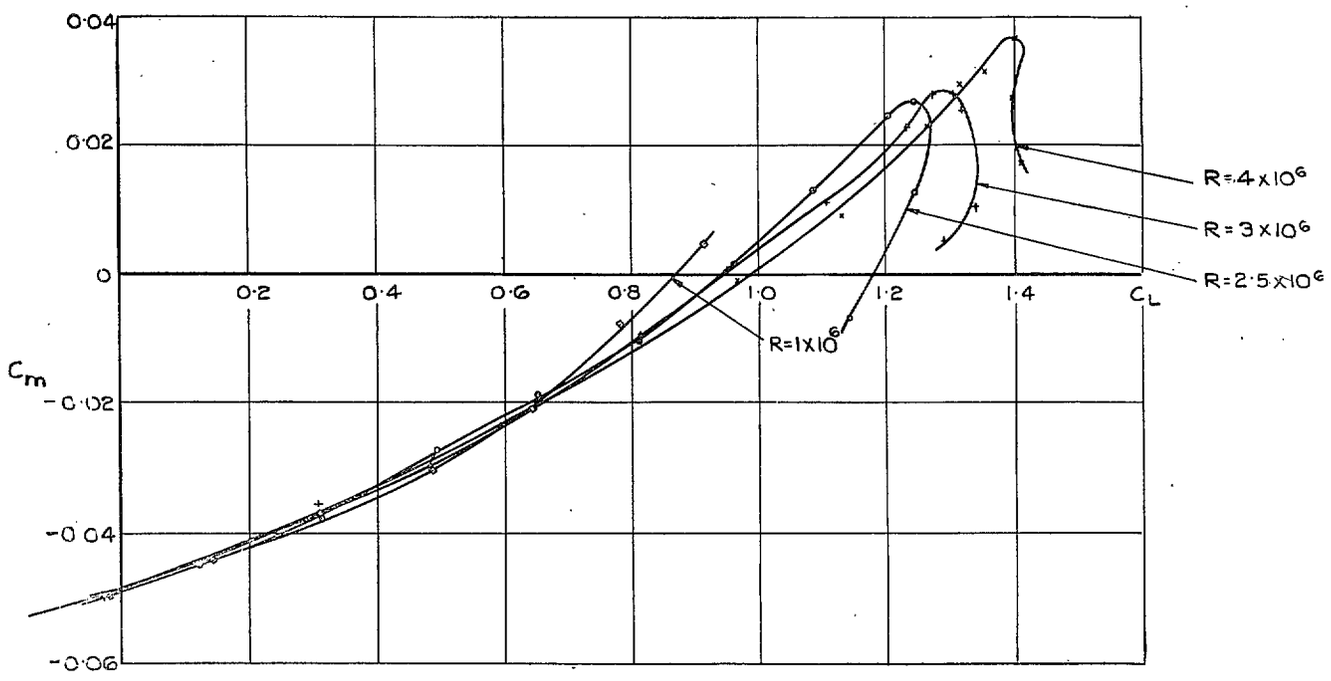

FIG. 21. Scale effect on pitching moment—wing ($M < 0 \cdot 2$).

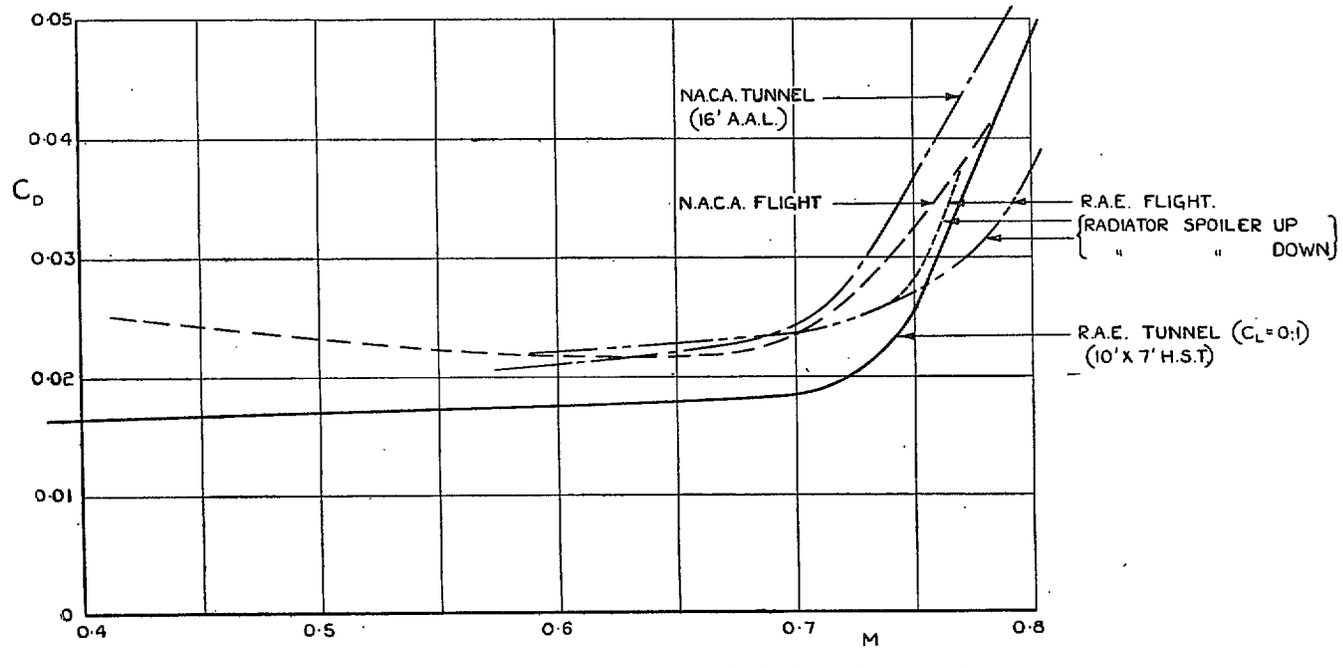

FIG. 22. Comparison of drag from N.A.C.A. and R.A.E. flight and tunnel tests.

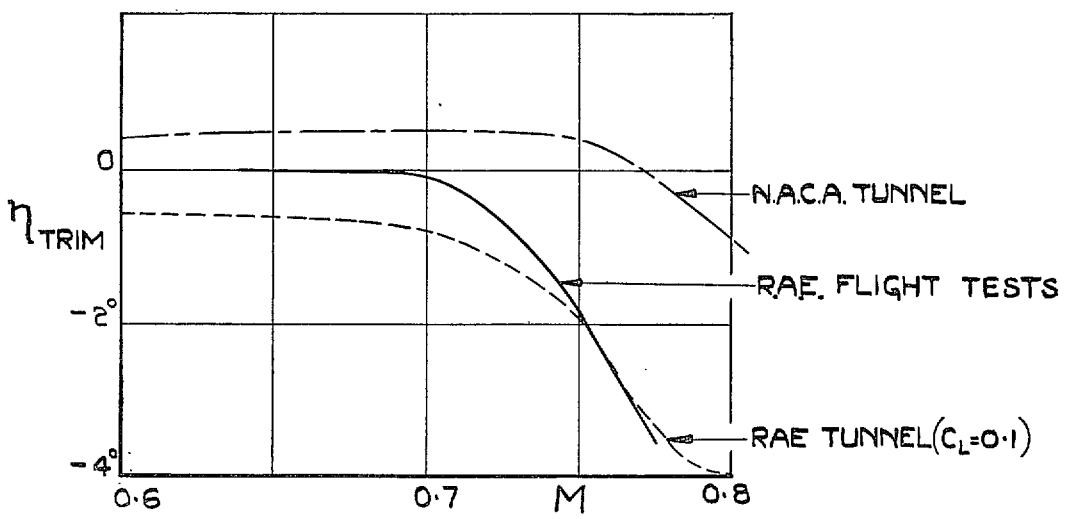

FIG. 23. Comparison of elevator angle to trim from flight and tunnel tests.

(92750) Wt. 13/806 K.5 11/51 Hw.

PRINTED IN GREAT BRITAIN

Publications of the Aeronautical Research Council

ANNUAL TECHNICAL REPORTS OF THE AERONAUTICAL RESEARCH COUNCIL (BOUND VOLUMES)—

1934–35 Vol. I. Aerodynamics. *Out of print.*
Vol. II. Seaplanes, Structures, Engines, Materials, etc. 40*s.* (40*s.* 8*d.*)

1935–36 Vol. I. Aerodynamics. 30*s.* (30*s.* 7*d.*)
Vol. II. Structures, Flutter, Engines, Seaplanes, etc. 30*s.* (30*s.* 7*d.*)

1936 Vol. I. Aerodynamics General, Performance, Airscrews, Flutter and Spinning. 40*s.* (40*s.* 9*d.*)
Vol. II. Stability and Control, Structures, Seaplanes, Engines, etc. 50*s.* (50*s.* 10*d.*)

1937 Vol. I. Aerodynamics General, Performance, Airscrews, Flutter and Spinning. 40*s.* (40*s.* 10*d.*)
Vol. II. Stability and Control, Structures, Seaplanes, Engines, etc. 60*s.* (61*s.*)

1938 Vol. I. Aerodynamics General, Performance, Airscrews. 50*s.* (51*s.*)
Vol. II. Stability and Control, Flutter, Structures, Seaplanes, Wind Tunnels, Materials. 30*s.* (30*s.* 9*d.*)

1939 Vol. I. Aerodynamics General, Performance, Airscrews, Engines. 50*s.* (50*s.* 11*d.*)
Vol. II. Stability and Control, Flutter and Vibration, Instruments, Structures, Seaplanes, etc. 63*s.* (64*s.* 2*d.*)

1940 Aero and Hydrodynamics, Aerofoils, Airscrews, Engines, Flutter, Icing, Stability and Control, Structures, and a miscellaneous section. 50*s.* (51*s.*)

Certain other reports proper to the 1940 *volume will subsequently be included in a separate volume.*

ANNUAL REPORTS OF THE AERONAUTICAL RESEARCH COUNCIL—

1933–34	1*s.* 6*d.* (1*s.* 8*d.*)
1934–35	1*s.* 6*d.* (1*s.* 8*d.*)
April 1, 1935 to December 31, 1936.	4*s.* (4*s.* 4*d.*)
1937	2*s.* (2*s.* 2*d.*)
1938	1*s.* 6*d.* (1*s.* 8*d.*)
1939–48	3*s.* (3*s.* 2*d.*)

INDEX TO ALL REPORTS AND MEMORANDA PUBLISHED IN THE ANNUAL TECHNICAL REPORTS, AND SEPARATELY—

April, 1950	R. & M. No. 2600.	2*s.* 6*d.* (2*s.* 7½*d.*)

INDEXES TO THE TECHNICAL REPORTS OF THE AERONAUTICAL RESEARCH COUNCIL—

December 1, 1936 — June 30, 1939.	R. & M. No. 1850.	1*s.* 3*d.* (1*s.* 4½*d.*)
July 1, 1939 — June 30, 1945.	R. & M. No. 1950.	1*s.* (1*s.* 1½*d.*)
July 1, 1945 — June 30, 1946.	R. & M. No. 2050.	1*s.* (1*s.* 1½*d.*)
July 1, 1946 — December 31, 1946.	R. & M. No. 2150.	1*s.* 3*d.* (1*s.* 4½*d.*)
January 1, 1947 — June 30, 1947.	R. & M. No. 2250.	1*s.* 3*d.* (1*s.* 4½*d.*)

Prices in brackets include postage.

Obtainable from

HIS MAJESTY'S STATIONERY OFFICE

York House, Kingsway, LONDON, W.C.2 429 Oxford Street, LONDON, W.1
P.O. Box 569, LONDON, S.E.1
13a Castle Street, EDINBURGH, 2 1 St. Andrew's Crescent, CARDIFF
39 King Street, MANCHESTER, 2 Tower Lane, BRISTOL, 1
2 Edmund Street, BIRMINGHAM, 3 80 Chichester Street, BELFAST

or through any bookseller.